Aus der Neurochirurgischen Klinik am Campus Großhadern

Klinik der Ludwig-Maximilians-Universität München

Vorstand: Prof. Dr. med. Jörg-Christian Tonn

angefertigt am

Helmholtz Zentrum München

Deutsches Forschungszentrum für Gesundheit und Umwelt

Institut für Molekulare Toxikologie und Pharmakologie

Nonsense-mediated decay factor SMG7
sensitizes cells to TNFα-induced apoptosis via CYLD tumor
suppressor and the noncoding oncogene *Pvt1* and lncRNA *Adapt33*

Dissertation

zum Erwerb des Doktorgrades der Naturwissenschaften

an der Medizinischen Fakultät der

Ludwig-Maximilians-Universität München

vorgelegt von

Limeng Yang

aus Shanghai

Jahr 2021

Mit Genehmigung der Medizinischen Fakultät
der Universität München

Betreuer:	Prof. Dr. rer. nat. Rainer Glaß
Zweitgutachter:	Prof. Dr. Oliver Gires
Dekan:	Prof. Dr. med. Thomas Gudermann
Tag der mündlichen Prüfung:	09.05.2022

Contents

1. List of Figures

2.   List of Tables

3. Abbreviations

3' UTR	3' untranslated region
ATCC	American Type Culture Collection
BAC	Bacterial artificial chromosome
BF	Bright-field
CCLE	Cancer Cell Line Encyclopedia
CDH1	E-cadherin
CHX	Cycloheximide
CLL	Chronic lymphocytic leukemia
CoVs	Coronaviruses
Cp	Crossing point
CRISPRa	CRISPR activation
CRISPRi	CRISPR interference
CYLD	Cylindromatosis
DCPC	Decapping complex
DECID	Decay-inducing complex
DEGs	Differentially expressed genes
DFS	Disease-free survival
DIA	Data-independent acquisition
DISC	Death-inducing signaling complex
Doxi	Doxycycline
DTT	Dithiothreitol
EEJ	Exon-exon junction
eIF4A3	Eukaryotic translation initiation factor 4A3

EJC	Exon junction complex
FBS	Fetal Bovine Serum
FLIPL	Long form of the FLICE-inhibitory protein
FPKM	Fragments per kilobase of transcript per million
GAS5	RNA-growth arrest-specific 5
GSEA	Gene set enrichment analysis
HCC	Hepatocellular carcinoma
HDGC	Hereditary diffuse gastric cancer
HR	Hazard ratio
hTNFα	Human tumor necrosis factor
IAPs	Inhibitors of apoptosis
IFNγ	Interferon-gamma
IKK	IκB kinase
IKKα or IKK1	IκB kinase α
IKKβ or IKK2	IκB kinase β
IκBs	Inhibitors of NF-κB
KD	Knockdown
KIRC	Kidney renal clear cell carcinoma
KIRC-TCGA	The Cancer Genome Atlas Kidney Renal Clear Cell Carcinoma
KO	Knockout
lincRNA	Long intergenic non-coding RNA
lncRNA	Long non-coding RNA
LoF	Loss-of-function
LPS	Lipopolysaccharide
MAGOH	Mago-nashi homolog

MAGOHB	mago homolog B
MF	Immortalized mouse fibroblasts
miRNA	MicroRNA
misc RNAs	Miscellaneous RNAs
miRISC	miRNA-induced silencing complex
MNU	N-methyl-N-nitrosourea
mORFs	Small ORFs
mRNA	Messenger RNA
mRNP	Messenger ribonucleoprotein
MSI	Microsatellite instable colorectal cancers
mTNFα	Mouse tumor necrosis factor
NA	Not available
NEMO or IKKγ	NF-κB Essential Modulator
NF-κB	Nuclear factor-κB
NLS	Nuclear localization signals
NMD	Nonsense-mediated decay
NSCLC	Non-small cell lung cancer
nt	Nucleotides
onco-lncRNA	Oncogenic lncRNA
OS	Overall survival
p-IκB	Phosphorylated IκB
p(adj)	*p*-value adjusted for multiple hypothesis testing
PAGE	Polyacrylamide gel electrophoresis
PI	Propidium iodide
pri-miRNAs	Primary microRNAs

PTC	Premature termination codon
Pvt1	Plasmacytoma variant translocation 1
qPCR	Quantitative PCR
RAP-MS	RNA antisense purification and mass spectrometry
RCC	Renal cell carcinoma
RHD	Rel Homology Domain
RIPK1	Receptor-interacting serine/threonine-protein kinase 1
RRIs	RNA-RNA interactions
rRNA	ribosomal RNA
SDS	Sodium dodecyl sulfate
siRNA	Small interfering RNA
SMG7	Suppressor with morphogenetic effect on genitalia 7
SURF	SMG-1–Upf1–eRF1–eRF3
sncRNAs	Small ncRNAs
SNHG12	Small nucleolar RNA host gene 12
snRNA	small nuclear RNA
SRA	Sequence Read Archive
STE	Stabilizer element
TCGA	The Cancer Genome Atlas
TNFα	Tumor necrosis factor-alpha
TNFαip3 or A20	TNF Alpha Induced Protein 3
TPR	Tetratricopeptide
TRAF2	TNF receptor-associated factor 2
TRAIL	TNF-related apoptosis-inducing ligand
TSS	Transcription start site

TWEAK	TNF-like weak inducer of apoptosis
untr	Untreated
uORFs	Upstream open reading frames
UPF1	Up-frameshift protein 1
UPR	Unfolded protein response
wt	Wild-type
zVAD	Z-VAD-FMK

4. Summary

Nonsense-mediated decay (NMD) factors play important roles in detection and degradation of abnormal RNAs. In humans, 10% of normal physiological messenger RNAs (mRNAs) are targets of NMD for degradation, and 30% of known disease-associated mutations are associated with premature termination codon (PTC)-containing mRNAs. Generally, PTC is a well-characterized and studied signal to induce NMD. However, there are exceptions to the rule that NMD can degrade even mRNAs without PTCs, including long non-coding RNAs (lncRNAs). The NMD pathway is comprised of a series of NMD proteins. Among which, suppressor with morphogenetic effect on genitalia 7 (SMG7) is a famous NMD factor and plays a key role in the regulation of tumor necrosis factor-alpha (TNFα)-induced extrinsic apoptosis; however, this novel mechanism behind it has not been thoroughly investigated.

In this study, I showed that there are similarities and differences among the NMD regulators. Knockout (KO) of *Smg7* by CRISPR Cas9 in mouse fibroblast (MF) cells inhibited TNFα-induced extrinsic apoptosis and allowed unrestricted expression of lncRNAs in addition to NMD targets. Similar to *Smg7 -/-* MF cells, transcriptome analysis revealed that knockout of NMD factor *Smg6* by gene targeting in mouse embryonic stem cell showed an increase in long intergenic non-coding RNAs (lincRNAs) while *Upf1* KD by siRNA in mouse myoblast cell C2C12 showed a predominant upregulation in microRNAs (miRNAs). Interestingly, *Smg7 -/-* MF cells shared 9 genes in common with *Smg6* KO and *Upf1* KD cells, and 6 of which were lncRNAs suggesting the vital role of the NMD system in controlling lncRNAs.

Smg7 -/- cells showed several salient features. Biochemical analysis of the apoptotic pathway in *Smg7 -/-* MF cells indicated that the tumor suppressor cylindromatosis (CYLD) was downregulated and caspase activity was reduced compared to parental MF cells, thereby, *Smg7 -/-* MF cells were switched to nuclear factor-κB (NF-κB)-mediated survival. A positive correlation between *SMG7* and *CYLD* expression levels was detected in both mouse and human cells, and this wide conservation was further confirmed in human cancer cells and the kidney cancer samples acquired from The Cancer Genome Atlas (TCGA). Apart from CYLD suppression in *Smg7 -/-* cells, overexpression of lncRNAs *Pvt1* and *Adapt33* by CRISPRa in MF cells increased the resistance to TNFα-induced apoptosis. In contrast, the application of pharmacologic IKK inhibitors in *Pvt1*-overexpressing TNFα-resistant cells and *Smg7 -/-* spheroid models restored TNFα-induced cell death. Unlike *Smg7* KD by CRISPRi in NIH 3T3 cells, *SMG7* KD by CRISPRi in HCT-116 and MCF-7 cells resulted in cell death and growth arrest. Moreover, *Adapt33* mRNA cross-linking precipitation showed that many enriched genes are involved in cell death and survival regulation network as well as the NMD pathway.

Furthermore, *Smg7 -/-* cells showed the TNFα-resistant performance when cultured in Matrigel matrix.

To summarize, these findings indicate a novel role of SMG7 in protecting TNFα-induced apoptosis through the regulation of tumor suppressor CYLD, onco-lncRNA *Pvt1* and lncRNA *Adapt33*, and implicate a comprehensive role of NMD factor in the regulation of NF-κB.

5. Zusammenfassung

Nonsense-mediated decay (NMD) Proteine sind für die Kontrolle und den Abbau von aberranten RNAs verantwortlich. In Menschen sind 10% der normalen physiologischen messenger-RNAs (mRNAs) NMD-Targets, während 30% der bekannten krankheitsassoziierten Mutationen mit vorzeitigen Stopcodons (PTCs) assoziiert sind. Diese PTCs sind charakteristische Merkmale zur Induktion von NMD. Abgesehen davon sind auch Ausnahmen bekannt, die zeigen das NMD sowohl mRNAs ohne PTCs als auchlanger nicht-kodierender RNAs (lncRNAs) abbauen kann. Der NMD-Signalweg besteht aus einer Vielzahl von NMD-Proteinen. Darunter ist der Suppressor mit morphogenetischer Wirkung auf die Genitalien 7 (SMG7) ein bekannter NMD-Faktor, der eine Schlüsselrolle bei der Regulierung der durch Tumornekrosefaktor-alpha (TNFα)-induzierten extrinsischen Apoptose spielt. Der neuartige Mechanismus, der dahinter steckt, ist jedoch noch nicht gründlich untersucht worden.

In dieser Studie habe ich gezeigt, dass es Gemeinsamkeiten und Differenzen zwischen den NMD-Regulatoren gibt. Das Knockout (KO) von *Smg7* durch CRISPR Cas9 in Mausfibroblastenzellen (MF) hemmt die TNFα-induzierte extrinsische Apoptose und ermöglicht die uneingeschränkte Expression von lncRNAs zusätzlich zu den NMD-Targets. Ähnlich wie bei *Smg7* KO MF-Zellen, zeigte die Transkriptomanalyse des Knockouts vom NMD-Faktor *Smg6* in embryonalen Stammzellen der Maus einen erhöhten Anteil an langen, intergenen nicht-kodierenden RNAs (lincRNAs) aufweist, während *Upf1* Knockdown (KD) in Maus- C2C12 Myoblastenzellen eine überwiegende Hochregulierung von microRNAs (miRNAs) zeigt. Interessanterweise haben *Smg7 -/-* MF-Zellen 9 Gene mit *Smg6* KO- und *Upf1* KD-Zellen gemeinsam, von denen 6 lncRNAs sind, was auf die wichtige Rolle des NMD-Systems bei der Kontrolle von lncRNAs hinweist.

Smg7 KO Zellen zeigten mehrere auffällige Merkmale. Die biochemische Analyse des apoptotischen Signalwegs in *Smg7* KO MF-Zellen zeigte, dass der Tumorsuppressor Cylindromatose (CYLD) herunterreguliert und die Caspase-Aktivität im Vergleich zu unmodifizierten MF-Zellen reduziert war, wodurch *Smg7 -/-* MF-Zellen auf ein durch den nuklearen Faktor-κB (NF-κB) gesteuertes Überleben umgestellt wurden. Des Weiteren wurde ein positiver Zusammenhang zwischen *SMG7* und *CYLD* in humanen Zellen und Mauszellen entdeckt und in menschlichen Krebszelllinien sowie Nierenkarzinom-Proben von The Cancer Genome Atlas (TCGA) bestätigt. Zusätzlich zur Suppression von CYLD in *Smg7 -/-* Zellen, erhöhte die Überexpression von lncRNAs *Pvt1* und *Adapt33* die Resistenz gegen TNFα induzierte Apoptose. Im Gegensatz dazu führte die Anwendung pharmakologischer IKK-Inhibitoren bei *Pvt1* überexprimierenden TNFα-resistenten Zellen und *Smg7* defizienten

Sphäroiden zur Wiederherstellung des TNFα-induzierten Zelltods. Auch KD von *SMG7* durch CRISPRi in humanen Krebszellen führte zum Zelltod und Wachstumsstillstand, eineIndikation von einem weiteren Zusammenhang zwischen NMD und Zelltod. Darüber hinaus zeigte eine *Adapt33* mRNA-Präzipitation eine erhöhte Anzahl von Genen in Überlebensregulierungs- und Zelltodnetzwerke, als auch im NMD Signalweg. Außerdem zeigten *Smg7 -/-* Zellen die TNFα-resistente Leistung, wenn sie in Matrigel-Matrix kultiviert wurden.

Zusammengefasst unterstützen diese Ergebnisse eine neuartige Funktion von SMG7 in der TNFα-induzierten extrinsischen Apoptose durch die Regulierung von onco-lncRNA *Pvt1*, lncRNA *Adapt33*, und Tumorsuppressor CYLD und legen eine umfangreiche Rolle als Regulator von NF-κB durch einen NMD Faktor nahe.

6. Introduction

6.1. NMD

6.1.1. The origin and function of NMD

Nonsense-mediated mRNA decay (NMD), a conservative quality-control system to reduce gene expression errors by eliminating transcripts that contain premature stop codons (PTC), has been extensively investigated in eukaryotic cells. The phenomenon of NMD was first described in human cells and yeast almost simultaneously 40 years ago [1, 2]. In 1993, the term "nonsense-mediated mRNA decay" was introduced to describe this phenomenon [3]. In plants, NMD degrades transcripts derived from not only protein-coding transcripts but also transposons, pseudogenes, natural antisense RNAs and mRNA-like non-coding RNAs [4]. In prokaryotes, mRNA cannot be degraded by NMD due to the lack of PTCs [5].

There are two NMD functions accepted widely in cellular processes: A), quality control of abnormal transcripts, for example, degrading mRNAs harboring PTCs to prevent the potentially deleterious truncated proteins; B), regulating the stability of many functional and full-length mRNAs in response to cellular needs [6, 7]. In humans, 10% of normal physiological mRNAs are targets of NMD for degradation, while the mechanism under this phenomenon remains incompletely clear [7-9]. Nevertheless, studies from many laboratories provided supportive evidence that NMD is closely associated with the translation termination process. At the end of the translation, cells need to make the final decision whether to continue using this mRNA as a template for the next round of translation or to degrade it by NMD [10].

6.1.2. NMD factors and their molecular mechanisms

The NMD pathway is constructed by a series of NMD factors, including, for example, up-frameshift protein 1 (UPF1) and SMG family proteins. The human UPF is known by its homologue in *S. cerevisiae*, which is the first identified NMD factor [11]. UPF1, UPF2 and UPF3 (UPF3A and UPF3B in mammals) are conserved from yeast to humans while SMG1, SMG5, SMG6 and SMG7 seem to be only found in the metazoans [12, 13]. SMG8 and SMG9 are two novel subunits of SMG family proteins in the SMG1 complex identified in 2009 [14].

The NMD process starts with PTC recognition by the so-called SURF (SMG-1–Upf1–eRF1–eRF3) surveillance complex, which contains SMG1, UFP1, eRF1 and eRF3 [15]. During RNA splicing, a protein complex, exon junction complex (EJC) is attached 20–24 nucleotides (nt) upstream of a pre-messenger RNA exon-exon junction (EEJ) [16]. EJCs are mainly composed

of four key elements including the eukaryotic translation initiation factor 4A3 (eIF4A3), the cancer susceptibility candidate 3 (CASC3), the RNA-binding motif protein 8A (RBM8A or Y14) and either the mago-nashi homolog (MAGOH) or the mago homolog B (MAGOHB) [17]. According to the established rule, NMD will be elicited if PTCs are presented more than 50–55 nt upstream of the last EEJ (Figure 6-1) [18]. Extreme evidence showed the distance between PTCs and nearest EEJ that NMD could identify can be up to 4.5 kb [19].
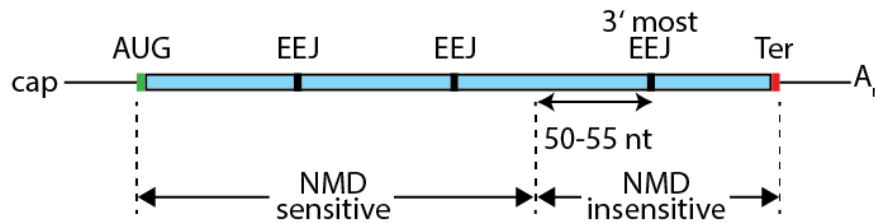
Figure 6-1. NMD depends on the position of PTC relative to the 3' most EEJ.

Exon junction complex (EJC) locates 20-24 nt upstream of the exon-exon junction (EEJ). During translation, the ribosome will remove all of the EJCs and their associated proteins. Generally, mRNAs with PTCs located 50-55 nt upstream of the 3' most EEJ is the signal for NMD degradation.

As shown in Figure 6-2, in the starting round of translation, the ribosome removes the EJC and other mRNP (messenger ribonucleoprotein) complexes from the entire coding region to maintain the standard translation process. When a translation is terminated at a PTC, the SURF surveillance complex is constructed. Subsequently, UPF1 and SMG1 are recruited to EJC complex through UPF2, forming the SURF-EJC complex, which is also known as decay-inducing complex (DECID), then resulting in the UPF1 phosphorylation by SMG1 [15]. The hyperphosphorylated UPF1 provides the binding platform for the NMD complex, including SMG5, SMG6 and SMG7, leading to the degradation of NMD targeted mRNAs by SMG6, SMG5-SMG7 or PNRC2 decapping route. SMG6 cleaves mRNA endonucleolytically near PTCs, the 3' and 5' fragment RNAs are rapidly degraded by XRN1 and exosome, respectively. In contrast, SMG5–SMG7 can recruit the deadenylation CCR4-NOT complex to the NMD-targeted RNAs, which are subsequently degraded by XRN1 [6].
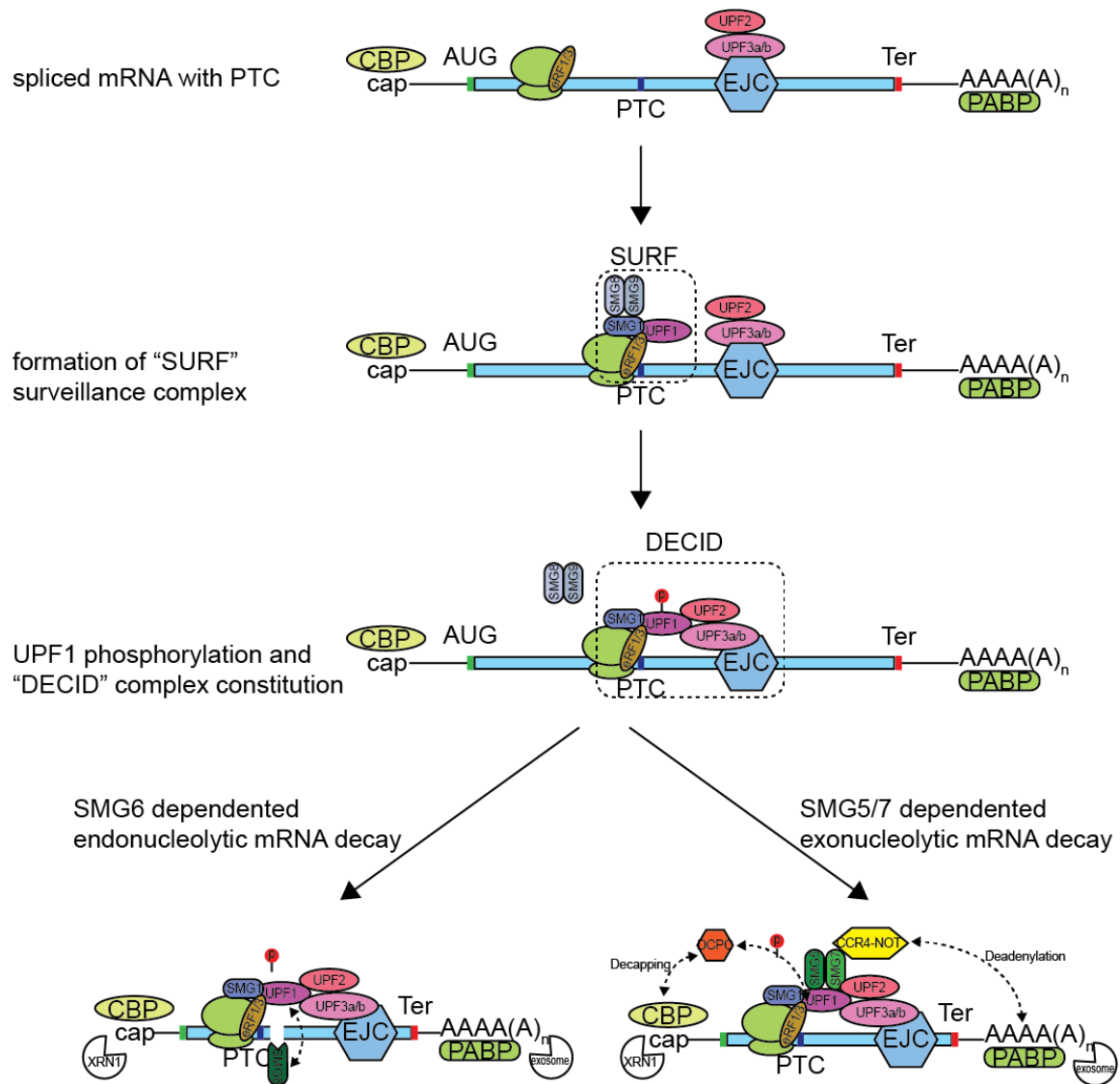
Figure 6-2. The activation of NMD and degradation of targeting mRNA.

The figure was modified from Karousis et al. and Kashima et al. [6, 15]. In the first round of translation, the EJCs and their associated proteins are dislocated by the ribosome. When the translating process terminates at the PTC, UPF1 and SMG8/9 are recruited to the translation termination complex which consists eRF1–eRF3 forming the "SURF" surveillance complex. Following the release of SMG8/9, UPF1 is phosphorylated by SMG1 and joins the downstream EJC to promote the formation of the decay-inducing (DECID) complex. In this situation, UPF1 can recruit SMG6 or SMG5/7 heterodimer, which results in the dephosphorylation of UPF1 and triggers the corresponding mRNA decay via an endonucleolytic or exonucleolytic method. SMG6 as an endonuclease can cleave mRNA near the PTC, and the 5' and 3' fragment RNAs are rapidly degraded by XRN1 and exosome, respectively. SMG5–SMG7 recruits the deadenylation CCR4-NOT complex via CNOT8 (POP2) to NMD targets, which are subsequently degraded by XRN1. The decapping complex (DCPC) is recruited directly by UPF1 or via PNRC2, leading to the degradation of target mRNA.

6.1.3.   General NMD targeting features

Generally, PTC is the well-characterized and studied signal to induce NMD. However, there are exceptions to this model that NMD can degrade even PTC-free mRNAs. Normal termination codons can also trigger NMD when it is too far away from the poly(A)-binding protein PABPC1. On the contrary, NMD can be inhibited by folding the poly(A) tail near the PTC or by tethering PABPC1 in the vicinity of the PTC [20]. Upstream open reading frames (uORFs) are another feature that can trigger the NMD pathway. The termination codon of a uORF can be recognized as a PTC that leads to mRNA degradation when the mRNA lacks a stabilizer element (STE), such as CPA1 [21, 22]. mRNAs with spliceable intron-containing 3' UTRs are also the targets of NMD. [23]. Apart from NMD, RNAs also can be degraded by other mechanisms. One well-known example would be microRNA (miRNA) which is involved in nearly all biological processes. miRNA (19–25 nt) can bind to Argonaute and other proteins to promote the formation of miRNA-induced silencing complex (miRISC) and guide this complex to its target RNAs to mediate the repression of protein production or the degradation of mRNAs by recruitment of CCR4-NOT deadenylase complex [24]. Dicer is a multi-domain RNase III-related endonuclease responsible for generating mature miRNA and small interfering RNA (siRNA) using the pre-microRNA and double-strand RNA (dsRNA), respectively. In contrast to miRNA that one miRNA can target many mRNAs, siRNA is a 21–22 nt dsRNA which can specifically cleave one mRNA with minor off-target exceptions [25, 26].

6.1.4.   NMD related disease

It is reported that 30% of known disease-associated mutations are associated with PTC-containing mRNAs [27]. Among these diseases, β-thalassemia is the earliest and most prototypical example. The disorder of hemoglobin production causes this disease. Hemoglobin is a tetramer composed of 2 α-globin and 2 β-globin chains. *β-globin* mRNA has typically three exons, and non-sense mutations that happen within the first two exons generally trigger NMD and protect heterozygotes from β-thalassemia. On the contrary, mRNAs harboring PTCs within the third exon are generally not targeted for NMD, and therefore, truncated β-globin leads to symptomatic, dominantly inherited β-thalassemia [28]. Several diseases like myotonia congenital [29], retinal degeneration [30, 31], robinow syndrome [32] and brachydactyly-type B [33] are all related to NMD. Moreover, coronaviruses (CoVs)

infection is under control by the NMD system. Many features in Cov, including long 3' UTR, make it appears to be targeted for NMD. Conversely, CoV replication also inhibits the function of NMD by one structural N protein of the virus [34].

Undoubtedly, NMD is involved in tumor development, though the mechanism is still quite poorly understood. Under certain circumstances, tumors use the NMD system to degrade the essential tumor suppressor. Under other circumstances, tumors adjust the activity of NMD to provide a microenvironment adapted to tumor growth [35]. Many kinds of cancer types exhibit mutated UPF1 protein, which is the core factor in the NMD system, especially in endometrial and ovarian cancers [36]. As a tumor suppressor, E-cadherin (CDH1) can suppress the invasion and metastasis of hereditary diffuse gastric cancer (HDGC) cells. The data showed that PTC-containing CDH1 transcripts were strongly downregulated in healthy gastric tissue, while HDGC patients with PTC-containing CDH1 alleles showed a relationship of their predicted NMD capacity and an earlier age of gastric cancer [37]. In microsatellite instable colorectal cancers (MSI), inhibition of NMD activity resulted in the re-expression of several of PTC mutant proteins, which possess potentially deleterious activity on MSI tumorigenesis and reduced tumor growth [38]. A genome-wide pan-cancer analysis across 24 cancers from TCGA revealed that NMD plays an essential role in promoting loss-of-function (LoF) of the affected genes, i.e., through loss of expression. Half of the highly mutated gastric adenocarcinomas were associated with NMD-inducible mutations in the translation promoters LARP4B and EIF5B [39]. Altogether, NMD is involved in different kinds of cancers and may be an effective strategy for cancer treatment.

6.2. SMG7

SMG7 (suppressor with morphological defects on genitalia 7), was first cloned in *Caenorhabditis elegans* and characterized as an NMD associated gene [40]. The structure revealed that SMG7 has a 14-3-3-like domain [41] and there are 2 tetratricopeptide (TPR) repeats at the N-terminal end, which is generally thought to mediate protein-protein interactions [42]. SMG7 can heterodimerize with SMG5 in an unusual perpendicular back-to-back orientation via their 14-3-3-like phosphopeptide recognition domains, thereby increasing the affinity between SMG5–SMG7 and UPF1 [43]. SMG7 localizes in cytoplasmic mRNA decay bodies and can degrade a reporter transcript tethered to it by the C-terminal domain in the absence of a PTC, UPF1, SMG5 or SMG6 [44]. The functions of SMG5-SMG7 complex and SMG6 have redundant parts in NMD via endo- and exonucleolytic mRNA degradation pathways [43, 45, 46]. Metze et al. showed that different NMD factors might have their specific

target transcripts, for example, SMG6 preferentially cleaved PTC-containing immunoglobulin μ reporter transcripts while SMG5/SMG7 predominantly degraded *β-globin* transcripts [45]. Furthermore, SMG7 recruits deadenylase complex CCR4–NOT via a catalytic subunit POP2 (also known as CNOT8), and thereby promotes deadenylation and subsequent decapping of NMD targets [46]. As reported recently, SMG7 is important to UPF1-dependent miRNA-mediated 3' UTR-length-dependent mRNA decay [47]. Moreover, two recent studies showed SMG7 interacts with p53 and influences cellular survival [48, 49]. The *SMG7* gene was also found to be associated with prostate cancer in a genome-wide scan [50]. We previously identified a role for *Smg7* in protecting cells from TNFα-induced apoptosis in a genome-wide mutation screen [51]. However, the downstream targets of SMG7 are not well understood in terms of their functional roles on TNFα and tumor biology.

6.3. Apoptosis

6.3.1. Apoptosis and its molecular mechanism

Apoptosis is a kind of programmed cell death which occurs in multicellular organisms. The German scientist Carl Vogt firstly described the apoptosis principle in 1842 [52]. In contrast to necrosis, which is an acute cell injury and always causes inflammation, apoptosis is a highly regulated and controlled process to eliminate the "unwanted" or damaged cells from multicellular organisms to prevent the release of intracellular components which can induce inflammation [53]. These apoptotic cells are shrunken, with condensed cytoplasm and pyknotic and fragmented nuclei, which are subsequently phagocytosed by other cells [54].

Like many other complex cellular processes, apoptosis is triggered by both exogenous and endogenous stimulus, including physical, chemical and biological factors [55]. Therefore, apoptotic pathways can be divided into extrinsic pathway and intrinsic pathway. In the extrinsic pathway of apoptosis, ligands bind to death receptors outside of the cell membrane, leading to trimerization of TNF receptors, which can recruit the receptor-specific adapter protein Fas-associated death domain (FADD). When the receptor is engaged, procaspase-8 will be recruited and cleaved into activated format to form the death-inducing signaling complex (DISC), which then initiates apoptosis by directly activating the executioner caspase-3 or switches to intrinsic apoptosis by cleaving Bid [56, 57]. In the extrinsic pathway of TNFα-induced apoptosis, the binding of TNFα to TNF-R1 recruits a few adaptors (for example TRADD, RIP1 and TRAF2) to form the membrane proximal complex I. Followed by this, the K-63-linked polyubiquitin chains on RIP1 and TRAF2 are cleaved by CYLD to promote the formation of complex II, also known as DISC, thus inducing apoptosis [58]. The intrinsic

(mitochondrial) pathway is activated by the potential alteration on mitochondrial membrane, resulting in the efflux of pro-apoptotic proteins into the cytoplasm. After the assembling of apoptosome by cytochrome c and Apaf-1, caspase-9 is activated and thus activates executioner caspase-3. The members of the Bcl-2 protein family are implicated in the intrinsic apoptosis pathway, playing either pro-apoptotic or anti-apoptotic roles [59].

6.3.2. NMD interacts with apoptosis

NMD can be shut down during apoptosis via caspase activity. The core NMD factors UPF1/2 are cleaved by caspases during apoptosis while, in turn, caspase-cleaved UPF fragments can promote apoptosis [60]. On the contrary, NMD also affects apoptosis. It has been reported that NMD might regulate Bax, Bcl-2, caspases-3 and PDE, and suppress N-methyl-N-nitrosourea (MNU)-induced apoptosis in rat photoreceptor cells [61]. Another study indicated that NMD could promote the timely termination of the unfolded protein response (UPR) to avoid apoptosis in response to ER stress, and that NMD also could buffer cells from an overactive UPR to avoid the unnecessary apoptosis [62]. Furthermore, *Upf1 -/-* blastocysts cells at 3.5 days post-fertilization underwent apoptosis after a short cell expansion in culture [63]. Interestingly, in human U2OS osteosarcoma cells, the depletion of another NMD factor, hSMG1, by small interfering RNA significantly increased the magnitude and rate of TNFα-induced apoptosis. However, this was not mediated by suppressing NMD, rather than by the decay of the long FLICE-inhibitory protein (FLIPL) [64].

6.4. LncRNA

6.4.1. The definition and classification of lncRNA

Long non-coding RNA is defined as a subtype of RNA where the length of the transcript is longer than 200 nt and cannot be translated into protein. The lncRNAs may have a total length of more than 100 KB and are typically expressed in a very low amount [65]. In total, protein-coding genes make up about 2% of the human genome, while about 98% of the genome is the birthplace of lncRNAs (perhaps 15,000 lncRNAs) [66, 67]. Similar to messenger RNA (mRNA), the lncRNA is transcribed by RNA polymerase II and undergoes capping, splicing and polyadenylation, leading to different isoforms from the same locus [68, 69].

Based on their genomic structure and origin, lncRNAs are divided into many different types. Many lncRNAs are overlapped with protein-coding genes. According to whether lncRNAs

overlap with protein-coding genes, lncRNAs consist of two major categories: non-overlapping and overlapping lncRNAs (Figure 6-3). The first group is non-overlapping lncRNAs, which are located and transcribed between two protein-coding genes using independent promoters; therefore, they are termed as intergenic lncRNAs (lincRNAs). Those lncRNAs that are located on the opposite strands of protein-coding genes, within 1 kB in distance, and share the same promoter with protein-coding genes are termed as bi-directional lncRNAs. The second group is overlapping lncRNAs, which are also made up of two subsets. The sense or anti-sense lncRNAs are overlapped with at least one exon of another gene and can be transcribed in any directions from the protein-coding gene. Similar to sense and anti-sense lncRNAs, the whole transcripts located between intronic regions with no overlap of the exonic sequences are classified as intronic lncRNAs.

Non-overlapping lncRNA:

Intergenic lncRNA (lincRNA)

Bi-directional lncRNA

<1Kb

Overlapping lncRNA:

Sence lncRNA

Anti-sense lncRNA

Sense intronic lncRNA

Anti-sense intronic lncRNA

Protein-coding gene   Protein-coding gene exon

LncRNA gene   LncRNA exon
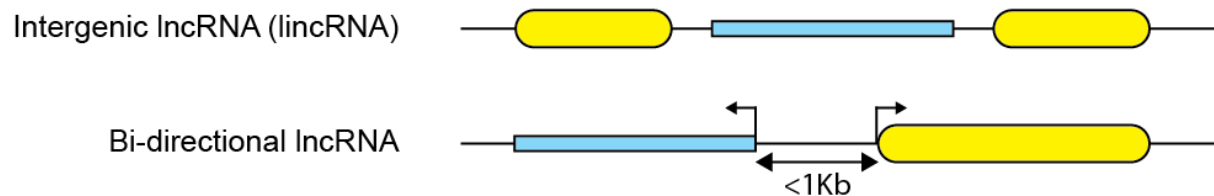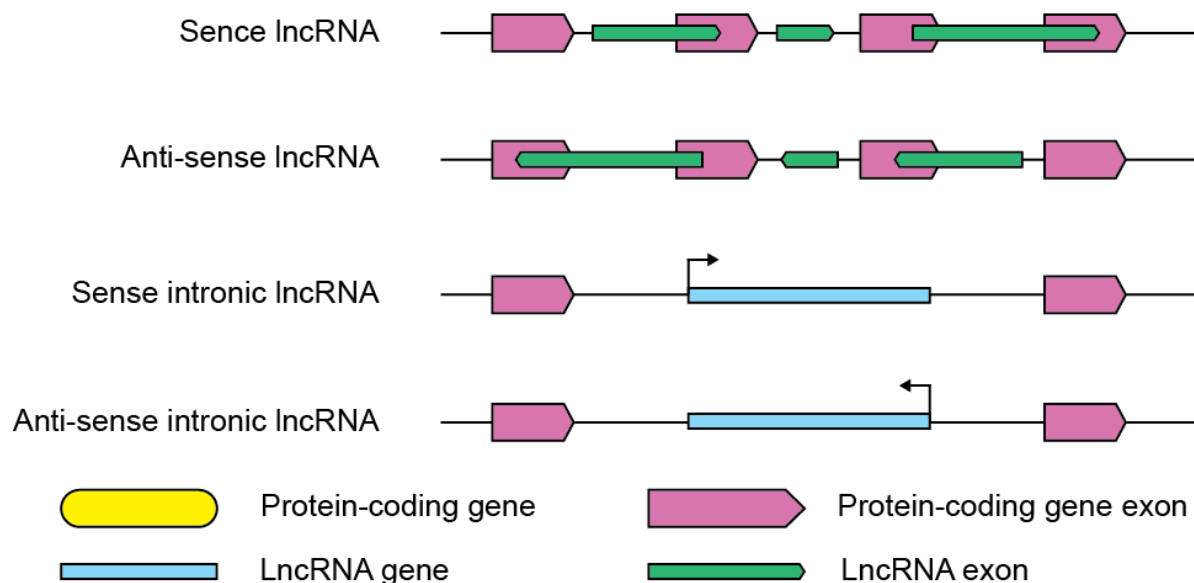
Figure 6-3. Classification of lncRNA due to the genomic location.

Based on the genomic locations and orientations, lncRNAs are divided into six categories. Intergenic lncRNAs are transcribed between two genes and do not overlap with protein-coding or any other lincRNA gene exons. Bi-directional lncRNAs are lncRNA sequences located on the opposite strand from protein-coding genes and head to head in a surrounding less than 1 kB in the distance. Sense and anti-sense lncRNAs overlap with the introns and/or exons of protein-coding genes, and the transcripts can initiate in the same or opposite direction from the protein-coding gene. Sense and anti-sense intronic lncRNAs are located between two introns of protein-coding genes in either sense or antisense orientation.

6.4.2. The function of lncRNA

In cells, lncRNAs show multiple functions in regulating gene expression as cis- or trans-regulators [70]. In *Malat1* knockout (KO) mice, many *Malat1*-adjacent genes were dysregulated, suggesting a prospective cis-regulatory function of *Malat1* [71]. The lncRNA *DLEU1* and *DLEU2* are found on chromosome band 13q14.3. DNA-demethylation of these two genes at transcriptional start sites that coincides with transcriptional dysregulations of their neighboring tumor suppressor genes in chronic lymphocytic leukemia (CLL) cells, suggesting a cis-regulatory role in this gene cluster [72]. In contrast, lncRNAs also regulate gene expressions at a distance from their transcription sites as trans-regulators. One RNA antisense purification and mass spectrometry (RAP-MS) experiment showed that lncRNA *AFAP1-AS1* is associated with more than 20 candidate proteins in vivo [73]. In lncRNA *Pnky*-deficient mice, overexpressed *Pnky* from a bacterial artificial chromosome (BAC) construct rescued the developmental phenotypes, indicating the lncRNA *Pnky* is a trans-regulatory progenitor that regulates development in mice. [74].

As reviewed in several papers, it is clear that lncRNAs are important in gene regulation (Figure 6-4), although their functions are still not fully understood. LncRNA transcripts transcribed upstream of a gene can influence their downstream genes in positive or negative ways, which is obtained by inhibiting the recruitment of RNA polymerase II or remodeling chromatin, respectively. Antisense-transcribed lncRNA can hybridize with the overlapping sense gene and inhibit the splice-site recognition, producing the alternatively spliced transcripts. The sense and antisense binding RNA complex is a resource for Dicer to generate endogenous siRNAs. It is also reported that lncRNA can act as a miRNA sponge to silence a miRNA. Additionally, lncRNA can be processed into small ncRNAs (sncRNAs). LncRNAs not only

interact with RNAs but also regulate gene expression in protein levels by modulating the activities of the partner proteins, serving as a structural component, enabling the formation of more abundant RNA-protein complexes, changing the localization of a protein within the cell and affecting epigenetic processes [75-77].
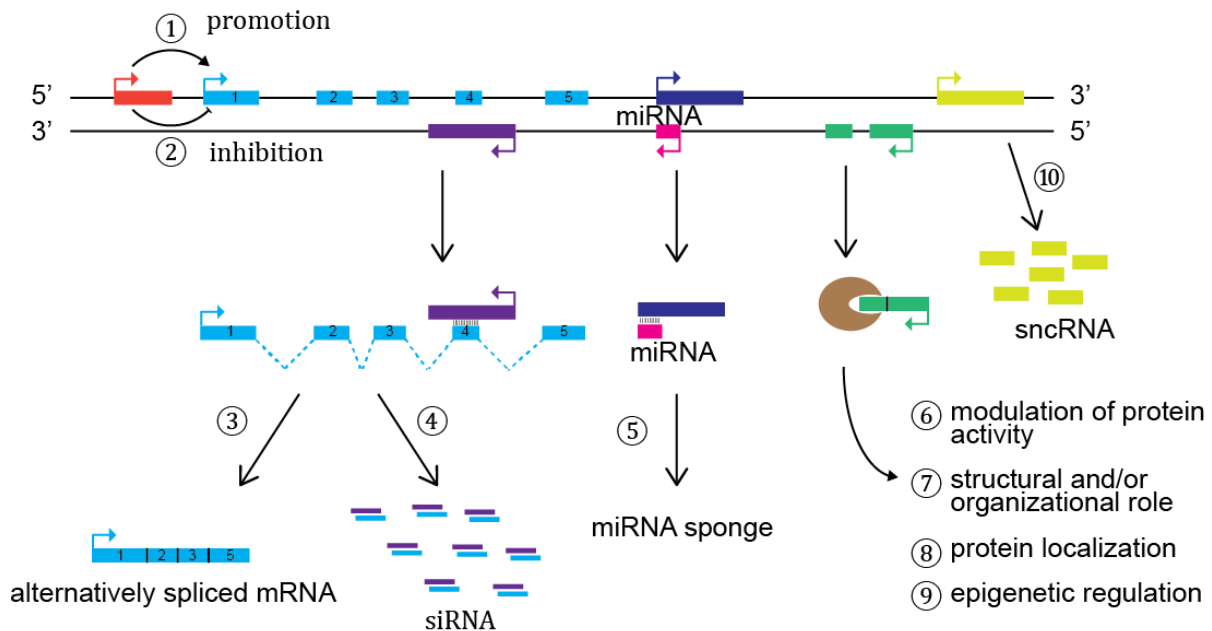
Figure 6-4. Summary of lncRNA functions.

The figure was modified from Wilusz et al. and Sana et al. [75, 76]. LncRNA upstream of a gene can either promote (1) or inhibit (2) the gene expression by inhibiting the recruitment of RNA polymerase II or remodeling chromatin, respectively. (3) The antisense lncRNA can form a dimer with the overlapping sense mRNA transcript and inhibit the splice-site recognition, producing the alternatively spliced mRNA. (4) In addition, the sense and antisense binding RNA complex is a resource for Dicer to generate endogenous siRNAs. (5) The hybridization of lncRNA and miRNA can lead to the silencing of miRNA. (6) LncRNAs are also able to bind to their partner proteins and participate in (7) cellular structural and/or organization, (8) altering the cellular localization of a protein and (9) affecting epigenetic processes. (10) Moreover, lncRNAs can be degraded into sncRNAs.

6.4.3. Dual functions of lncRNA in apoptosis

LncRNAs have dual functions (either promotion or inhibition) in response to apoptosis. One main function of lncRNAs is to induce apoptosis. For example, knockdown of lncRNA growth arrest-specific 5 (*GAS5*) diminished apoptosis in THP-1 cells under OxLDL treatment [78]. LncRNA *TUG1* is a tumor suppressor that can promote apoptosis in human glioma cells [79].

Additionally, lncRNAs are also able to inhibit apoptosis. For example, lncRNA *SNHG12* inhibits apoptosis in colorectal cancer cells [80], and lncRNA *CASC9* suppresses apoptosis in oral squamous cell carcinoma [81]. Furthermore, the same lncRNA can display different roles in different cells. For example, lncRNA *HOTAIR* can induce apoptosis in chondrocytes [82] and MCF-7 [83] cells, while inhibiting apoptosis in PANC-1 [84], nucleus pulposus [85] cells.

6.4.4. LncRNA in human diseases

As a result of this versatility, lncRNAs perform a widespread effect in human diseases, in particular, human cancer [86, 87]. A database for lncRNA–associated disease (LncRNADisease, version 1.0) showed around 480 experimentally supported lncRNAs contribute to 166 diseases, including 39.8% cancer, 10.8% cardiovascular disease and 8.4% neurodegeneration disease [88]. In 2019, LncRNADisease 2.0 was published where 19166 lncRNAs, 823 circRNAs and 529 diseases were included. Cancer still ranked the top associated disease (44.2%) followed by cardiovascular disease (11.6%) and neurodegeneration disease (7.3%) [89]. Dysregulation of lncRNAs was found in a lot of cancers, such as breast cancer [90-92], leukemia [93, 94], colorectal cancer [95, 96], liver cancer [97-99]. Lots of oncogenic-lncRNAs (onco-lncRNAs), such as *ANRIL*, *MALAT1* and *GAS5*, are increasingly being characterized as cancer-associated genes [100, 101], while others, e.g., *HOTAIR* and *H19* are used as biomarkers [102-104]. Moreover, many reports showed that lncRNAs exert impacts on cellular activities including proliferation, migration, invasion, apoptosis and cell cycle [105, 106].

6.4.5. LncRNA *Pvt1*

Plasmacytoma variant translocation 1 (*Pvt1*) was firstly reported in 1984 in mouse [107]. Soon afterwards, the human *PVT1* (homologous to *Pvt1*) was also observed in human Burkitt's lymphomas serving as a variant translocation site and in T lymphoma possessing a retroviral integration site, suggesting its involvement in carcinogenesis. Later, *PVT1* was found to be frequently upregulated and amplified in a variety of cancers [108]. *Pvt1* is a large lincRNA and spans more than 200 kb in the genome. *PVT1* is located downstream of c-myc, within the well-known cancer-related 8q24.21 chromosomal region, where is considered to be a "gene desert" as approximately two megabases of nucleotides contain only four genes [109]. *PVT1* is a well-characterized oncogene and involved in many cancers, for example, gastric cancer [110], lung cancer [111], pancreatic cancer [112], liver cancer [113], ovarian and breast cancer [114].

PVT1 is a biomarker for non-small cell lung cancer (NSCLC) diagnosis and prognosis, patients with higher *PVT1* expression experienced shorter disease-free survival (DFS) and overall survival (OS) times [115]. A similar phenomenon was also found in osteosarcoma patients, where the overexpression of *PVT1* decreased the survival time [116]. Moreover, *PVT1* serves as a sponge for many miRNAs such as *miR-195* [116], *miR-448* [117], *miR-152* [118], *miR-488-3p* [119], *miR-203* [120] and *miR-149* [121] and involves in cancer dynamic gene regulation. Interestingly, several publications mentioned *PVT1*-targeted miRNAs promote apoptosis in cancer cells [116, 122-126]. In contrast, *PVT1* encodes a group of six miRNAs, including *miR-1204*, *miR-1205*, *miR-1206*, *miR-1207-3p*, *miR-1207-5p* and *miR-1208* in human [127]. Colombo et al. also showed *PVT1* preferred to bind the mir-200 family, which under normal conditions antagonistically regulates hundreds of genes; moreover, *PVT1* showed increased expression in tumors and a high Pearson correlation with *MYC* [108].

6.5. NF-κB

6.5.1. Components and activation of NF-κB

NF-κB family proteins are inducible transcription factors that regulate an extensive array of genes involved in inflammation, immunity, cell proliferation, differentiation and survival [128]. These factors include five genes *NF-κB1* (*p50/p105*), *NF-κB2* (*p52/p100*), *RelA* (*p65*), *c-Rel* and *RelB*. They contain a Rel homology domain (RHD) and thus can mediate dimerization, interaction with their specific repressors and binding DNA. NF-κB proteins can be synthesized in a mature or precursor form. Thus they are divided into two groups: RelA, c-Rel, and RelB can directly interact with the transcription elements while NF-κB1 and NF-κB2 need to be proteolyzed by the proteasome and converted into an active format from p100 and p105 to p50 and p52 [129]. Within a cell, NF-κB forms either homo- or hetero-dimers. Rel-A, c-Rel and RelB have a trans-activation domain by which they can recruit co-activator and initiate transcription. On the contrary, p50 and p52 don't carry the trans-activation domains, so they need to form heterodimerization either with p65, cRel or RelB or with non-Rel transcription factors, including specific inhibitors of NF-κB (IκBs) proteins [130]. In quiescent cells, NF-κB stays in an inactive status due to the binding of IκBs. IκBs consist of four members, including IκBα, IκBβ, IκBε and Bcl-3, which bind to the RHD domains of NF-κB through their ankyrin repeats, resulting in NF-κB transcriptional inactivation. Interestingly, p105 and p100 also have ankyrin repeats through which they maintain their inactivity [131]. Since p105 and p100 possess the inhibition activities like IκB, they are also treated as IκB proteins [132].

6.5.2. The role of CYLD in the NF-κB pathway

As a tumor suppressor, the deubiquitinase CYLD plays an essential function in the activation of the NF-κB signaling. In complex I, polyubiquitinated RIP1 and TRAF2 recruit and activate IκB kinase (IKK) and transforming growth factor-β-activated kinase 1 (Tak1), which in turn activate NF-κB. The absence or downregulation of CYLD results in the increase of TRAF2 and RIP1 K-63 polyubiquitination, therefore, pronouncing the activation of the IKK complex [58]. IKK complex consists of NF-κB essential modulator (NEMO or IKKγ), IκB kinase α, (IKKα or IKK1) and IκB kinase β (IKKβ or IKK2) [131]. CYLD can also inhibit IKK by the removement of K-63 polyubiquitin chains from IKKγ. As a result of reduced CYLD expression, IKK activation accelerates the phosphorylation and K-48 polyubiquitination of IκB and subsequent degradation of the proteasome. Eventually, NF-κB is activated and transferred into the nucleus facilitating NF-κB-targeted genes transcription [58].

6.5.3. NF-κB regulates apoptosis by promoting anti-apoptotic genes expression

TNFα is a proinflammatory cytokine that has diverse roles in cellular events, including NF-κB activation and apoptosis. In 1996, Van et al. showed that the inhibition of NF-κB activity by blocking IκB degradation promoted TNFα-induced apoptosis in several cell lines [133]. Following this, in 1998, Van et al. showed a set of genes induced by NF-κB activation downregulated the apoptosis signal upon TNFα treatment [134], suggesting that NF-κB mediated survival. Now NF-κB is commonly accepted to be involved in apoptosis by upregulating anti-apoptotic genes. One of these genes is FLIP, which is highly homologous to caspase-8 but does not have the function of degrading proteins, therefore, it inhibits apoptosis by competing with caspase-8 for binding to DISC. The inhibitors of apoptosis (IAPs) and several Bcl-2 family proteins are also the NF-κB-targeted genes. In addition, NF-κB may disrupt p53 by upregulating anti-apoptotic genes, which results in the inhibition of p53-induced apoptosis [129].

7. The goal of this study

SMG7 is a well-known NMD factor that functions together with UPF1 to deadenylate and degrade target RNAs [43, 46]. Recently, SMG7 was also reported to interact with p53 in HCT-116 cells [48, 49] and found to be associated with prostate cancer [50]. We previously identified that knockout of *Smg7* can protect MF cells from TNFα-induced apoptosis in a genome-wide mutation screen [51]. TNFα has been shown to cause tumor cytotoxicity [135], but it also has a key function in the activation of NF-κB and inflammation. However, the mechanism of SMG7 involved in TNFα-induced extrinsic apoptosis and its tumor biology, as well as its downstream targets, are still poorly understood.

The following questions will be addressed in this dissertation:

1. Does SMG7 influence the global NMD system, and what kind of RNAs does SMG7 prefer to target?

2. What are the genes that are differentially expressed in *Smg7 -/-* MF cells? Especially in the TNFα pathway.

3. Can other NMD factor deficiency protect cells against TNFα-induced apoptosis, and what are the expression profiles of other NMD factors in *Smg7 -/-* cells?

4. Do SMG6 and UPF1 target the same cluster of RNAs and which genes do they share with *Smg7 -/-* cells?

5. What is the functional role that SMG7 plays in TNFα-induced apoptosis and its potential target genes?

6. What is the role of SMG7 in human cancer and cancer cell lines?

8. Results

8.1. *Smg7 -/-* cells are resistant to TNFα-induced apoptosis

Data in this section have been published in Molecular Oncology [136].

When stimulated by TNFα, the cells can decide either to initiate cell death by triggering apoptosis pathway or remain alive by activating the NF-κB pathway. In our previous work, we showed that *Smg7* knockout immortalized mouse fibroblasts (MF) only exhibit the protection against TNFα-induced apoptosis but not any other cell death inducers [51]. Here I re-conducted the TNFα sensitivity experiment with parental MF cells in the presence of a caspase inhibitor Z-VAD-FMK (zVAD) and observed a rescue, suggesting caspase involvement in TNFα-induced extrinsic apoptosis (Figure 8-1A). I also conducted an *Smg7* knockdown by CRISPR interference (CRISPRi) [137] in NIH 3T3 cells (*Smg7* KD) and achieved a similar result as in *Smg7 -/-* MF cells (Figure 8-1B). In both CRISPR KO and CRISPRi cases, a consistent pattern was found that cells were not sensitive to TNFα-induced apoptosis any more, possibly due to blocked signaling in TNFα-insensitive cells.
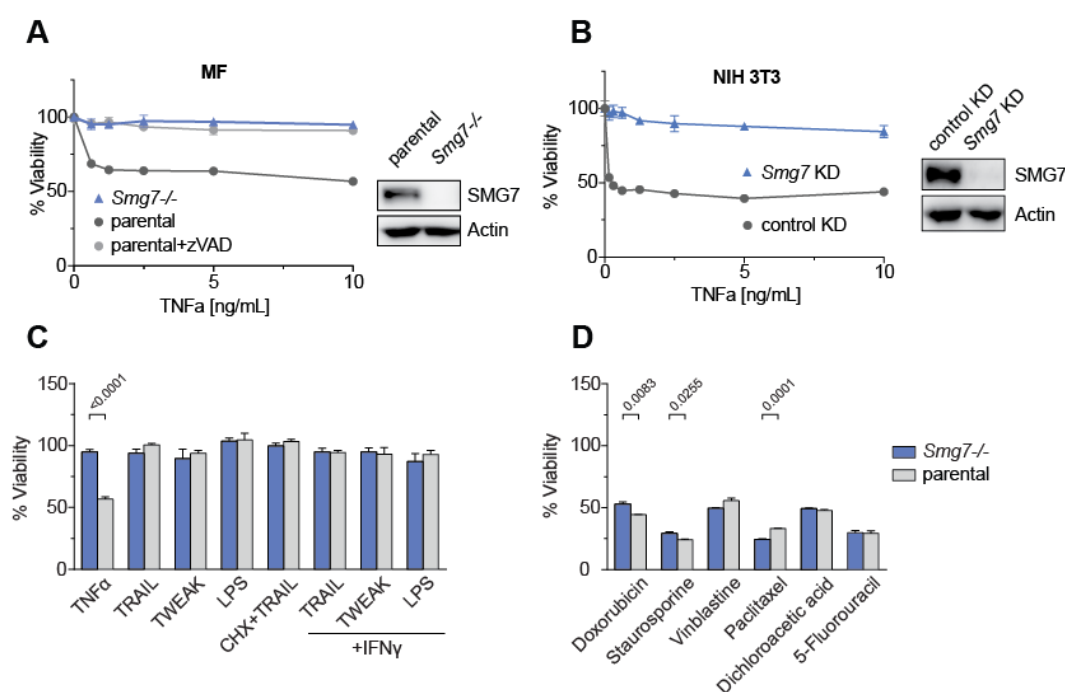
Figure 8-1. Effects of *Smg7* ablation on cell death inducers.

(**A**) TNFα dose-response curves in *Smg7 -/-* cells compared to parental MF cells (parental) with caspase inhibitor Z-VAD-FMK 10 μM (zVAD) and validation of ~127 kD protein absence by Western blot. Viability is represented as mean ± SEM of n = 4 technical replicates. The experiment was repeated independently N = 3 times with similar results and a representative example is shown. (**B**) TNFα dose-

response curves of *Smg7* CRISPRi knockdown (*Smg7* KD) compared to empty KD vector control NIH 3T3 cells (control KD). Viability data represent mean ± SEM of n = 4 technical replicates of two independent experiments. Western blot showed the *Smg7* KD efficiency. (**C**) Viability of *Smg7 -/-* compared to parental MF cells (parental) against apoptosis inducers: 10 ng/mL tumor necrosis factor (TNFα), 100 ng/mL TNF-related apoptosis-inducing ligand (TRAIL), 12.5 ng/mL TNF-like weak inducer of apoptosis (TWEAK), 10 µg/mL lipopolysaccharide (LPS), co-treatment with 20 pg/mL cycloheximide (CHX) or 20 ng/mL interferon-gamma (IFNγ). (**D**) Viability of *Smg7 -/-* compared to parental MF cells (parental) against chemotherapeutic drugs: 20 µM Doxorubicin, 2 µM Staurosporine, 0.05 µM Vinblastine, 0.4 µM Paclitaxel, 250 mM Dichloroacetic acid, 50 µM 5-Fluorouracil. Viability data (**C**, **D**) are plotted as mean ± SEM of n = 3 or 4 technical replicates. Data were analyzed by Vanessa Kraft and me. Data and figure legend were published in Molecular Oncology [136].

Next, I investigated whether SMG7 deficiency exclusively affects TNFα signaling engaged by other ligands or leads to other cell death forms. To this end, *Smg7 -/-* and parental MF cells were treated with TNF-related apoptosis-inducing ligand (TRAIL), TNF-related weak inducer of apoptosis (TWEAK) and lipopolysaccharide (LPS) separately. However, none of them can induce cell death, regardless of extra sensitization of cycloheximide (CHX) or IFNγ (Figure 8-1C). There was marginal defense against doxorubicin and staurosporine, and partial zVAD-independent cell death to paclitaxel in *Smg7 -/-* cells when treated with a group of chemotherapeutic agents (Figure 8-1D) [51]. In short, this sensitivity to TNFα-induced apoptosis in *Smg7 -/-* MF cells is inducer-dependent and functions primarily through the TNF signaling pathway.

8.2. Apoptosis-resistant *Smg7 -/-* cells upregulate non-coding RNAs

Data in this section have been published in Molecular Oncology [136].
PTC-containing transcripts and lncRNAs are the well-known targets of NMD. In order to determine the downstream effects on SMG7 ablation, four hallmark lncRNAs were picked for quantitative PCR (qPCR). In *Smg7 -/-* cells, three of the four transcripts, *Gas5, Anril* and *Hotair,* were up-regulated roughly ~2 to 6-fold, whereas *Malat1* was reduced (Figure 8-2A). A hypothesis is that these transcriptional modifications were caused by the functional redundancy in the NMD complex or as compensation for SMG7. The qPCR study of a group of core NMD factors, on the other hand, showed only slight increases in transcripts *Smg5* and *Upf3b*, indicating mild compensation (Figure 8-2B). Next, I investigated if the ablation of the same NMD factors in Figure 8-2B could also protect cells against TNFα-induced apoptosis by reanalyzing data from a TNFα pan-genomic mutagenesis screen in the same cells [51]. The

result showed only a small fraction of guides against *Smg7* and *Upf2* were observed to be enhanced, suggesting the insensitivity to the TNFα-induced apoptosis is achieved by a dedicated SMG7 mechanism instead of by global destruction of NMD (Figure 8-2C). I did not investigate UPF2 further in this study.
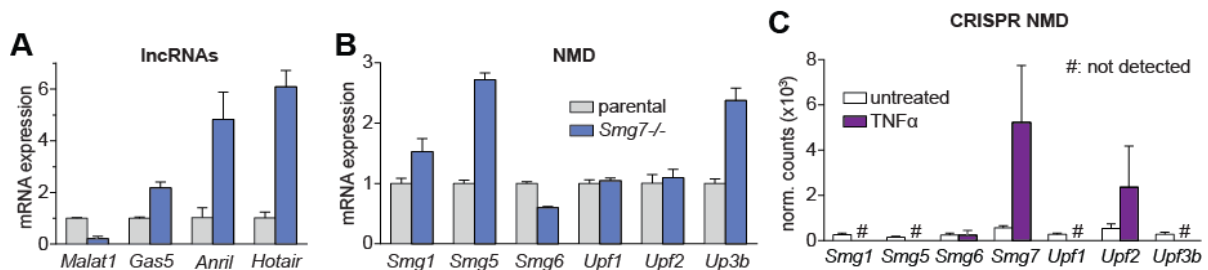
Figure 8-2. SMG7 can protect cells against TNFα.

(**A**, **B**) Gene expression analysis by qPCR of hallmark long non-coding RNA (lncRNA) targets and a panel of NMD regulators in *Smg7 -/-* relative to parental MF cells. Expression data are shown as mean ± SD of n = 3 technical replicates. Experiments were conducted by Susanne Pfeiffer and me. (**C**) Normalized read counts of NMD regulators from a pan-genomic CRISPR mutagenesis screen in MF cells after TNFα selection. Data represent mean ± SEM of n = 2-5 guides per gene according to [51]. #, not detected. Data were analyzed by Joel Schick and me. Data and figure legend were published in Molecular Oncology [136].

Next, I tested if specific groups of transcripts are impacted in *Smg7 -/-* cells using RNA sequencing. The top 100 upregulated and downregulated transcripts were collected for analyzing. The transcripts were grouped by biotype and, as expected, canonical NMD targets were the most prominent cluster (33%) among the top 100 upregulated transcripts. In specific, protein-coding genes comprised 29%, while lncRNAs and ncRNAs made up 35% of the highest upregulated transcripts (Figure 8-3A, Table 13-1). In comparison, the bulk (78%) of the top 100 downregulated transcripts were almost entirely protein-coding genes.

Remarkably, general biotype differential expression analysis indicated that the most substantially upregulated biotypes were long intergenic non-coding RNAs (lincRNA, Figure 8-3B, p(adj) ≈ 0.0000) and antisense transcripts (p(adj) = 1.84E-67), while protein-coding genes displayed just a minimal reduction (Figure 8-3B). Separate subclasses of lncRNAs, which include sense intronic, macro lncRNA and 3' overlapping ncRNA, were similarly slightly elevated. Pseudogenes are similar to functional genes and usually contain frameshifts and PTCs. In this study, pseudogenes showed a mild decrease, whereas global NMD targets only

showed a small increase (log2(FC) = 0.26) in comparison. The miRNA transcripts were reduced (log2(FC) = -0.62, p(adj) = 5.65E-22, Table 13-1), as forecast, in line with the position of the lncRNA as the miRNA sponges [13].
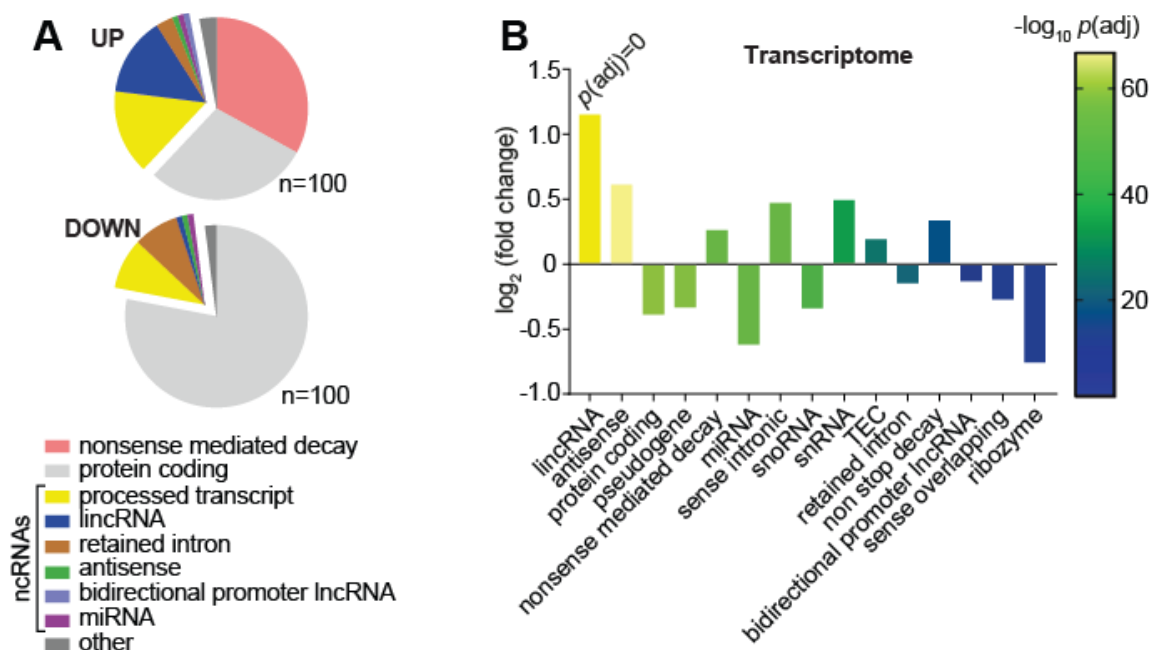
Figure 8-3. *Smg7 -/-* cells upregulate non-coding RNAs.

(**A, B**) Differential gene expression of *Smg7 -/-* compared to parental MF cells. RNA of n = 3 technical replicates were deep sequenced as 100 bp paired-end runs on an Illumina HiSeq4000 platform and gencode transcripts and significance were evaluated using DESeq2. (**A**) Biotype classification of the top 100 up- and downregulated genes. (**B**) Global analysis of differentially expressed biotypes of *Smg7 -/-* transcripts compared to parental, evaluated by log2 fold change and significance. ncRNAs, non-coding RNAs, p(adj), p-value adjusted for multiple hypothesis testing. See text for additional abbreviations. Data and figure legend were published in Molecular Oncology [136]

Gene set enrichment study was conducted in *Smg7 -/-* cells by using top 100 up- and down-regulated genes showing the characteristics of cancer pathway and reduction of apoptotic genes (Figure 8-4). I have also conducted a proteomic study in *Smg7 -/-* cells and found elevated expression of cytokine response factors (such as Mgst3) as well as caspase-1 (Figure 8-5). In *Smg7 -/-* cells, proteins that negatively control viruses have also been identified, potentially as a result of unorthodox transcription.

	Gene Set Name	Description	*p*-value	FDR
Upregulated	MLL-AF4 fusion targets	Specific signature shared by cells expressing AF4-MLL alone and those expressing both AF4-MLL and MLL-AF4 fusion proteins.	2.61E-09	5.90E-05
	Matrisome	Ensemble of genes encoding extracellular matrix and extracellular matrix-associated proteins	8.65E-08	9.77E-04
	Prostate cancer	Genes up-regulated in prostate cancer samples from African-American patients compared to those from the European-American patients.	6.12E-07	4.61E-03
Downregulated	Apoptosis by serum deprivation	Genes up-regulated in ME-A cells (breast cancer) undergoing apoptosis upon serum starvation	9.47E-11	1.16E-06
	Stem cell	Genes up-regulated in freshly isolated CD31- (stromal stem cells from adipose tissue) versus the CD31+ (non-stem) counterparts.	5.18E-10	3.19E-06
	Stem cell cultured vs fresh	Genes up-regulated in cultured stromal stem cells from adipose tissue, compared to the freshly isolated cells.	2.14E-09	8.01E-06

Figure 8-4. Gene Set Enrichment Analysis in *Smg7 -/-* cells.

Top identified clusters identified using top 100 up-/down-regulated genes in *Smg7 -/-* cells relative to parental cells detected in triplicate RNAseq samples. Gene set enrichment analysis was performed by Joel Schick and me. Data and figure legend were published in Molecular Oncology [136].

Pseudogenes are mRNAs containing PTCs that target them for NMD degradation; thus, they are predicted to be increased [138]. Conversely, in *Smg7 -/-* cells, the global analysis result showed that pseudogene transcripts were decreased (log2(FC) = -0.33, Figure 8-3B). Taken together, the findings indicate that SMG7 prefers to degrade processed transcripts including the lncRNAs than PTC-containing RNAs. Moreover, as seen in section 8.7, SMG7 selectively targets individual lncRNAs for degradation.

Figure 8-5. Quantitative mass spectrometry analysis of *Smg7 -/-* cells.

(**A**) The log$_2$ of the normalized protein abundance ratios between *Smg7 -/-* and parental cells and the -log$_{10}$ of corresponding *p*-values were plotted in a volcano plot. Proteins quantified by at least two unique peptides from three replicate samples were used in this analysis. Proteins being significantly ($p < 0.05$) more abundant in *Smg7 -/-* are given in yellow and less abundant in *Smg7 -/-* are given in blue (with a fold-change cut-off of 2-fold). Data and figure legend were published in Molecular Oncology [136]. (**B**) Proteins quantified by at least 2 unique peptides and showing a significant ($p < 0.05$) and at least 2-fold difference in their abundance between *Smg7 -/-* and parental were used for network generation using Genomatix GePX (evidence filter "function word level"). Unconnected proteins were deleted. Yellow,

more abundant in *Smg7 -/-*; blue, less abundant in *Smg7 -/-*. Experiments were conducted by Juliane Merl-Pham and me.

8.3.   *Smg6* KO and *Upf1* KD upregulate lincRNA and miRNA, respectively

To better understand which transcripts NMD targets, I performed the same global biotype analysis using *Smg6* KO and *Upf1* KD transcriptome data. RNAseq data for *Upf1* KD and *Smg6* KO were download from Sequence Read Archive (SRA, accession number: PRJNA548061, mouse C2C12 cells, PRJNA215086, mouse ES cells [139]). The results in Table 8-1 showed that protein-coding transcripts made 60% or 29% of the top 100 upregulated transcripts in *Smg6* KO or *Upf1* KD samples. 16% and 8% of transcripts were subject to NMD (Figure 8-6A, B and Table 8-1). Moreover, 24% and 47% were non-coding transcripts in *Smg6* KO or *Upf1* KD samples, respectively (Figure 8-6A, B, Table 8-1). In the top 100 downregulated transcripts, most of them were protein-coding transcripts (82% in *Smg6* KO and 58% in *Upf1* KD samples, Figure 8-6C, D, Table 8-2). 3% and 8% of transcripts belong to nonsense-mediated decay (Table 8-2). Furthermore, ncRNAs were much less in the *Smg6* KO group compared to the *Upf1* KD group within the top 100 downregulated genes (10% vs. 33%).

Table 8-1. Top 100 up-regulated transcripts in *Smg6*, *Upf1* and *Smg7*-deficient cells.

Biotypes	*Smg6*	*Upf1* (%)	*Smg7* (%)
protein_coding	60	29	29
nonsense_mediated_decay	16	8	33
retained_intron	11	21	3
processed_transcript	10	12	15
lincRNA	1	5	14
antisense	1	1	1
sense_intronic	0	1	0
miRNA	0	4	1
misc_RNA	0	1	0
ribozyme	0	2	0
pseudogene	0	2	2
bidirectional promoter lncRNA	0	0	1
snRNA	1	0	0
TEC	0	14	1

Table 8-2. Top 100 down-regulated transcripts in *Smg6, Upf1* and *Smg7*-deficient cells.

Biotypes	*Smg6* (%)	*Upf1* (%)	*Smg7* (%)
protein_coding	82	58	78
processed_transcript	3	13	9
lincRNA	1	0	1
retained_intron	4	17	8
antisense	2	3	1
nonsense_mediated_decay	3	8	0
miRNA	0	0	1
IG gene	0	0	1
pseudogene	5	1	1
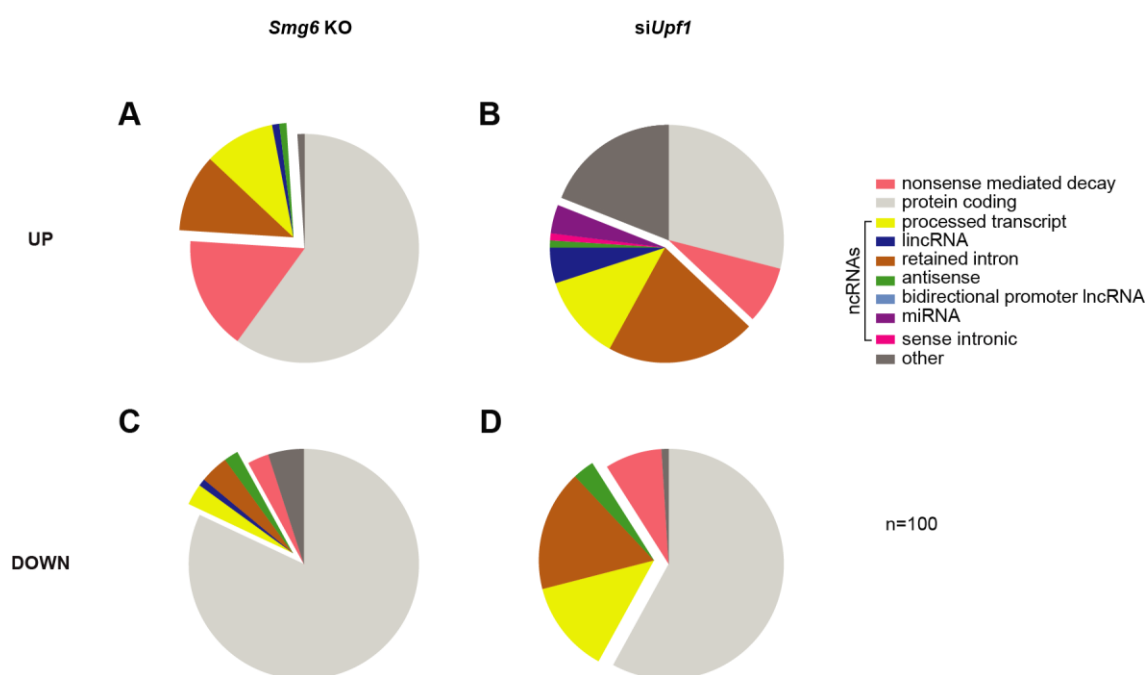
Figure 8-6. Top 100 up- and downregulated transcripts in *Smg6* KO and *Upf1* KD cells.

Mouse *Smg6* KO and *Upf1* KD RNAseq data were downloaded from SRA (accession number: PRJNA215086, PRJNA548061). RNA of n = 2 and 3 technical replicates were deeply sequenced and transcripts of gencode and significance were analyzed by DESeq2. Differential gene expression of *Smg6* KO and *Upf1* KD cells were compared to control cells. (**A-D**) Classification of the top 100 up- and downregulated genes by biotype.
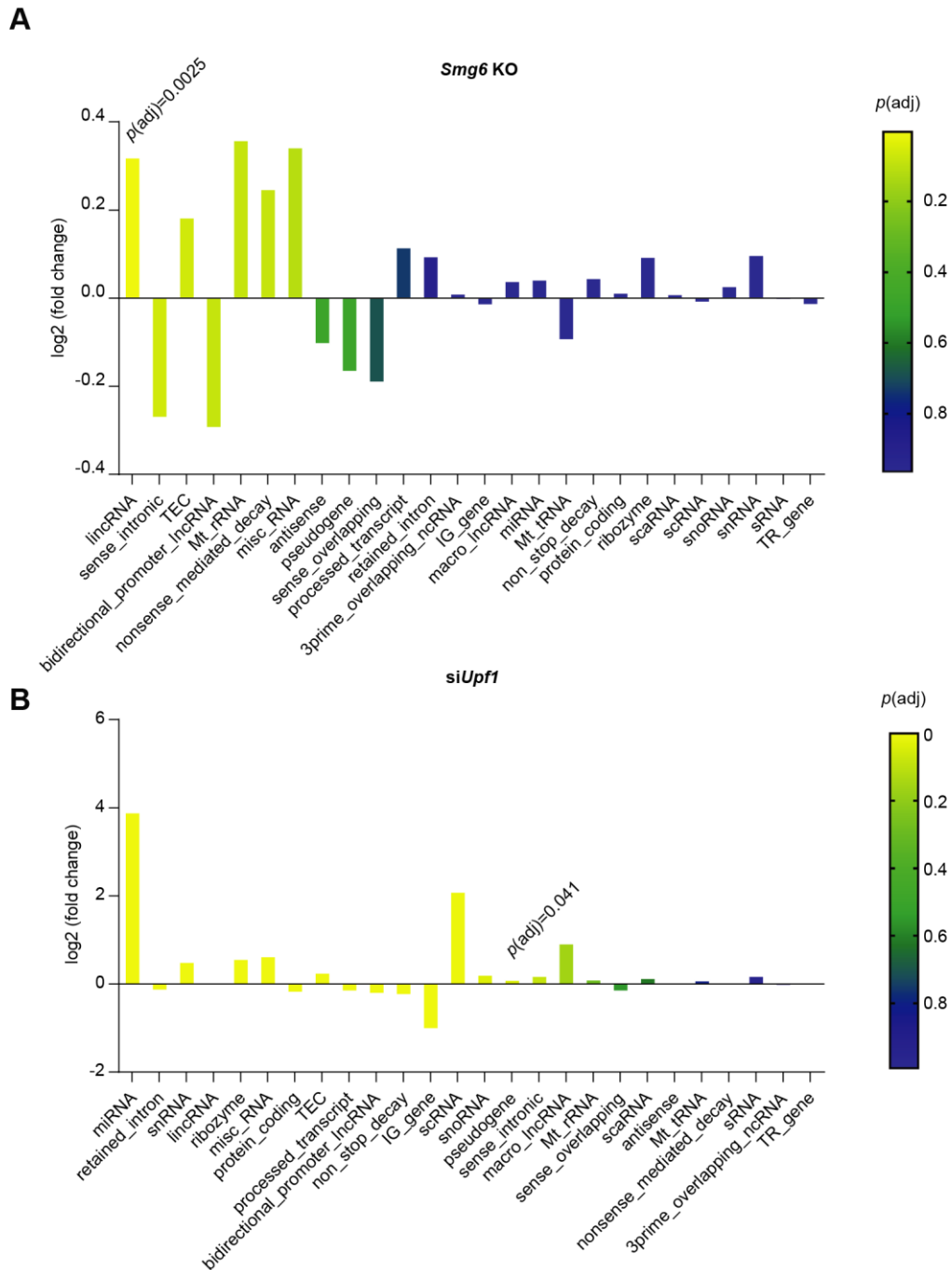
Figure 8-7. *Smg6* KO and *Upf1* KD upregulate lincRNA and miRNA, respectively.

Mouse *Smg6* KO and *Upf1* KD RNAseq data were downloaded from SRA (accession number: PRJNA215086, PRJNA548061). RNA of n = 2 and 3 technical replicates were deeply sequenced and transcripts of gencode and significance were analyzed by DESeq2. Global analysis of differentially expressed biotypes of *Smg6* KO (**A**) and *Upf1* KD (**B**) transcripts compared to control were analyzed by log$_2$ fold change and significance.

Interestingly, global differential expression analysis revealed lincRNAs were significantly upregulated in the *Smg6* KO group (p(adj) = 0.0025, Figure 8-7A, Table 13-2), which is similar to *Smg7 -/-* where the significantly upregulated biotype was lincRNA. Nonsense-mediated decay transcripts also increased slightly (log2(FC) = 0.25), while protein-coding genes almost remained unchanged (log2(FC) = 0.010, Figure 8-7A). Strikingly, microRNAs (miRNAs) were highly upregulated (log2(FC) = 3.87, p(adj) ≈ 0.0000, Figure 8-7B) in *Upf1* KD samples. However, lincRNA which was significantly upregulated in *Smg7 -/-* and *Smg6* KO samples, slightly downregulated in *Upf1* KD samples by 0.91-fold. Protein-coding transcripts showed a slight decrease with 0.89-fold in *Upf1* KD cells (Figure 8-7B, Table 13-3).

8.4. *Smg7 -/-* cells share upregulated ncRNAs with *Smg6* KO and *Upf1* KD cells

SMG7, SMG6, and UPF1 are three well-known factors involved in the NMD system. SMG7 and SMG6 are responsible for RNA degrading through different mechanisms, while UPF1 is the core factor for NMD-targeted RNAs recognition. Therefore, it will be interesting to identify the genes which are targeted by these three proteins. I analyzed RNAseq data of these three genes in wt and KO or KD mouse cell lines. *Smg7 -/-* and *Smg6* KO cells had more identified genes with p(adj) < 0.05 compared to *Upf1* KD cell lines, which may be due to the inefficient gene silencing by siRNA in *Upf1* KD samples (Table 8-3). Additionally, *Smg6* KO samples showed more upregulated genes compared to downregulated genes by 1.58-fold (Table 8-3). The DEseq2 analysis showed that they shared only 9 common genes in the top 1000 upregulated gene list (Figure 8-8A). Among these 9 genes, 6 of them were lncRNAs (processed transcript *Zfas1*, *2410006H16Rik* and *Snhg16* are also predicted as lncRNAs, Figure 8-8B). Surprisingly, most of these frequently up-regulated genes have been implicated in cancer and apoptosis. The small nucleolar RNA host gene 12 (*SNHG12*) inhibited cell apoptosis in colorectal cancer cells and promoted tumorigenesis and metastasis in hepatocellular carcinoma [80, 140]. *SNHG6,* as a biomarker for hepatocellular carcinoma (HCC), was overexpressed in HCC tissues and hepatoma cell lines and promoted HCC progression [141, 142]. LncRNA *SNHG16* was identified as an oncogene and served as a sponge for mir-4518 [143]. LncRNA *ZFAS1* was found to be increased in multiple cancers and contributed to cancer development and progression [144]. *LncRNA241* (*2410006H16Rik*) was reported to inhibit 1,2-Dichloroethane-induced hepatic apoptosis [145]. *DDIT3* was important within lung cancer cells for endoplasmic reticulum stress-induced apoptosis [146]. Moreover, *PVT1* is a well-characterized oncogene involved in many cancers [110-114].

Table 8-3. Quantified significant genes calculated by DESeq2.

condition	p-adj < 0.05	up	down	ratio
Smg7	11950	5801	6149	0.94
Smg6	6846	4196	2650	1.58
Upf1	5725	2762	2963	0.93

A
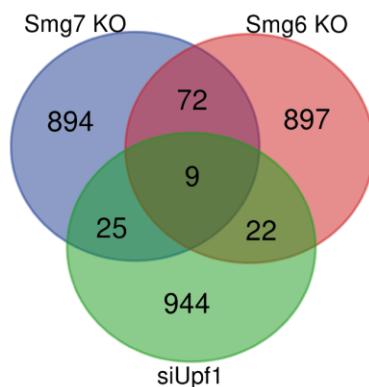
B

Gene name	Biotype
Snhg12	lincRNA
Ddit3	protein coding
Zfas1	lncRNA
Rasgrf2	protein coding
Pvt1	lincRNA
Gm42546	TEC
2410006H16Rik	lncRNA
Snhg6	lincRNA
Snhg16	lncRNA

C
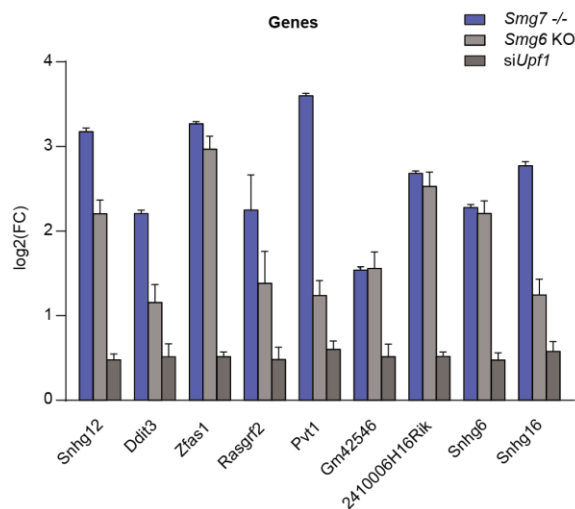
D
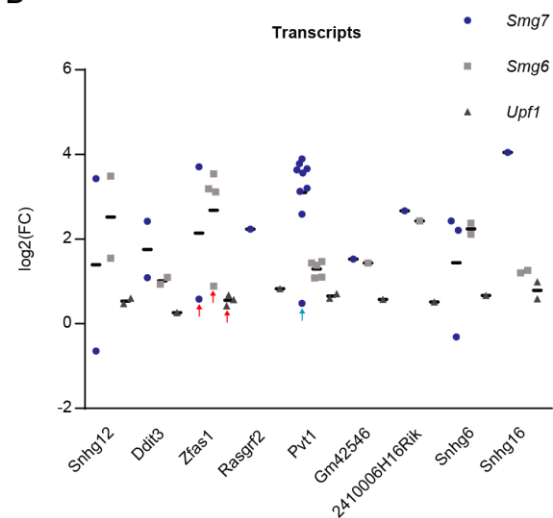
Figure 8-8. NMD factor-deficient cells share upregulated lncRNAs.

(**A**) Top 1000 upregulated genes in three NMD factor-deficient cell lines were selected to generate the Venn diagram (http://bioinformatics.psb.ugent.be/webtools/Venn/). 9 common genes intersected into a subcluster. (**B**) Biotypes of 9 common genes. 6 out of 9 turned out to be lncRNAs. Processed transcript *Zfas1*, *2410006H16Rik* and *Snhg16* are also predicted as lncRNAs. Biotypes were annotated at bioDBnet using db2db function (https://biodbnet-abcc.ncifcrf.gov/db/db2db.php#biodb). (**C**) Relative mRNA expression levels of 9 common genes. Data are shown as mean ± SD. (**D**) Relative expression

levels of individual spliced variants in 9 common genes. The red arrow indicates *Zfas1-201* and the blue arrow indicates *Pvt1-202*.

Next, I analyzed the expression levels of the 9 common genes and their spliced variant transcripts under three conditions (*Smg7* KO, *Smg6* KO and *Upf1* KD, Figure 8-8C, D). Gene expressions in *Smg7* KO cell lines had a dominant upregulation profile. Especially for *Pvt1*, which had the highest expression (log2(FC) = 3.60, p(adj) ≈ 0, Figure 8-8C, Table 13-4) among all of these 9 genes. Except for *Gm42546*, all of the expression showed high upregulation levels higher than 4-fold in *Smg7 -/-* cells (Figure 8-8C, Table 13-4). In *Smg6* KO cells, *Zfas1* showed the highest expression level with a log2(FC) = 2.97, and all expression levels were higher than 2-fold. Interestingly, gene expression levels in *Upf1* KD cells did not show an evident upregulation, in contrast, all of the upregulation levels were less than 1.52-fold (log2(FC) = 0.60, Figure 8-8C, Table 13-4). This may occur due to the inefficient KD by siRNA or UPF1 regulates different genes via a specific mechanism. Moreover, I tested if all of the spliced transcripts of these 9 genes were equally affected by NMD factors KO or KD (Figure 8-8D, Table 13-5). Therefore, I analyzed all of the spliced transcripts whose expression levels were significant with p(adj) < 0.05 (Table 13-5). As shown in Figure 8-8D, the expressions of spliced transcripts were varied compared to gene expression, indicating NMD factors modulate specific transcripts other than the whole gene. Even though gene expression levels were upregulated, the specific transcript expression levels can be downregulated (*Snhg12-207* and *Snhg6-205* in *Smg7* KO cells, Figure 8-8D, Table 13-5). NMD can target alternative spliced RNAs. Hansen et al. showed that NMD has a distinct impact on various alternative isoforms and preferentially degrades alternative spliced transcripts with longer 3′ UTRs in *Drosophila* [147]. In our case, for example, *Pvt1-202* and *Zfas1-201* showed lower upregulation levels, which may be due to specific alternative spliced RNAs losing their NMD-targeting features. Thus, these isoforms (transcripts) escaped the degradation by NMD (Figure 8-9).
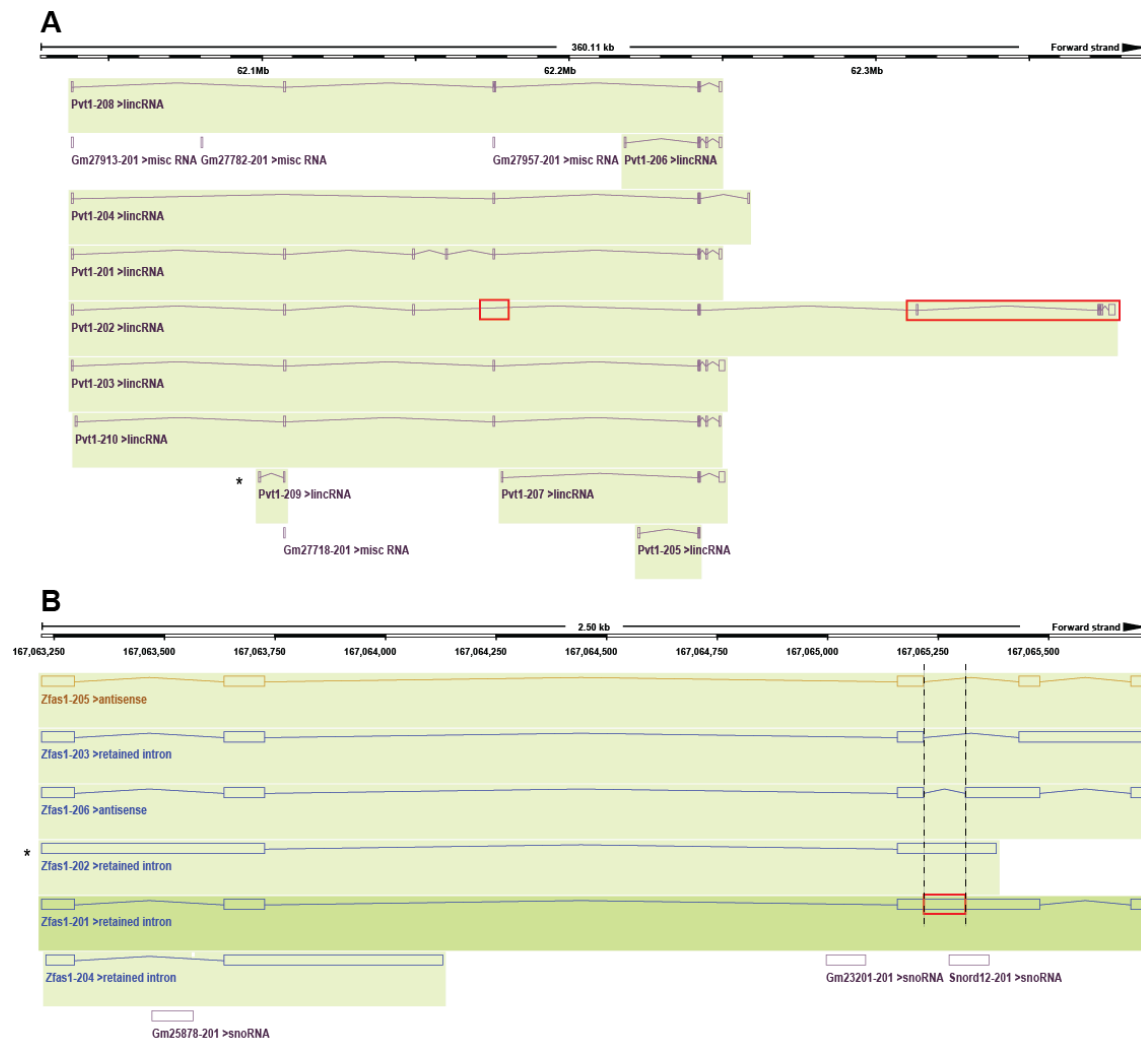
Figure 8-9. Transcript structures overview of lncRNA *Pvt1* and *Zfas1*.

Different transcript structures of lncRNA *Pvt1* (**A**) and *Zfas1* (**B**) were downloaded from the Ensembl Genome Browser. *Pvt1-202* and *Zfas1-201* had relatively lower upregulation levels. Red boxes labeled the unique parts which may be the potential targeting sites by NMD factors. * indicates undetected transcripts in this analysis.

8.5. *Smg7 -/-* cells show decreased caspase activity and CYLD levels

Data in this section have been published in Molecular Oncology [136].

When the death-inducing ligands bind to the death receptors, the DISC is built at the membrane, which executes extrinsic apoptosis by activating caspases. I first tested the caspase-8 and 3 activities utilizing a luminescence assay to evaluate where the SMG7 works in TNFα signaling pathway. The results showed that caspase-8, and more notably, caspase-3 activity was sharply decreased in *Smg7 -/-* cells treated with 20 ng/mL TNFα (Figure 8-10A).

A similar result was observed by Western blot in a TNFα timecourse condition. Pro-caspase-8 was largely degraded into the active form and cleaved caspase-3 was also increased in parental cells. In contrast, *Smg7 -/-* cells showed significantly less cleaved caspase-8 and -3 (Figure 8-10B).
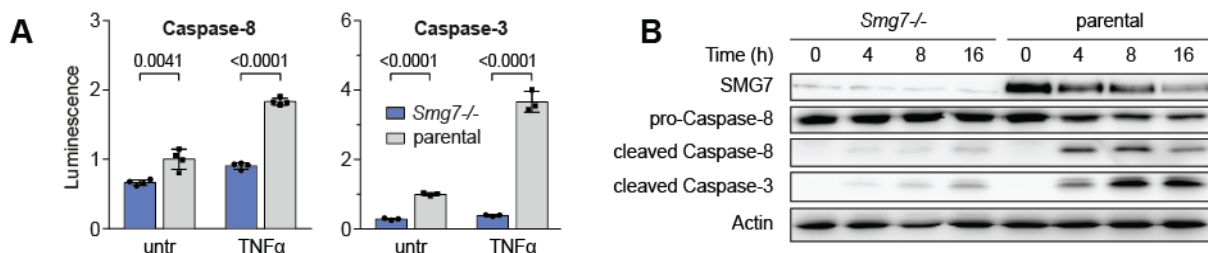
Figure 8-10. *Smg7 -/-* blocks caspases-8 and -3 activities.

(**A**) Caspase-8 and caspase-3 activity in *Smg7 -/-* cells compared to parental MF cells in untreated (untr) conditions and after 20 ng/mL TNFα treatment for 8 h. Luminescence intensity in arbitrary units is shown as mean ± SD of n = 3 or 4 technical replicates. The experiment was repeated independently N = 2 times with similar outcomes. (**B**) pro- and cleaved caspase-8 and caspase-3 proteins Western blot in *Smg7 -/-* and parental MF cells after 20 ng/mL TNFα treatment at indicated time points. ACTIN was served as the loading control. Data and figure legend were published in Molecular Oncology [136].

In the view of decreased caspase activity, I suspected that SMG7 had to function on- or upstream of caspase-8 and 3. I next checked TNFα signaling receptors TNFR1 and -2, however the protein expression levels did not explain the inhibition of apoptosis (Figure 8-11A). The receptor-interacting serine/threonine-protein kinase 1 (RIPK1) and TNF receptor-associated factor 2 (TRAF2) also remained the same. CYLD deubiquitinase, however, demonstrated a marked decline in basal levels in *Smg7 -/-* cells (Figure 8-11A).

CYLD serves as an intermediate for cell death and survival pathways. Less CYLD expression accelerates IκB phosphorylation and promotes NF-κB transfer into the nucleus. Therefore, IκB was phosphorylated as p-IκB in *Smg7 -/-* cells, indicating NF-κB pathway activation (Figure 8-11A).
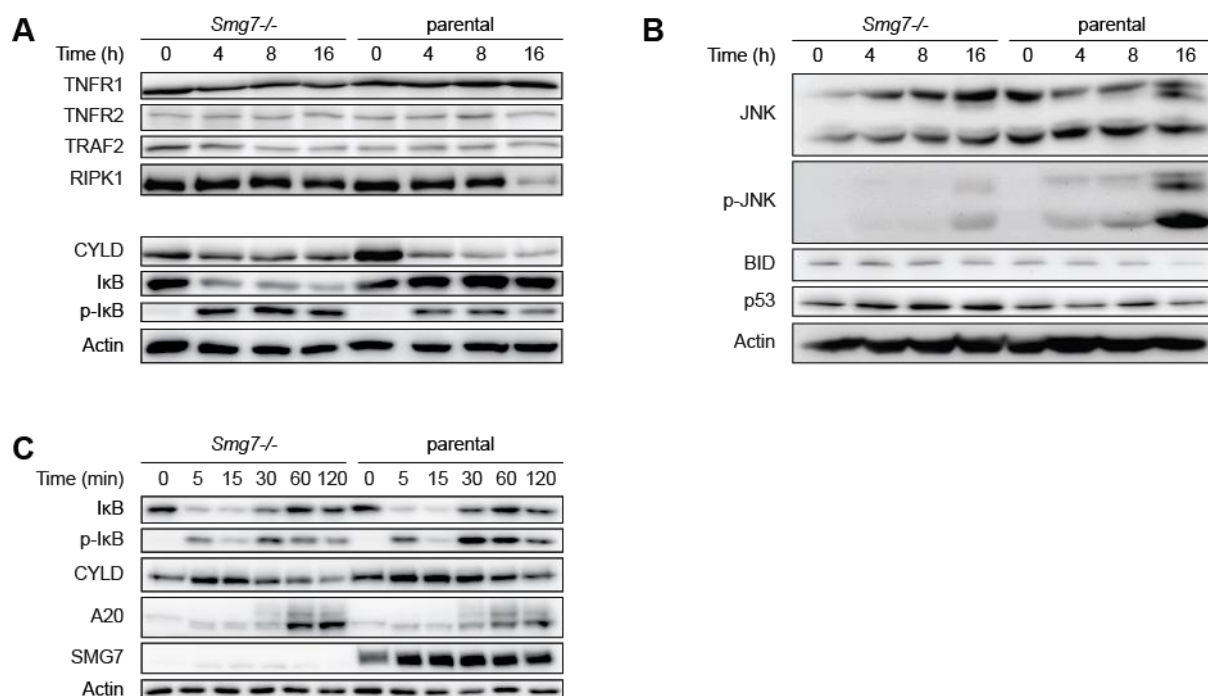
Figure 8-11. *Smg7 -/-* induces p-IκB and blocks p-JNK.

TNFα pathway-related expression levels determined by Western blot in *Smg7 -/-* and parental MF cells after 20 ng/mL TNFα treatment at indicated time points. Western blots were divided into 3 groups: (**A**), TNF-receptor and NF-κB related proteins, (**B**), mitochondrial apoptosis-associated proteins. (**C**), short interval TNFα treatment of NF-κB proteins. ACTIN was served as the loading control. Data and figure legend were published in Molecular Oncology [136].

In parental cells, the active format of Jun-kinase (phospho-JNK) was increased [148], while other mitochondrial apoptotic effectors like p53 and BID stayed unchanged in *Smg7 -/-* cells (Figure 8-11B). In conclusion, these results showed that SMG7 involves the sensitization of cells to TNFα-induced apoptosis in the upstream of JNK/caspases but downstream of the TNF receptors.

CYLD is a well-known tumor suppressor which can directly deubiquitinate K63 chains downstream of TNF receptors. Downregulation of CYLD results in the activation of the NF-κB survival pathway [149]. Therefore, I detected the NF-κB signal by checking IκB under TNFα condition. The result showed that the classical activation-feedback and inhibition-activation responses were unaffected in *Smg7 -/-* cells treated with TNFα (Figure 8-11C), suggesting the receptor protein can still transmit the signal frequently. Moreover, NF-κB inducible effector A20 was sharply increased in *Smg7 -/-* cells.
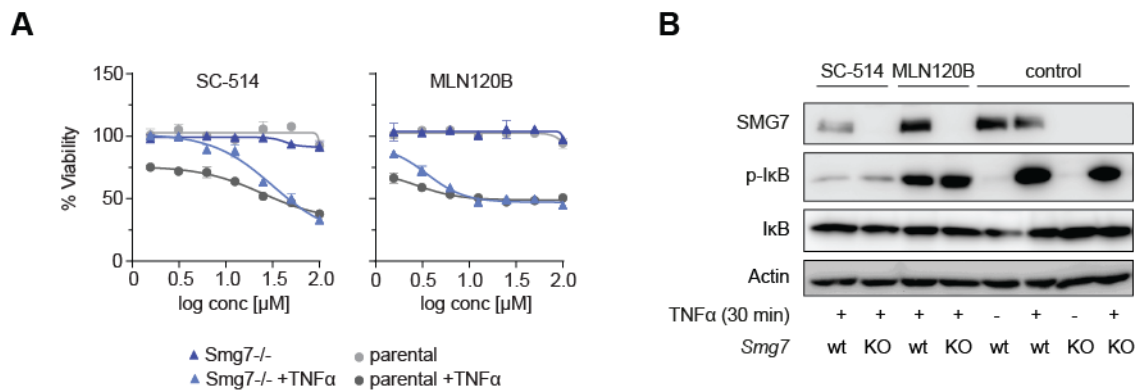
Figure 8-12. IKKβ inhibitors SC-514 and MLN120B sensitize cells to apoptosis.

(**A**) Dose-response curves of IKK inhibitors SC-514 or MLN120B in *Smg7 -/-* compared to parental MF cells. Cells were pre-treated with IKK inhibitors for 2 h followed by 20 ng/mL TNFα addition for 36 h. Viability is represented as mean ± SEM of n = 3 technical replicates. The experiment was conducted by Vanessa Kraft and me. Data and figure legend were published in Molecular Oncology [136]. (**B**) Corresponding Western blots to examine the IKK inhibitors' efficiency. *Smg7 -/-* and parental MF cells were pre-treated with IKK inhibitors (MLN120B, 30 µM, SC-514, 60 µM) for 2 h accompanied by 30 min TNFα treatment. ACTIN was served as the loading control.

As TNFα can induce NF-κB activation in both *Smg7 -/-* and parental cells, however it remains unclear whether NF-κB can rescue *Smg7 -/-* cells. Therefore, pharmacological IKK inhibitors SC-514 and MLN120B were used to block NF-κB, and then the cell viabilities were checked under TNFα treatment (Figure 8-12A). As shown in Figure 8-12B, TNFα could induce the phosphorylation of IκB in both *Smg7 -/-* and parental cells and IKKβ inhibitors (SC-514 and MLN120B) could block the phosphorylation of IκB (Figure 8-12B). Cell viability was sharply decreased when treated with TNFα in the condition of IKKβ inhibitors. Interestingly, in order to reach similar degrees of cell death, *Smg7 -/-* cells often needs higher concentrations of both inhibitors compared to parental cells (Figure 8-12A). Thus, I conclude that CYLD/NF-κB mediates the resistance of TNFα-induced apoptosis in *Smg7 -/-* cells.

8.6. CYLD and SMG7 coordinate apoptosis sensitivity

Data in this section have been published in Molecular Oncology [136].
As shown in Figure 8-11A, CYLD expression was decreased in *Smg7 -/-* cells. I want to know if this is a universal phenomenon that also exists in other cell lines. Therefore, I tested this relationship in other cell types. One mouse cell line NIH 3T3 and one human breast cancer

cell line MCF-7 were chosen for further analysis. SMG7 knockdown by siRNA (siSmg7) in these two cell lines restored viability upon TNFα treatment (Figure 8-13). Strikingly, CYLD proteins also significantly decreased correspondingly to SMG7 KD. These data suggest a conservational relationship between SMG7 and CYLD (Figure 8-13).
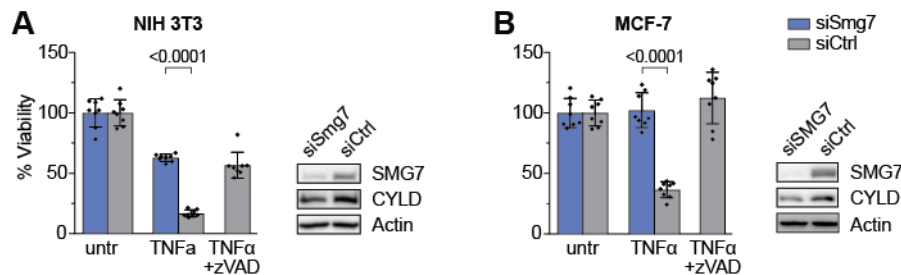
Figure 8-13. *SMG7* KD rescues cells from apoptosis and reduces CYLD.

Viability of siRNA-mediated *Smg7* knockdown (siSmg7) compared to control siRNA (siCtrl) in NIH 3T3 (**A**) and human MCF-7 cells (**B**) exposed to 10 ng/mL TNFα with 10 µM Z-VAD-FMK (zVAD) control. Western blots of SMG7 knockdown efficiency and CYLD expression. Viability data are represented as mean ± SD of n = 8 technical replicates of at least N = 2 independent repetitions with similar outcomes. untr, untreated. Data and figure legend were published in Molecular Oncology [136].

CYLD showed a diminished expression level in both *Smg7* KO and KD cells. I supposed that ectopic overexpression of *Cyld* (*Cyld* OE) might restore TNFα-sensitivity in *Smg7 -/-* cells. As shown in Figure 8-14A, *Cyld* overexpressing *Smg7 -/-* cells were partially re-sensitized compared to control empty vector *Smg7 -/-* cells, while *Cyld* siRNA knockdown (siCyld) showed partially increasing cell viability in response to TNFα-induced apoptosis (Figure 8-14B). The above data suggest that CYLD expression levels are qualified by SMG7 and CYLD expression directly influences apoptosis sensitivity.
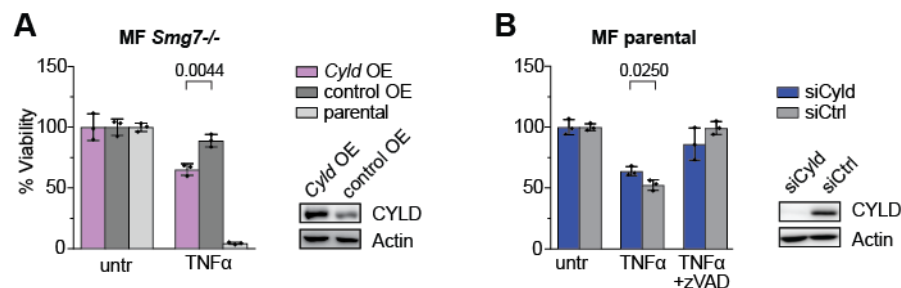
Figure 8-14. CYLD controls apoptosis in MF cells.

(**A**) Viability of *Cyld* overexpression (*Cyld* OE) compared to empty vector control (control OE) in *Smg7 -/-* MF cells or parental MF cells treated with 5 ng/mL TNFα. (**B**) Viability of siRNA *Cyld* knockdown (siCyld) compared to control (siCtrl) in parental MF cells exposed to 10 ng/mL TNFα with 10 μM zVAD control. Western blots of CYLD overexpression and knockdown efficiency. Viability data are represented as mean ± SD of n = 3 technical replicates. untr, untreated. Data and figure legend were published in Molecular Oncology [136].

In order to investigate whether the relationship is universal, we evaluated the expression levels of *CYLD* and *SMG7* in 1164 human cancer cell lines [150] acquired from The Cancer Genome Atlas. Strikingly, *CYLD* expression showed a comprehensive positive correlation with *SMG7*. The strongest Pearson correlations were detected in soft tissue (R = 0.65, Figure 8-15), multiple myeloma (R = 0.58), rhabdoid (R = 0.605), upper aerodigestive (R = 0.397) and gastric cancers (R = 0.407).
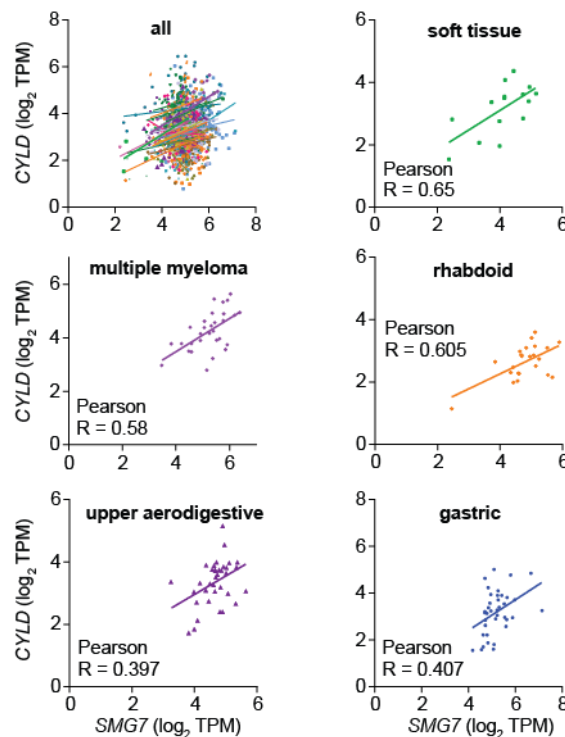
Figure 8-15. *SMG7* shows a positive relationship with *CYLD* in cancer lines.

The relationship between *CYLD* and *SMG7* expression levels in 1164 human cancer cell lines in the CCLE database determines by linear regression. Data were acquired from The Cancer Genome Atlas (TCGA). Selected cell lines with indicated tissue of origin and a high degree of association by Pearson's

R-value are shown. TPM, transcripts per million. Data were analyzed by Joel Schick and me. Data and figure legend were published in Molecular Oncology [136].

A moderate association (R = 0.41) was found between *CYLD* and *SMG7* in primary renal cell carcinoma samples (Figure 8-16A) [151]. RCC cells are susceptible to TNF-family induced apoptosis [152, 153], and TNF alpha levels are considered a prognostic marker for RCC progression. Therefore, refractory, or NF-κB activating tumors may be indicated by higher TNFα levels. This result was consistent with a Kaplan-Meier plot study between the expression level of *SMG7* and survival in 516 KIRC-TCGA (The Cancer Genome Atlas Kidney Renal Clear Cell Carcinoma) patients. The elevated *SMG7* expression has a strong correlation with survival rate (p(HR) = 0.00022, Figure 8-16B), indicating cancers with higher *SMG7* expression may undergo apoptosis and thus, increase the patients' survival rates.
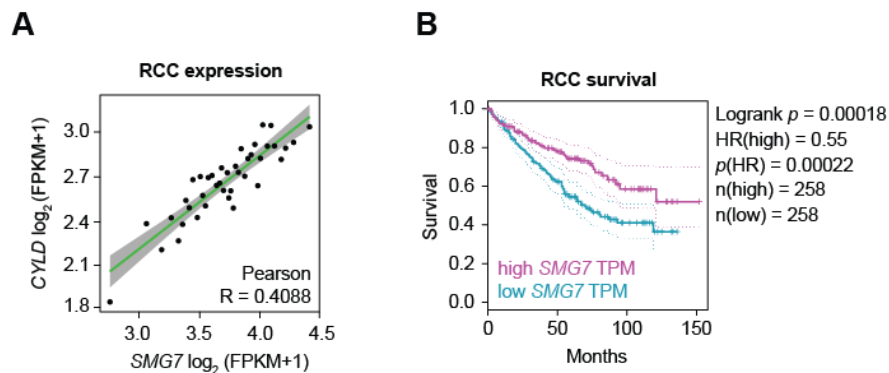
Figure 8-16. Correlation of *SMG7* between *CYLD* expression and survival in RCC.

Data were analyzed by Xuanwen Bao. Correlation of *CYLD* and *SMG7* expression in renal cell carcinoma (RCC, **A**) and Kaplan-Meier plot of *SMG7* expression and survival in RCC patients (**B**). FPKM, fragments per kilobase of transcript per million. HR, hazard ratio. Data and figure legend were published in Molecular Oncology [136].

8.7.   *SMG7* regulates anti-apoptotic lncRNAs *Pvt1* and *Adapt33*

Data in this section have been published in Molecular Oncology [136].
Cyld overexpression could only incompletely restore TNFα sensitivity in *Smg7 -/-* cells (Figure 8-14A). To investigate whether RNAs are also involved in the regulation of apoptosis, we conducted RNA differential expression analysis in *Smg7 -/-* and parental MF cells without ribosomal RNA. As shown in Figure 8-2B, rest of NMD elements generally remained unchanged in *Smg7 -/-* cells. Therefore, I suspected that SMG7-degraded RNAs should

increase in *Smg7 -/-* cells. Surprisingly, relative to control, only 38 out of the top 332 known significant genes were upregulated (Figure 8-17A). These upregulated genes include apoptosis resistance genes (*Nupr1*, *Sulf1*, *Tnfrsf11b*), known oncogenes (*Pvt1*, *Klf4*), and small nucleolar RNA host genes (lncRNAs *Snhg1, -5, -6, -12, -15*). In *Smg7 -/-* cells, 13.5% reads were mapped to lncRNA transcripts (gencode vM12) compared to parental cells (7.3%, Figure 8-17B).
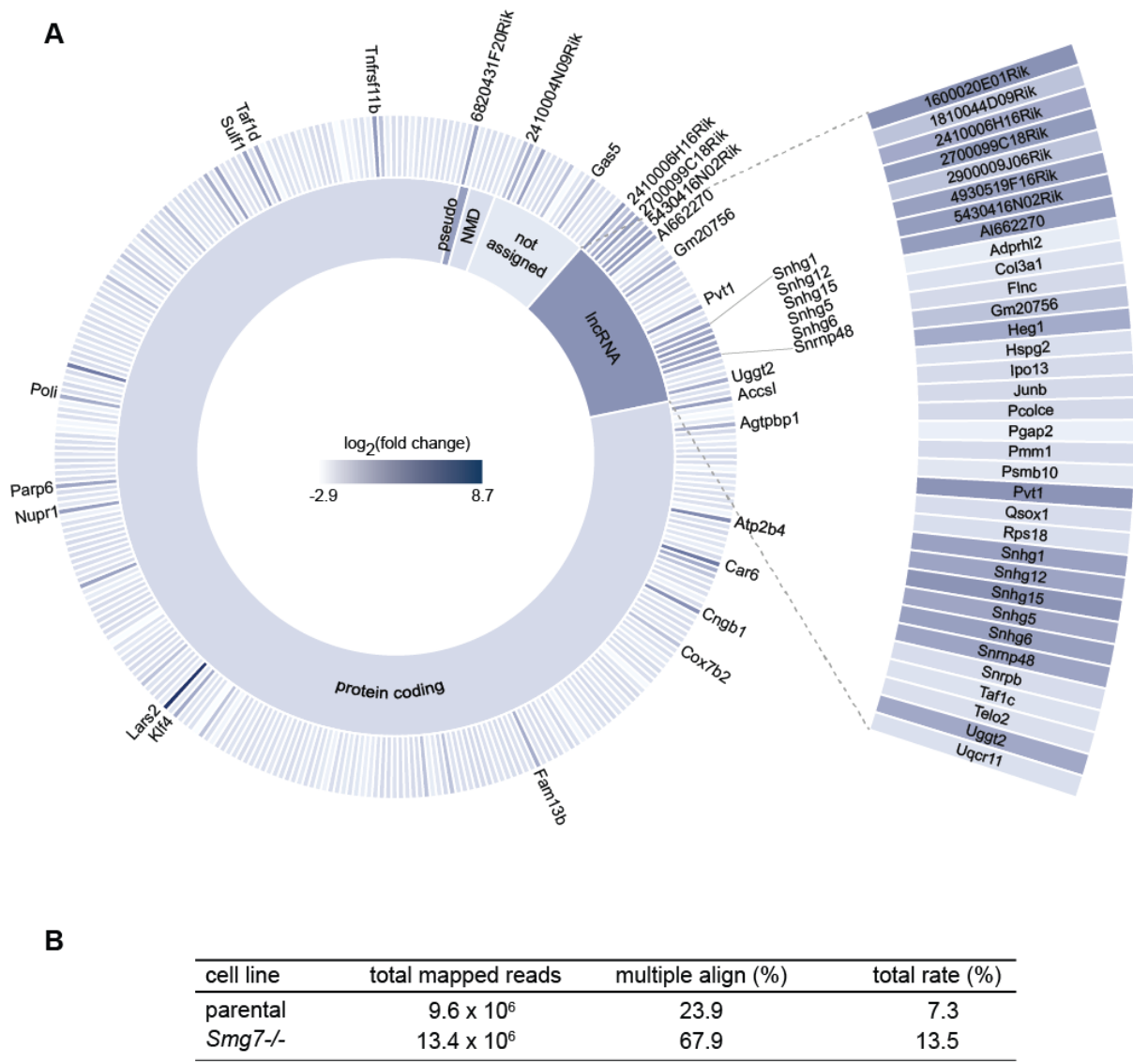
Figure 8-17. Transcriptional changes in *Smg7 -/-* cells.

Data analysis was conducted by Joel Schick and me. (**A**) Sunburst chart with indicated gene fold changes in *Smg7 -/-* cells. LncRNAs were exploded from the pie chart. (**B**) Quantification of mapped non-coding reads in parental and *Smg7 -/-* cells. Data and figure legend were published in Molecular Oncology [136].

Many lncRNAs have not been functionally characterized yet. I wondered whether the overexpression of these top enriched lncRNAs as well as protein-coding genes in parental cells could functionally recapitulate the resistance of *Smg7 -/-* cells to TNFα. To this end, I applied a CRISPR activation [154] library in parental cells targeting the top upregulated genes (Figure 8-17A and Figure 8-18A, B). As shown in Figure 8-18C, guides from 29 out of 31 genes presented in the library and distributed quite evenly. After multiple hypothesis correction, there were three genes, of which only the overexpression of two lncRNAs showed significant protective effect against TNFα-induced apoptosis: the oncogene Plasmacytoma variant translocation 1 (*Pvt1*; $p = 0.000865$, FDR = 0.0031) and *5430416N02Rik* (*Adapt33*, $p < 0.0001$, FDR < 0.0001, Figure 8-18B). Another one, the decoy TNF receptor *Tnfrsf11b,* as well displayed defense, which may be mediated by interaction with TNF receptors. Considering the activation of downstream NF-κB in *Smg7 -/-* cells (Figure 8-11A, C), the TNF signaling is not substantially impeded. Therefore, I chose these two lncRNAs as my primary research subjects.

50
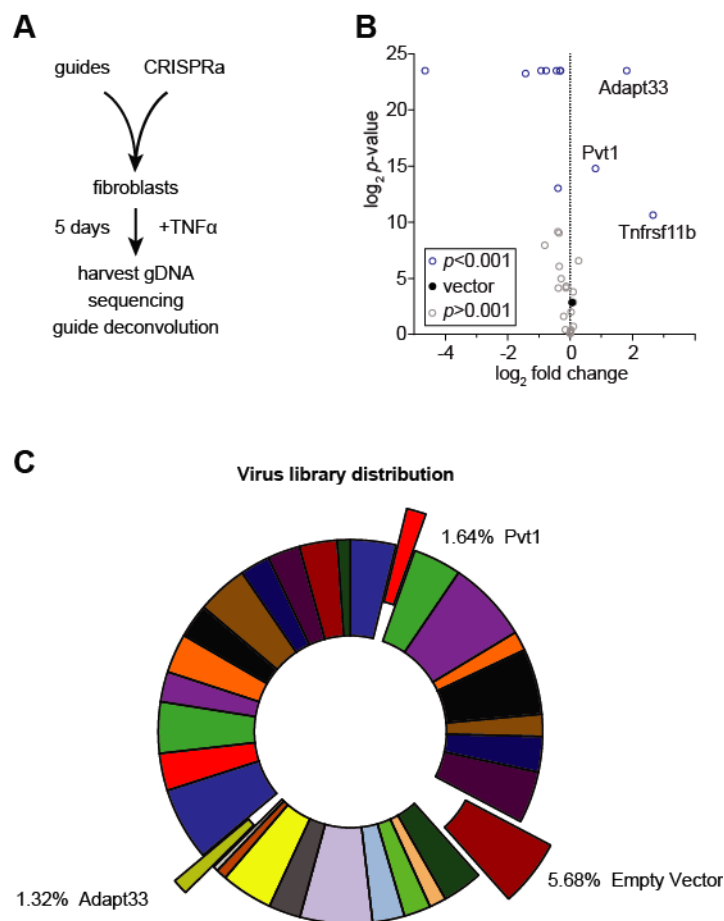
Figure 8-18. The mini gain of function screen by CRISPRa.

(**A**) CRISPR activation screen workflow. A mini-library was designed for upregulated genes from *Smg7 -/-* MF cells. Parental cells expressing CRISPRa components were infected with the pooled guide library followed by 20 ng/mL TNFα treatment for 5 days. Genomic DNA was extracted from surviving cells and guide sequences were amplified for sequencing and deconvolution. Data and figure legend were published in Molecular Oncology [136]. (**B**) Identification of anti-apoptotic genes from *Smg7 -/-* cells. Guides from positively scoring genes are displayed in the upper right corner. Data and figure legend were published in Molecular Oncology [136]. (**C**) Guide sequences distribution in the lentiviral library. *Pvt1*, empty vector and *Adapt33* were shown from the pie chart.

It has been reported that lncRNA *Adapt33* expression level can be induced by hydrogen peroxide or staurosporine in response to apoptotic stimuli [155]. Thus, I tested the levels of lncRNA expression in *Smg7 -/-* cells with or without the presence of 20 ng/mL TNFα for 8 h. *Pvt1* and *Adapt33* transcripts increased 7- and 10-fold in *Smg7 -/-* cells, respectively (Figure 8-19). Notably, *Adapt33* mRNA increased 26-fold upon TNFα treatment (Figure 8-19).
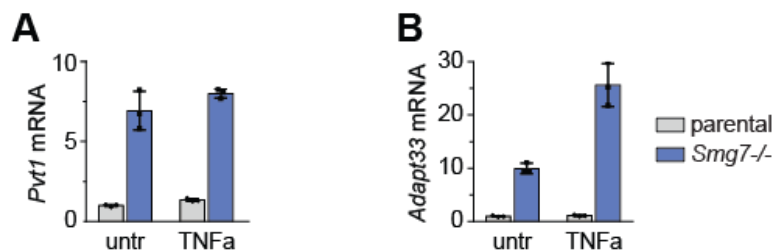
Figure 8-19. *Pvt1* and *Adapt33* mRNA are upregulated in *Smg7 -/-* cells.

qPCR analysis of *Pvt1* (**A**) and *Adapt33* (**B**) expression in parental and *Smg7 -/-* MF cells stimulated with 20 ng/mL TNFα for 8 h or untreated (untr). Data and figure legend were published in Molecular Oncology [136]. Expression data are shown as mean ± SD of n = 3 technical replicates. untr, untreated.

I generated *Pvt1* and *Adapt33* overexpressing cell lines with three guides by CRISPRa (OE, Figure 8-20A, B and C) and checked cell viability by TNFα challenge. *Pvt1* OE cells showed significantly more viability treated with 5 ng/mL TNFα compared to control cells ($p = 0.0001$; Figure 8-20A). *Adapt33* OE also showed protection against TNFα, but at lower levels ($p = 0.0013$). However, overexpressing these two lncRNAs cannot restore resistance to TNFα completely. This incomplete protection may be due to the overexpressed transcripts being surveilled by SMG7 persistently. Forced siRNA knockdown of *Smg7* (siSmg7, Figure 8-20D) increased the resistance of *Pvt1* and *Adapt33* OE cells to TNFα (Figure 8-20A). *Pvt1* OE and *Adapt33* OE, however, did not detectably decrease CYLD levels (Figure 8-20B), suggesting

the decreased CYLD expression may be due to other effectors other than *Adapt33* and *Pvt1* or they derived miRNA. The cleavage of caspase-8 and -3 was similarly unchanged in both cell lines (Figure 8-20E).
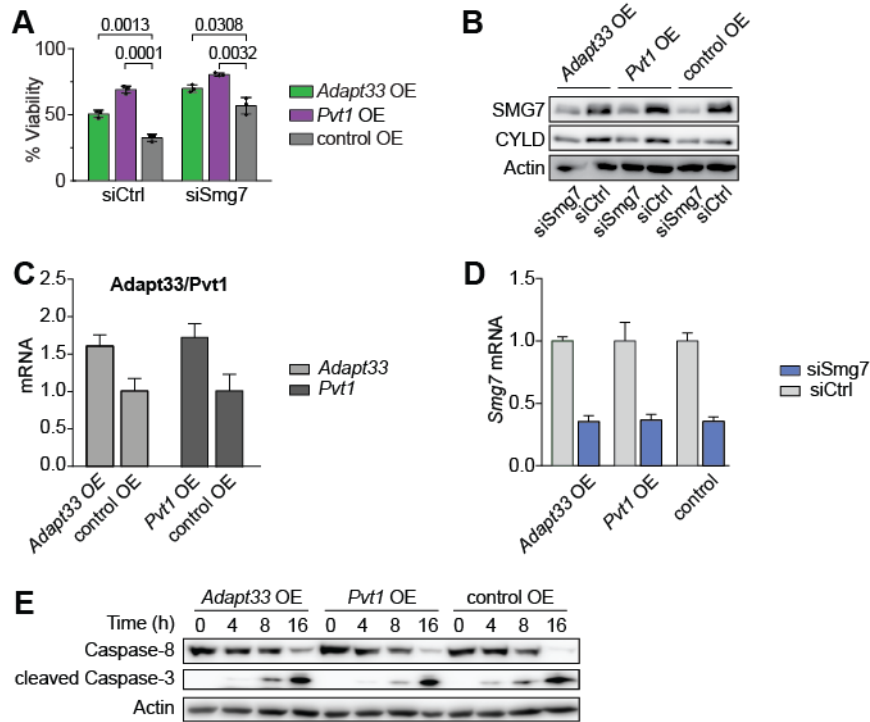
Figure 8-20. Overexpression of *Pvt1* and *Adapt33* decrease sensitivity to apoptosis.

(**A**) Viability of *Pvt1* or *Adapt33* overexpression cells (*Pvt1* OE, *Adapt33* OE) compared to negative OE vector control (control OE) cells upon 5 ng/mL TNFα treatment for 36 h. Additional siRNA *Smg7* knockdown (siSmg7) compared to control siRNA (siCtrl). Viability is shown as mean ± SD of n = 3 technical replicates. A typical result of N = 2 independent repetitions is shown. (**B**) Western blot of *Pvt1* OE, *Adapt33* OE, and control OE cells with siSmg7 knockdown and corresponding CYLD protein levels. (**C**) qPCR validation of *Pvt1* and *Adapt33* overexpression. (**D**) qPCR validation of *Smg7* KD efficiency in *Pvt1* OE, *Adapt33* OE, and control OE cells. (**E**) Western blot corresponding to (**A**) showing caspase-8 and cleaved caspase-3 protein levels following 20 ng/mL TNFα stimulation at respective time points in *Pvt1* OE, *Adapt33* OE, and control OE cells. Data and figure legend were published in Molecular Oncology [136].

Interestingly, a synergistic sensitization effect on TNFα was detected in *Cyld* overexpressing cells upon *Pvt1* knockdown (Figure 8-21A). Thus, to some degree, the protection acquired from these lncRNAs may be mechanistically complementary to the SMG7-CYLD relationship to some extent. Nonetheless, the IKK inhibitor SC-514 re-established sensitization of *Pvt1* OE

cells to TNFα (Figure 8-21B), implying that NF-κB plays an important role in *Pvt1* OE mediated resistance to TNFα.
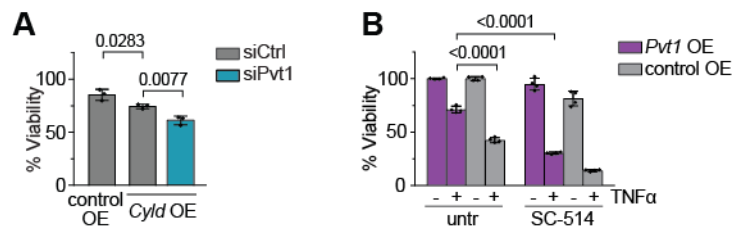
Figure 8-21. Overexpressing cells can be re-sensitized by *Pvt1* KD and SC-514.

(**A**) Viability of siRNA knockdown of *Pvt1* (siPvt1) compared to control (siCtrl) in *Cyld* OE and empty OE vector control (control OE) cells treated with 10 ng/mL TNFα. Viability is shown as mean ± SD of n = 3 technical replicates. A representative result of N = 2 independent repetitions is shown. (**B**) Viability of *Pvt1* OE compared to empty OE vector control cells (control OE) treated with 10 µM SC-514 in the presence or absence of TNFα for 48h. Viability data represent mean ± SD of n = 4 technical replicates. untr, untreated. The experiment was conducted by Vanessa Kraft and me. Data and figure legend were published in Molecular Oncology [136].

8.8. Sensitization of *Smg7 -/-* cells to TNFα in the 3D spheroid model

Data in this section have been published in Molecular Oncology [136].

In the tumor microenvironment, TNFα has pluripotent impact on cancer growth and autocrine function. In this study, to simulate in vivo tissue and cellular connectivity, I checked the impact of *Smg7* deletion against TNFα in a 3D spheroid model [156] (Figure 8-22A). Compared to parental cells, *Smg7 -/-* cells showed a growth disadvantage (Figure 8-22B). Thereby, I seeded 1000 *Smg7 -/-* and 500 parental cells to compensate for this disparity to yield comparable spheroids. TNFα-triggered apoptosis was stained by propidium iodide (PI). TNFα-induced apoptosis was still obviously observed in parental cells with a 3D spheroid model and synthetic lethality with a 10 µM SC-514 IKK inhibitor also promoted cell death in both cells (Figure 8-22A). Moreover, compacted, sharply defined spheroids were observed in *Smg7 -/-* cells upon TNFα treatment.
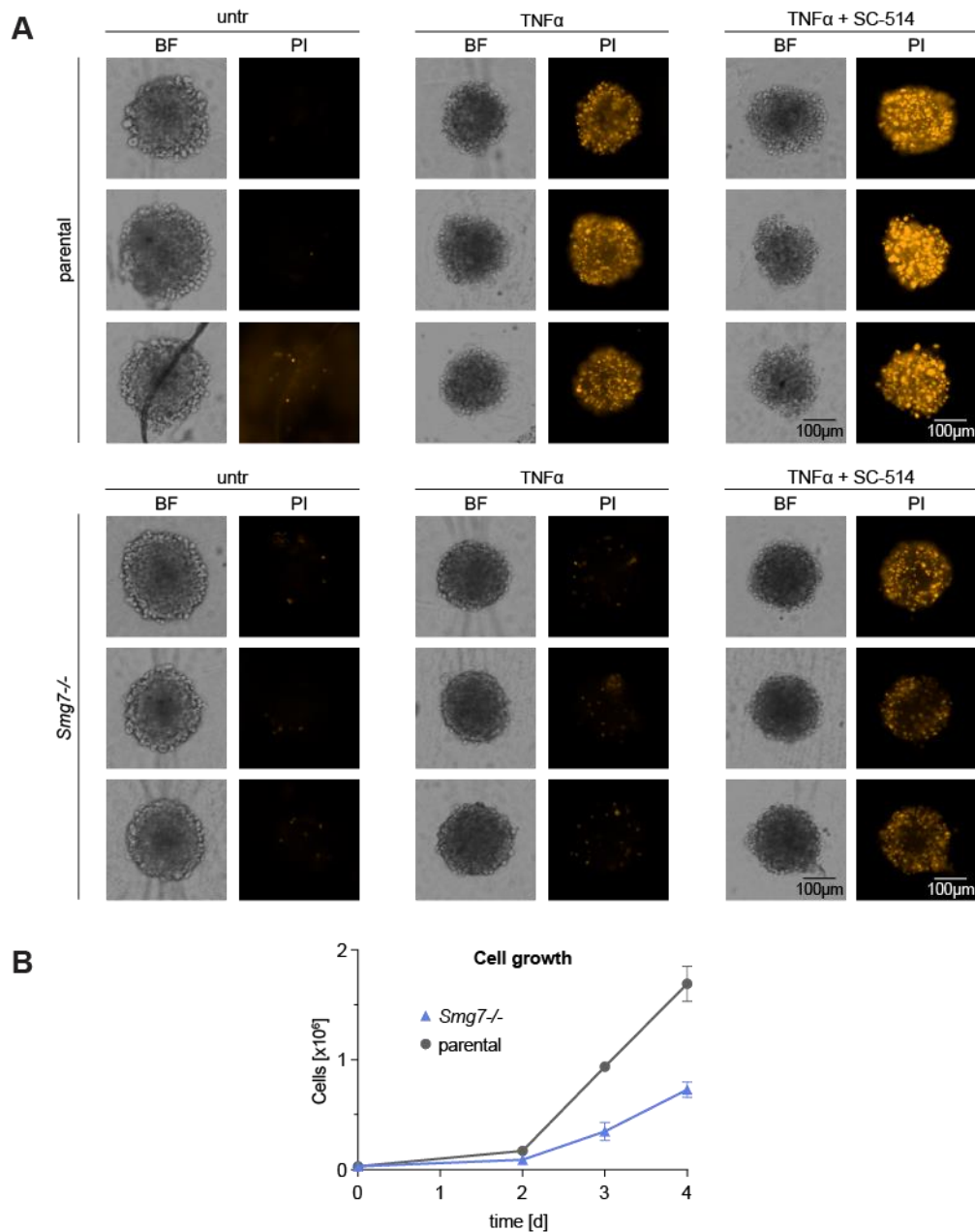
Figure 8-22. Pharmacological sensitization of *Smg7 -/-* cells to TNFα in the 3D spheroid model.

(**A**) Three-dimensional spheroids of *Smg7 -/-* and parental MF cells were grown for 4 days and treated with 20 ng/mL TNFα and addition of 10 µM SC-514 for 48 h. Propidium iodide (PI) staining indicates dead cells next to corresponding bright-field images (BF). Scale bar = 100 µM. untr, untreated. The experiment was conducted by Vanessa Kraft and me. (**B**) Growth characteristics of *Smg7 -/-* compared to parental MF cells in culture. Cells were counted in n = 3 technical replicates and a typical result of N = 3 independent repetitions is shown. Data and figure legend were published in Molecular Oncology [136].

8.9. TNFα sensitive cell lines
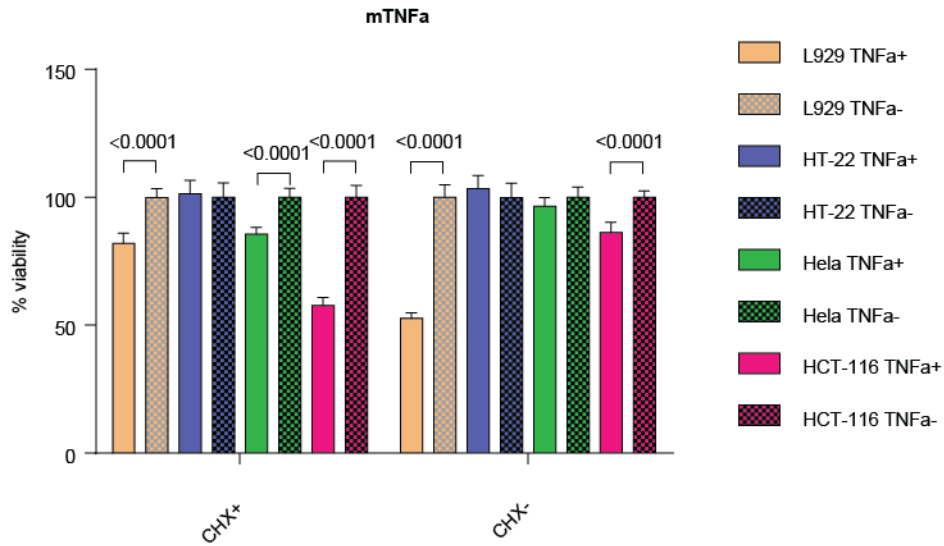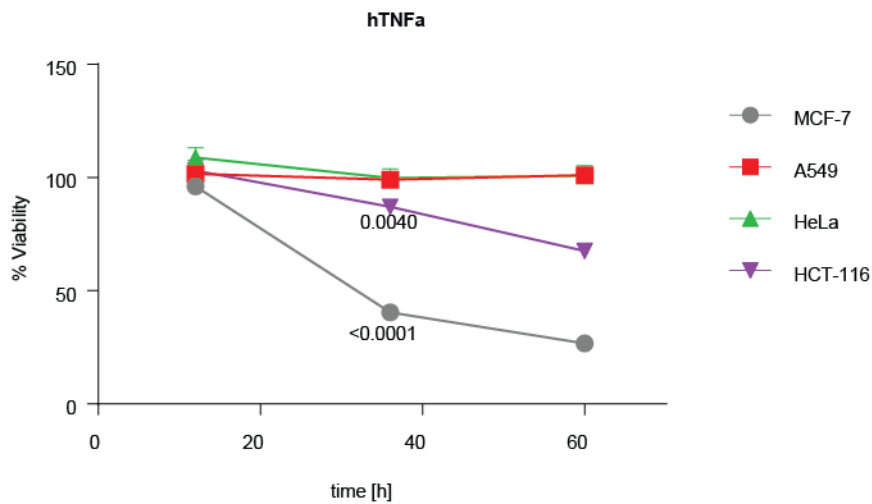
Figure 8-23. Variation of apoptotic sensitivities in different cell lines.

(**A**) L929, HT-22, Hela and HCT-116 cells were incubated with 20 ng/mL mouse tumor necrosis factor (mTNFα) in the presence or absence of CHX (100 ng/mL) overnight. Viability is represented as mean ± SD of n = 6 technical replicates. (**B**) 4 human cancer cell lines, MCF-7, A549, Hela and HCT-116 were treated with 20 ng/mL human tumor necrosis factor (hTNFα). Cell viabilities were measured at 12 h, 36 h, and 60 h post hTNFα exposure. Data are shown as mean ± SD of n = 3 technical replicates.

TNFα can cause tumor cytotoxicity [135], but it also plays a crucial role in triggering NF-κB and inflammation. The sensitivity of various cell types to TNFα-induced apoptosis can differ significantly, but most of the cells become very responsive when treated simultaneously with protein synthesis inhibitors [134]. Cycloheximide, an inhibitor of protein biosynthesis in eukaryotic cells, was applied in my study to inhibit protein synthesis. Here, I treated L929, HT-22, Hela, HCT-116 and A549 cells with either mouse TNFα (mTNFα) or human TNFα (hTNFα, 20 ng/mL), as indicated in Figure 8-23 in the absence or present of CHX (100 ng/mL) overnight. The results showed that L929, HCT-116 and MCF-7 cells could be sensitized to TNFα-induced apoptosis (Figure 8-23). However, only in HCT-116 and Hela cells, CHX promoted cells undergoing apoptosis induced by TNFα (Figure 8-23 A). Moreover, Hela cells could only be sensitized in the condition of CHX. Interestingly, both human and mouse TNFα could contribute to apoptosis in human HCT-116 colon cancer cell lines, which may be due to human and mouse TNFα are homologous genes and have a similar function.

8.10. SMG7 KD in HCT-116 and MCF7 cells results in lethal and growth defect

To confirm the SMG7 KD phenotype in human cells, I generated *SMG7* KD in HCT-116 and MCF-7 cells using the CRISPRi method. *SMG7* KD in HCT-116 cells caused cell disruption and cell death (Figure 8-24). Moreover, SMG7 protein levels showed a negative correlation to cell death (Figure 8-24A, B), which means less SMG7 protein leads to more cell death. However, why less SMG7 resulted in cell death and which kind of cell death remains unclear. In MCF-7 cells, *SMG7* KD by CRISPRi (Figure 8-24C) caused a growth defect. *SMG7* KD MCF-7 cells grew much slower compared to control cells (Figure 8-24C, upper panel). In addition to growth defects, many *SMG7* KD MCF-7 cells also showed a star-like cell structure with a plurality of tentacle-like branched structure (Figure 8-24C, D). Similarly, the mechanism behind the phenotype also needs to be further investigated. One suspicion may be that insufficient NMD resulted in the accumulation of truncated proteins, which may be toxic to cells. Nevertheless, loss of SMG7 in two human cancer cell lines resulted in cell death or growth arrest, indicating SMG7 or NMD plays an essential role in cancer cells.
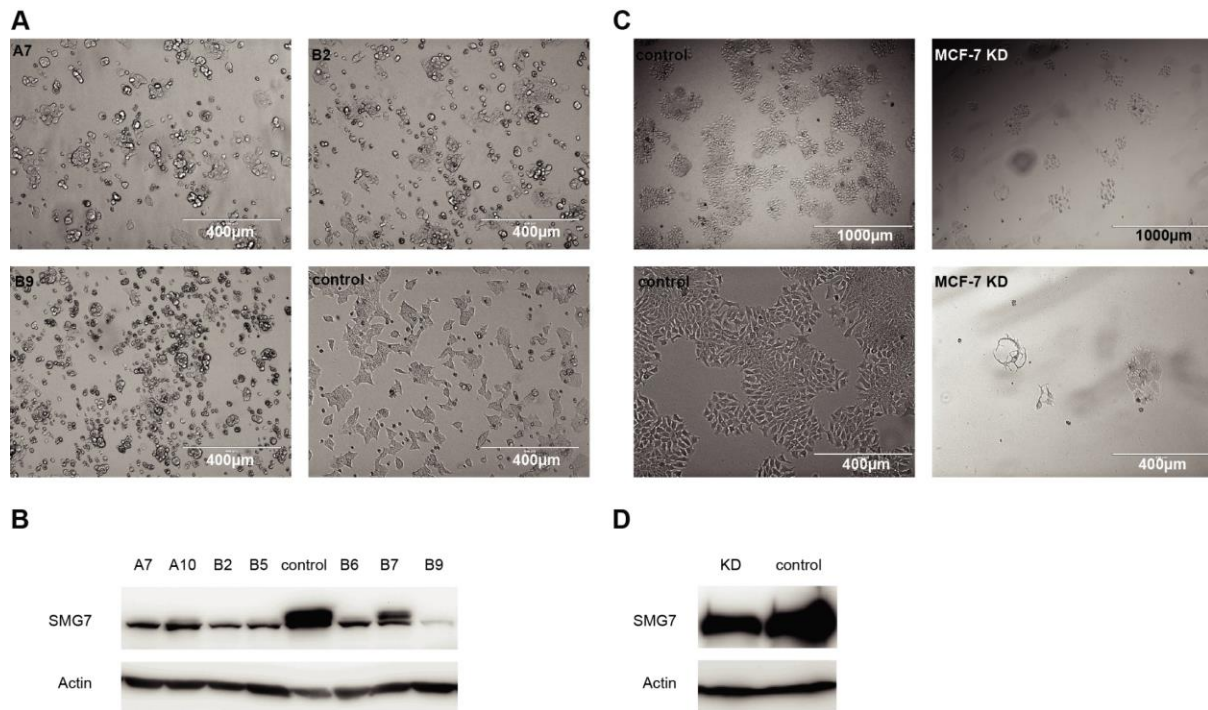
Figure 8-24. *SMG7* silencing leads to lethal and growth defects in HCT-116 and MCF-7 cells.

(**A**) The phenotype of HCT-116 *SMG7* KD and control cells. Scale bar = 400 µM. (**B**) SMG7 protein levels detected by Western blot corresponding to (**A**). (**C**) The phenotype of MCF-7 *SMG7* KD and control cells. Scale bar = 1000 µM in the upper panel, and scale bar = 400 µM in the lower panel. (**D**) SMG7 KD efficiency in MCF-7 cells. ACTIN served as a loading control.

8.11. Global NMD examination in MF cells

To investigate whether SMG7 affects and how much it affects the global NMD, I performed a test using doxycycline (Doxi) inducible *β-globin* construct (pTRE-Tight-BI-Gl NORM-LacZA-TER-LacZB, Addgene_86194, Figure 8-25A) [157]. This vector contains one wt *β-globin* transcript (NORM) and one mutated one at site 39 with a PTC (TER). *β-globin* expressing vector was co-transfected with a pLenti_CMV_rtTA3_Hygro vector (Addgene_26730) which can start the transcription of both *β-globin* transcripts in the presence of Doxi (Tet-on system). The transfected *Smg7* -/-, *Upf1* -/- (Figure 8-25B) and parental cell were induced by1 µg/mL Doxi for 36 h, and then cells were harvested for a qPCR analysis. Without the Doxi induction, almost no *β-globin* RNAs were detected. The same level of *β-globin* RNAs was detected using vector DNA as a template, suggesting the same amplification efficiency of both *β-globin* primers. Unexpectedly, I found mutated *β-globin* can be degraded in parental cells and also

in the *Smg7* -/- and *Upf1* -/- cells. Similar results were also found in *Upf1* shRNA KD MF cells (Figure 8-25C, D), where mutated *β-globin* RNAs were also degraded compared to wt *β-globin* RNAs. Surprisingly, *Smg7* -/- and *Upf1* -/- cells showed a lower mutated *β-globin* expression, which may be due to the compensatory effect of other NMD factors.
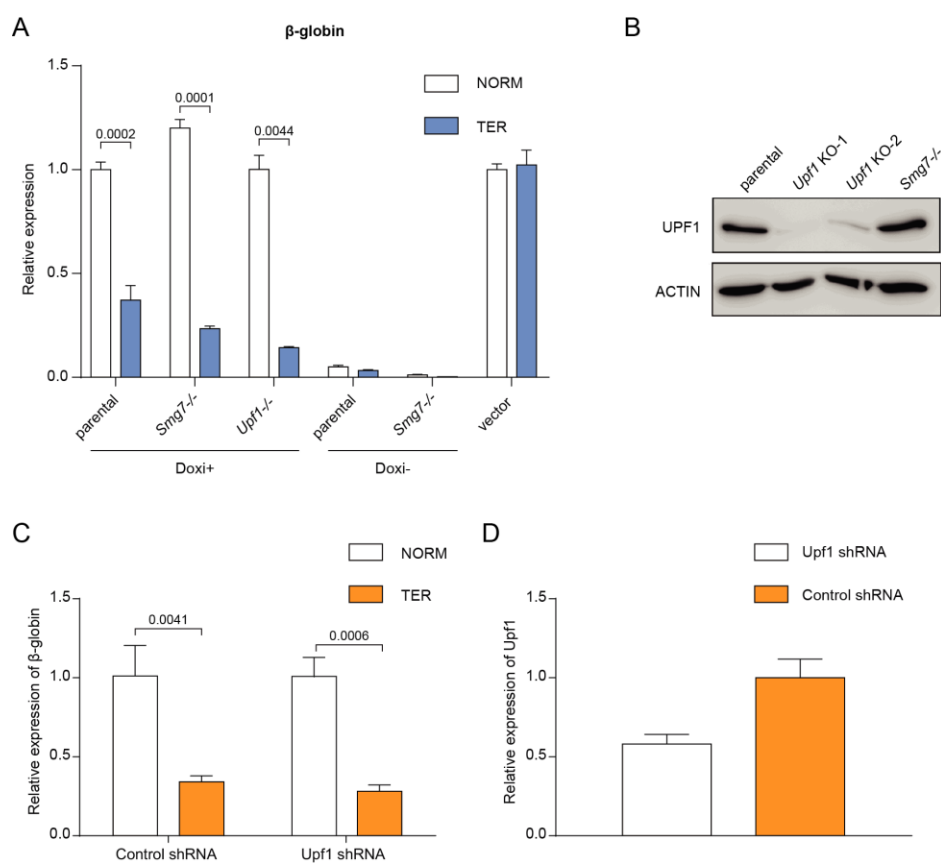
Figure 8-25. Global NMD examination in MF cells.

(**A**) *Smg7* -/-, *Upf1* -/- and parental cells were co-transfected with Tet-on system which can express wt *β-globin* (NORM) and mutated *β-globin* at site 39 with a PTC (TER). *β-globin* RNAs were induced with the presence of 1 µg/mL Doxi or not. (**B**) Efficiency analysis of UPF1 CRISPR knockdown by Western blot. ACTIN served as a loading control. (**C**) *β-globin* expression levels in *Upf1* shRNA KD MF cells. (**D**) *Upf1* shRNA KD efficiency test. Data are shown as mean ± SD of n = 3 technical replicates. NORM, wt *β-globin*. TER, mutated *β-globin*. Doxi, doxycycline.

8.12. *Adapt33* RNA targets in *Smg7 -/-* cells

Adapt33, as a stress-induced transcript, was reported to be upregulated to respond to apoptosis and promote ES cells proliferation [155, 158, 159]. Its role, however, has not yet been proven. Here, I have stated that the *Adapt33* RNA increased in *Smg7 -/-* MF cells and especially when treated with TNFα. The over-expression of *Adapt33* by CRISPRa could shield MF cells from apoptosis triggered by TNFα. However, the fundamental anti-apoptotic function of *Adapt33* remains unelucidated.

	Smg7 -/-			UV-crosslink			glutaraldehyde		
Adapt33	20,4	20,36	20,31	20,94	20,92	20,83	25,25	25,26	25,25
GAPDH	22,77	22,9	22,89		37,59		36,13		
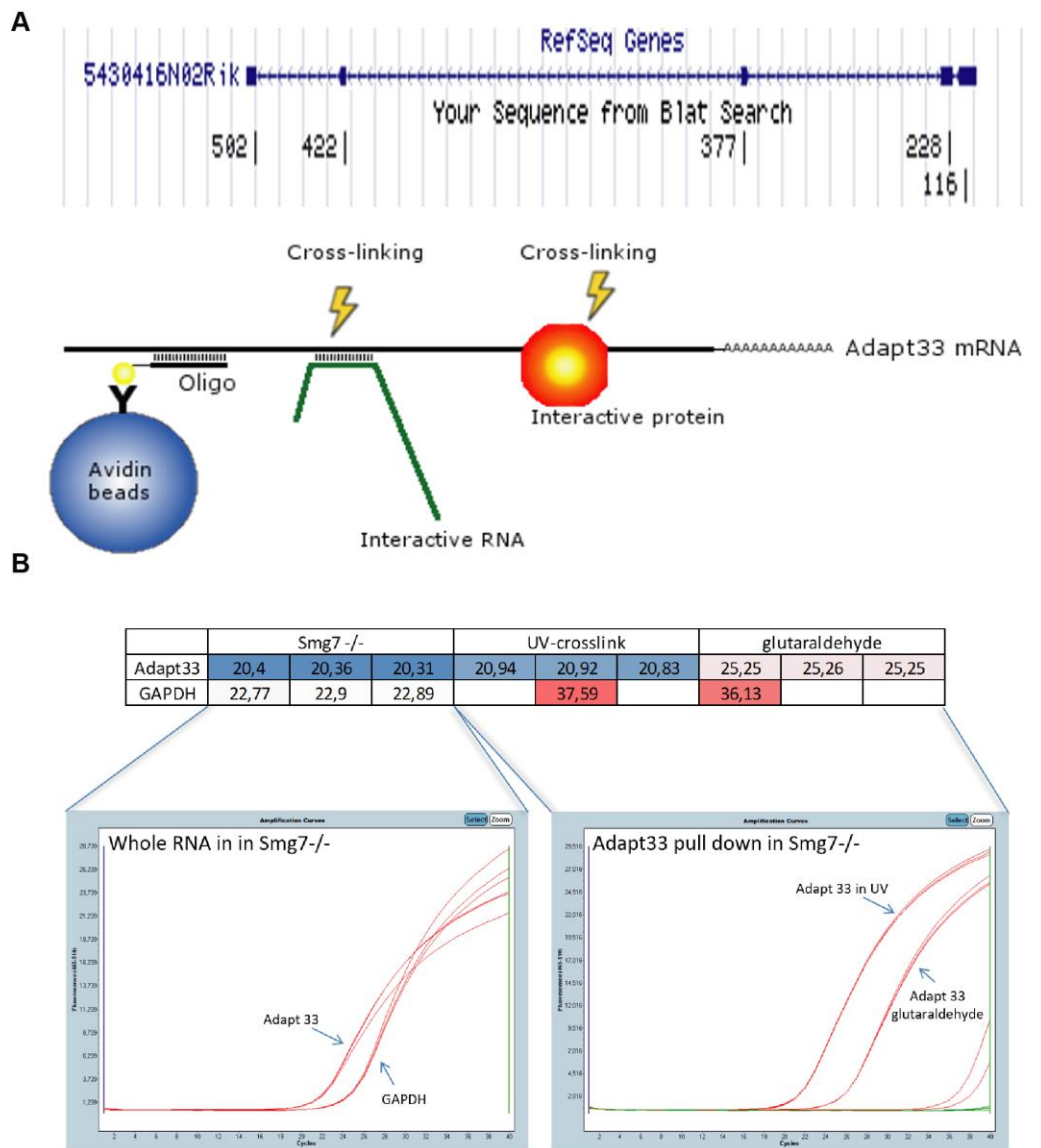
Figure 8-26. UV and glutaraldehyde cross-linking precipitation of *Adapt33* RNA.

(**A**) *Adaapt33* (*5430416N02Rik*) RNA has 5 exons. For each exon, I designed one biotinylated oligo (ssDNA, upper panel). The numbers on the left side indicate the oligos' positions. In total, 5 oligos were

aligned using the blat tool at UCSC (https://genome.ucsc.edu/). The lower panel shows the schematic diagram of RNA cross-linking precipitation. The interactive RNAs and proteins were cross-linked to *Adapt33* RNA using UV light or glutaraldehyde and the complex was pulled down with biotin-labeled oligos using avidin agarose beads. (**B**) *Adapt33* cross-linking precipitation efficiency was examined by qPCR and the data were presented with Cp values and amplification curves. The difference in Cp values is much more significant in cross-linking groups than *Smg7 -/-* cells. The blank Cp values mean undetectable.

Figure 8-27. Upregulated genes and pathway enrichment analysis.

(**A**) The top 200 upregulated genes (*p*-value < 0.05) in UV and glutaraldehyde cross-linking conditions were selected to generate the heat map. Gene names were sorted by mean $\log_2$(FC) of relative expression level. Glu, glutaraldehyde cross-linking. UV, UV cross-linking. Upper gene symbols are corresponding to the upper two rows of the heat map. Lower gene symbols are corresponding to the lower two rows of the heat map. (**B**) Gene set enrichment analysis of the top 200 upregulated genes (167 were annotated) in *Adapt33* RNA precipitation using Metascape [160]. The results showed the top 20 clusters.

To better understand how *Adapt33* is involved in apoptosis response and regulating RNAs, I conducted the cross-linking pulldown experiment in *Smg7 -/-* cells (Figure 8-26A). 5 biotin-labeled antisense oligos were designed against each exon of *Adapt33* RNA (Table 11-4). UV-crosslinking and glutaraldehyde were used to cross-link *Adapt33* RNA to interactive RNAs and proteins. The enriched *Adapt33* RNAs were verified by qPCR (Figure 8-26B). As shown in Figure 8-26B, compared to the reference gene *Gapdh*, the Cp (crossing point) values between *Adapt33* and *Gapdh* were much more abundant in UV cross-linked and glutaraldehyde cross-linked groups than *Smg7 -/-* cells, implicating a high enrichment of the *Adapt33* RNAs. Then the precipitated RNAs from the UV and glutaraldehyde cross-linking groups were sent to RNAseq. The RNAseq data were analyzed using the DESeq2 program on the Galaxy platform by comparison with *Smg7 -/-* cells. The result showed that 3199 and 640 genes were significantly enriched in UV and glutaraldehyde cross-linked samples, respectively ($p < 0.05$). Then the top 200 upregulated significant ($p < 0.05$) genes presented in both UV and glutaraldehyde cross-linking conditions were chosen for subsequent analysis. As expected, *Adapt33* (*5430416N02Rik*) was highly upregulated (mean log2(FC) = 8.56, Figure 8-27A) in both conditions compared to *Smg7 -/-* cells.

To investigate the pathways and biological functions, 200 genes (167 were annotated) were uploaded into Metascape bioinformatics resources [160]. As the results showed in Figure 8-27B, the corresponding genes were mainly enriched in TNF signaling pathway (mmu04668), Apoptosis (mmu04210) and NF-kappa B signaling pathway (mmu04064) and GO biological processes, for example, I-kappaB kinase/NF-kappaB signaling (GO:0007249), interspecies interaction between organisms (GO:0044419), response to interferon-beta (GO:0035456), reactive oxygen species metabolic process (GO:0072593), as well as reactome gene sets Nonsense-Mediated Decay (NMD, R-MMU-927802). Unsurprisingly, the top-ranked pathways and biological processes were involved in cell death and survival regulation network, implicating the novel role of *Adapt33* in cell fate decisions. Interestingly, the target genes of

Adapt33 were also associated with the nonsense-mediated decay process (Figure 8-27 and Table 8-4).

Table 8-4. Enriched gene sets of *Adapt33* pulldown in different pathways and biological processes.

Pathways and biological processes	Genes
TNF signaling pathway	Fas, Cxcl1, Nfkbia, Ccl2, Ccl5, Cx3cl1, TNFαip3, Traf1, Vcam1, Gbp2, Nos2, Ccl7, Gbp3, Stx11, Parp14, Noct, Ncl, Nr1h2, Hmgb2, Abr, Hdac5, Nfkb2, Relb, Saa3, Tnip1, Stab1, Muc19, Pecam1, Sgsm1, Rgs8, Sh3bp4, Tbc1d14, Dock10, Hip1r, Ndufa13, Itpr2, Trim30a, Polr3d, Dtx3l, Csf2rb2, Prkn, Osr1, Tacr2, Npffr1, Ank3, Comt, Mafg, Atp6v1g1, Car12, Ank2, Pde6a, Map2k2
I-kappaB kinase/NF-kappaB signaling	Nfkb2, Nfkbia, Relb, Saa3, Cx3cl1, TNFαip3, Traf1, Prkn, Tnip1, Ccl5, Fas, Ndufa13, Hmgb2, Pak2, Cxcl1, Nos2, Trim30a, Oasl2, Dtx3l, Hip1r, Comt, Pde1a, Tenm4, Ncl, Ccl2, Polr3d, Trim16, Tacr2, Abr
Apoptosis	Csf2rb2, Gadd45a, Fas, Itpr2, Nfkbia, Traf1, Map2k2, TNFαip3, Abr, Lamb3, Nos2, Pik3r5, Prkn
response to interferon-beta	Gbp2, Gbp3, Ndufa13, Xaf1, 9930111J21Rik1
NF-kappa B signaling pathway	Nfkb2, Nfkbia, Relb, TNFαip3, Traf1, Vcam1, Hdac5, Nfkbie, Polr3d, Psmb10, Pak2, Gadd45a, Fas, Map2k2, Cxcl1
Nonsense-Mediated Decay (NMD)	Rpl19, Rps27, Rplp2, Rpl34, Rpl10, Smg1, Ncl, Psmb10, Snrpf

Next, I checked apoptosis and NF-κB related mRNA expression levels in *Smg7 -/-* cells. LncRNAs can hybridize with RNAs and allow Dicer to generate endogenous siRNAs, thereby suppressing the expression of target RNAs [75, 76]. Therefore, I only focused on downregulated RNAs in *Smg7 -/-* cells. Surprisingly, NF-Kappa-B Inhibitor Alpha (Nfkbia) was significantly decreased (Log2(FC) = -0.54, Table 8-5). TNF Alpha Induced Protein 3 (TNFαip3,

A20), whose expression can inhibit NF-κB activation and TNF-mediated apoptosis, was also downregulated in *Smg7 -/-* cells. *Polr3d*, also named as RNA polymerase III subunit C4, can transcribe miRNA [161], snRNA, tRNA and rRNA [162], showed a decrease in *Smg7 -/-* cells.

Table 8-5. Apoptosis and NF-κB related mRNA expression levels in *Smg7 -/-* cells.

apoptosis		NF-κB	
Gene	Log2(FC)	Gene	Log2(FC)
Traf1	1.77	Polr3d	-0.08
Nfkbia	-0.54	Traf1	1.77
Csf2rb2	1.86	Nfkbia	-0.54
Gadd45a	1.66	Psmb10	-0.56
Itpr2	1.57	Gadd45a	1.66
Fas	N/A	Fas	N/A
Abr	0.57	Cxcl1	-1.83
Pik3r5	-0.93	Relb	-0.26
Lamb3	0.16	Pak2	-0.14
Map2k2	-0.32	Hdac5	-0.81
Prkn	0.17	Vcam1	-2.02
TNFαip3	-0.73	Nfkb2	N/A
Nos2	-2.26	Map2k2	-0.32
		Nfkbie	N/A
		TNFαip3	-0.73

8.13. Sensitization of *Smg7 -/-* cells to TNFα in Matrigel basement

I also tested cell viability in a 3D cell culture condition conducted using Matrigel (Figure 8-28). TNFα could still sensitize parental MF cells in the Matrigel condition. As time went on, the viability dropped from 64.49% (12 h) to 35.77% (96 h) compared to *Smg7 -/-* cells, suggesting MF cells can grow in the Matrigel matrix and still maintain resistance to TNFα induced-apoptosis.
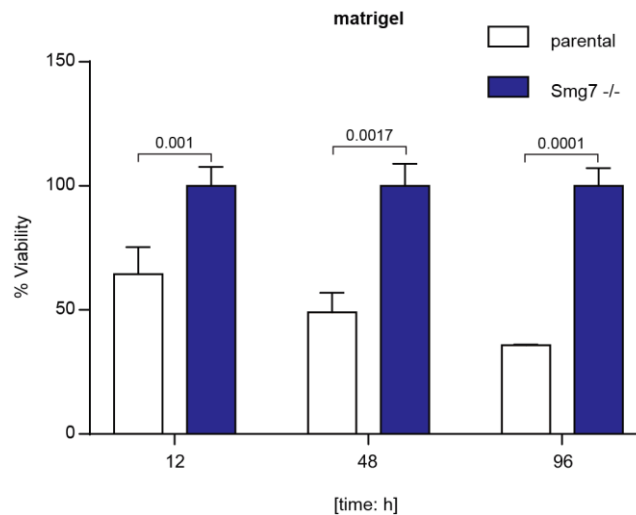
Figure 8-28. Cell viability analysis in Matrigel.

Cell viability assay was performed in a Matrigel-based 3D cell culture system. *Smg7 -/-* and parental MF cells were treated with 20 ng/mL TNFα and cell viabilities were measured 12, 48, and 96 h post-treatment. Data are shown as mean ± SD of n = 3 technical replicates

9. Discussion

SMG7 specifically protects TNFα-induced apoptosis by targeting lncRNAs

TNFα is a proinflammatory cytokine that has diverse roles in cellular events, including NF-κB activation and apoptosis. In human malignancies, TNFα plays a variable and contradictory role [163]. Lower levels of TNFα can stimulate the inflammatory and pro-survival pathways through NF-κB, while higher local levels of TNFα, i.e. monocyte presentation or natural killer-induced cytotoxicity, can trigger apoptosis in tumors [164, 165]. A high concentration of TNFα, as well as other physical, chemical and biological stimuli, is necessary to induce apoptosis. In contrast, the biological characteristics of cells also determine their fates towards TNFα. In this study, I observed *Smg7 -/-* MF cells and *Smg7* knockdown NIH 3T3 cells showed resistance to TNFα-induced apoptosis. In MF cells, this apoptosis was rescued by a caspase inhibitor zVAD, implicating the involvement of caspase (Figure 8-1A, B). CHX, a protein synthesis inhibitor, can markedly sensitize HT-29 human colon epithelial cells to apoptosis by TRAIL [166]. IFNγ, a proinflammatory cytokine, is able to induce apoptosis by upregulation of Fas and FasL in many cell lines [167, 168]. TNFα and IFNγ costimulation synergistically reduced cell viability via apoptosis in mouse osteoblasts [169]. Surprisingly, in my case, only TNFα induced cell death in MF cells independent of other apoptotic inducers. Neither CHX nor IFNγ

was able to reduce cell viabilities when combined with TNFα (Figure 8-1C), suggesting MF cells are insensitive to these other challenges. Re-analysis of other cell death inducers did not show exceptional protection in *Smg7 -/-* MF cells (Figure 8-1D). These data showed this resistance to TNFα-induced apoptosis in *Smg7 -/-* MF cells was convincingly stimulus-dependent and mediated by TNFα signaling.

It remains unclear whether SMG7 can directly modulate specific RNAs in addition to NMD. The present result showed that *Smg7* modulated a subset of lncRNAs specifically. Whether this is occurred in addition to NMD or instead of NMD is still unproven. However, whether SMG7 can directly target specific RNAs by itself or collaborate with other NMD members remains to be further investigated. The other NMD factors would have to be individually knocked out in order to specifically test whether they can control the same transcripts involved in apoptosis. The pan-genomic mutagenesis analysis showed that SMG7 KO protected so well against TNFα-induced apoptosis (Figure 8-2C) than other factors. Since other factors did not protect, the subset of transcripts they regulate is probably quite different, suggesting SMG7 may have the capacity to degrade transcripts by itself. Indeed, SMG7 could degrade RNA transcripts alone through CNOT8 interaction [46] and could also degrade 3' UTR-length based transcripts via a miRNA mediated mRNA degradation mechanism [47]. Interestingly, SMG7 can degrade the reporter mRNA independently of PTC, SMG5, UPF1 and SMG6 when tethered to a reporter transcript [44]. In this study, a transcriptome analysis of differentially expressed biotypes in *Smg7 -/-* cells revealed lncRNA (lincRNA and antisense, log2(FC) = 1.15 and 0.61, Figure 8-3B and Table 13-1) rather than nonsense-mediated decay transcripts (log2(FC) = 0.26) were highly increased. Moreover, knockout of NMD effectors in the CRISPR screening, excluding *Smg7* and *Upf2*, did not show any defense against TNFα (Figure 8-2C). These data support a model that over a generalized NMD substrate, *Smg7* contributes to specialized transcript degradation, where lncRNAs upregulation in response to *Smg7*-deletion increases cells viability against TNFα challenge.

Smg7 -/- causes NMD factors compensatory regulation

When the balance of NMD factor levels is disturbed, cells can upregulate unaffected NMD factors to compensate and maintain NMD activity [170]. For example, SMG7 was upregulated in response to UPF3B depletion in HeLa cells, which maintained the NMD function by repression of known NMD-targeted RNAs. However, this compensation also showed a tissue-specific pattern in various *Upf3b*-null tissues. In extreme cases, no changes were detected among these NMD factors in some tissues [170]. Similarly, in the present study, qPCR analysis of a group of crucial NMD factors showed upregulation in *Upf3b* and *Smg5* (Figure 8-2B), indicating a functional compensation in response to the loss of *Smg7*. Interestingly,

SMG7 was upregulated in UPF3B knockout Hela cells [170]; similarly, I observed that *Upf3b* increased in *Smg7 -/-* cells (Figure 8-2B), implying a delicate connection between these two factors. SMG5 can heterodimerize with SMG7 via their 14-3-3-like phosphopeptide recognition domains to increase the affinity to UPF1 [43]. In the present study, the expression of *Smg5* also upregulated in *Smg7 -/-* cells, which may result in the compensation regulation due to the loss of SMG7. However, NMD is not systematically affected because NMD factors were not dramatically changed. The pan-genomic mutagenesis analysis revealed that the basal guides directed against *Smg7* were highly enriched and *Upf2* guides also showed a slight enrichment (Figure 8-2C). In *Drosophila*, *Upf2* mutant cell clones were unable to grow and underwent apoptosis [171]. Weischenfeldt et al. showed that *UPF2* depletion in thymocytes resulted in apoptosis [172]. In contrast, my data showed that *Upf2* KO protected MF cells against TNFα-induced apoptosis (Figure 8-2C), however, only one out of 5 guides against *Upf2* was protective in the TNFα screening assay. Nevertheless, these data suggested that loss of SMG7 caused the compensatory regulation of other NMD factors and the protection against TNFα was mediated by a specialized function of SMG7 rather than by the general damage of NMD. Indeed, as shown in Figure 8-25, NMD is not that affected in *Smg7 -/-* cells.

Specific RNA targets of NMD factors

Strikingly, several independent experiments indicated that SMG7 and SMG6 played partially redundant roles to promote the NMD targets degradation in the endo- and exonucleolytic decay routes, respectively [43, 45, 46, 173]. However, these two NMD factors have different capacities in the degradation of specific RNAs. SMG6 preferentially degrades NMD substrates over SMG5/7-dependent deadenylation and decapping, and PTC-containing transcripts are constitutively involved in SMG6-dependent exonucleolytic decay [174]. A transcriptome-wide analysis of human NMD targets showed NMD also modulates lncRNAs, miRNA and snoRNA host genes [173], which is consistent with my results that lincRNAs were dramatically elevated in *Smg7 -/-* and *Smg6* KO cells while miRNAs were intensively enriched in *Upf1* KD cells (Figure 8-3B and Figure 8-7). Moreover, almost exclusively lncRNAs (except sense intronic and macro lncRNA) were decreased in *Upf1* KD mouse C2C12 cells regardless of the remarkable upregulation of miRNAs (Figure 8-7B). This is consistent with a model showed that lncRNAs as primary microRNAs (pri-miRNAs) which can be degraded into miRNAs [175-177].

UPF1, SMG7 and SMG6 are three core effectors involved in NMD-mediated RNA regulation. The first step of NMD is the recognition of PTC by the SURF surveillance complex composed of UPF1, while SMG7 and SMG6 are responsible for the RNA degradation via endo- and

exonucleolytic decay routes. Surprisingly, I observed that loss of these well-known NMD factors indeed affected typical NMD substrates, while the most obvious alteration was found not to be these NMD-targeted transcripts in the global differential expression analysis. Instead, ncRNAs, including lincRNA and miRNA, were dramatically upregulated (Figure 8-6 and Figure 8-7). Even within one gene, NMD was found to target specific transcripts rather than the entire gene (Figure 8-8D). So, I hypothesized that different NMD factors might have their specific target transcripts, target a subcluster of RNAs possessing particular features, or have novel uncharacterized RNA-degrading mechanisms other than the unique roles in NMD surveillance system. For example, SMG6-mediated endonucleolytic route preferentially cleaved PTC-containing immunoglobulin μ reporter transcripts, whereas SMG5/SMG7-dependent pathway predominantly degraded *β-globin* transcripts [45]. Recently, Park et al. demonstrated that miRNAs, not nonsense mRNAs, are responsible for 3′UTR-length-dependent mRNA decay via Ago-associated UPF1/SMG7 [47], suggesting novel roles of NMD factors in mediating RNA degradation rather than the basic functions in NMD. This information opens the door to a more profound realm for reconsidering the redundant functions of NMD factors in response to RNA degradation, as previously thought.

In Hela cells, UPF1, SMG6 and SMG7-deficient cells have extensive overlapping genes within the top 1000 targets [173]. In contrast, I found that, over the top 1000 upregulated genes, these NMD factor-deficient cells barely shared nine genes (Figure 8-8A). Environmental and technological variables can have a substantial impact on the results when comparing RNAseq data sets from different publications. Notably, in my case, these mouse RNA-seq data sets come from different cell lines, which caused the massive variation in NMD factor-targeted transcripts. Interestingly, in the commonly targeted genes, 6 out of 9 genes were lncRNAs (Figure 8-8B). NMD starts with PTC recognition and is a translation-dependent process. LncRNAs cannot be translated into protein; thus, they do not have PTCs. However, recent studies have shown that a significant fraction of lncRNAs expressed in cells are also associated with ribosomes [178-181], indicating cells want to translate these lncRNAs. Indeed, a considerable number of reports have revealed that lncRNAs are able to encode short polypeptides [181, 182]. These putative small ORFs (mORFs) of lncRNAs often correspond to regulatory ORFs (uORFs) in the 5′ UTR region [181], which may end the translation in an mRNP complex and activate NMD to degrade the corresponding lncRNAs. Colombo et al. found the number of predicted ORFs on an ncRNA and the likelihood of it being identified as an NMD target were highly correlated [173]. At this point, the enriched lncRNAs in *Smg7 -/-* and *Smg6* KO cells, as well as overlapping transcripts in three NMD factor-deficient cell lines,

should also be involved in NMD regulation through these mORFs, though different effectors may have their favorite targets and cleave a specific transcript to varying degrees.

More remarkably, *SMG7* KD in Hela cells only weakly impaired NMD compared to *SMG6* and *UPF1* [173]. However, I found that *Smg7 -/-* and *Smg6* KO cells had more significant effect on NMD targets in the nine common genes (Figure 8-8C). The inefficient siRNA KD may cause this in *Upf1* group. For some genes, such as *Zfas1*, *Gm42546*, *2410006H16Rik* and *Snhg6*, expression levels were comparable in *Smg7* and *Smg6*-deficient cells, while others, especially *Pvt1*, had a dramatical higher expression level in *Smg7 -/-* cells (Figure 8-8C). This suggests different RNAs cleaving routes in NMD preferentially target specific genes or have different mechanisms to degrade genes over typical NMD. Indeed, previous data showed that SMG6 and SMG7 could preferentially target specific transcripts [45]. However, how they may choose their targets and whether they can independently affect the same classes of RNAs still need to be further confirmed.

NMD has differential effects on distinct alternative RNAs of the same gene [147]. In my analysis, though the whole gene was upregulated, the different transcripts encoded by this gene could vary considerably (Figure 8-8, Table 13-5). Two examples are given here, almost all of the *Pvt1* transcripts were highly upregulated while transcript *Pvt1-202* remained nearly unchanged (log2(FC) = 0.49, other transcripts were higher than log2(FC) = 2.59 in *Smg7 -/-* cells). According to the *Pvt1-202* transcript structure, *Pvt1-202* loses one exon that encodes one misc RNA *Gm27957-201* and has three more exons in the 3' UTR (Figure 8-9A). When it comes to *Zfas1*, the alternative spliced isoform *Zfas1-201* showed a relatively lower expression in both *Smg7* and *Smg6*-deficient cells (log2(FC) = 0.58 and 0.89, other transcripts were higher than log2(FC) = 3.11 in *Smg7 -/-* and *Smg6* KO cells). As shown in Figure 8-9B, compared to *Zfas1-206*, the only difference is that the third intron in *Zfas1-206* is transcribed in *Zfas1-201*. These changes between different transcripts caused by alternative splicing may result in loss of NMD-targeted features, consequently, leading them to escape NMD degradation. Several interesting experiments, including accurately expressing exogenetic NMD-targeted transcripts, for example, overexpressing *Zfas1-201* and *Zfas1-206* independently by cDNA in *Zfas1* KO cells, could be conducted to identify which exons and introns contain NMD signatures. The exons that determine degradation could be further mind by bioinformatics, perhaps comparing them to each other and trying to distinguish what exactly causes them to be more stable or more susceptible to degradation.

SMG7 dictates CYLD levels, which in turn mediates NF-κB activation

In this study, I detected a diminished caspase activity in *Smg7* -/- cells and a caspase inhibitor zVAD rescued TNFα-induced apoptosis in parental cells (Figure 8-10A and B), indicating TNFα-triggered cell death is mediated by caspases. SMG7 regulates CYLD deubiquitinase levels, so losing SMG7 resulted in lower CYLD expressions (Figure 8-11A). In necrosis, caspase-8 cleaves CYLD to generate a survival signal following TNF stimulation [183]. Similarly, parental cells showed distinctly lower CYLD levels when treated with TNFα, likely due to the cleavage by caspase-8. However, a lower level of CYLD was still detected even in resting *Smg7* -/- cells, suggesting this downregulation of CYLD in resting *Smg7* -/- cells was mediated by loss of SMG7 other than caspase-8 cleavage. In turn, CYLD also promotes caspase-8 activation via RIP1 deubiquitination [184]. Consistent with my data, I also observed a decreased caspase-8 activity in *Smg7* -/- cells upon TNFα stimuli, which may be caused by the less basal amount of CYLD. Taken together, these data suggest that loss of SMG7 blocks caspases-mediated apoptosis triggered by TNFα and that SMG7 interferes with CYLD levels, possibly by which it regulates NF-κB activation and switches apoptosis to survival.

The downregulation of CYLD mainly leads to the activation of the NF-κB pathway. TNFα-resistant *Smg7* -/- cells have less CYLD and more phosphorylated IκB and can be sensitized by NF-κB inhibitors when treated with TNFα (Figure 8-12), suggesting the activation of NF-κB mediates the survival due to the loss of SMG7. On a deeper level, this means that tumors with higher NF-κB expression levels are more easily affected by SMG7. In reality, SMG7 was identified as a new risk factor in NF-κB treatment of prostate cancer [50], showing the potential role in regulating tumorigenesis and development [185]. In prostate cancer cells, the paracrine application of TNFα was also confirmed to promote apoptosis and result in cell cycle arrest [186]. In testicular cells, *CYLD* ablation activated NF-κB and promoted the expression of a large number of anti-apoptotic genes [187]. These pieces of evidence are totally consistent with what I found here in *Smg7* -/- cells, including insensitivity to TNFα challenge and pharmacological sensitization in the presence of NF-κB inhibitors in monolayers and 3D spheroids, indicating NF-κB mediates the resistance in *Smg7* -/- cells through the deregulation of CYLD.

More interestingly, these diminished CYLD levels were also found in NIH 3T3 and MCF-7 cells following SMG7 KD by siRNA (Figure 8-13). Furthermore, this positive correlation between *CYLD* and *SMG7* was further confirmed in 1164 human cancer cell lines (Figure 8-15). These data imply a novel function of SMG7 in CYLD expression and establish a bridge between SMG7 and survival mediated by NF-κB. K-63 polyubiquitination of RIP1 and TRAF2 promotes NF-κB, while its removal by CYLD facilitates the conversion of complex I to complex IIa, at which DISC is built up, leading to the induction of apoptosis as well as caspase-8-mediated

cleavage of CYLD. K-63 polyubiquitin chains may also be removed from IKKγ by CYLD, leading to the inhibition of IKK activation and reduced NF-κB activity. Conversely, loss of CYLD expression results in the K-63 polyubiquitination of TRAF2, RIP1and IKK, thereby switches apoptosis to NF-κB-mediated survival [58, 188]. Therefore, SMG7 may dictate the level of CYLD, which in turn mediates survival through activation of NF-κB. However, it is not clear how SMG7 is involved in the regulation of CYLD. One possible explanation is that SMG7-deficient cells upregulate lncRNAs and these lncRNA-derived miRNAs may have the function to regulate CYLD. Another possibility may be that these upregulated lncRNAs in *Smg7 -/-* cells are acting as transcriptional repressors on genomic DNA [75, 76], which downregulates *Cyld* mRNA. Indeed, I saw *Cyld* mRNA was downregulated in *Smg7 -/-* cells (Figure 13-1). Similarly, I also observed this positive correlation between *SMG7* and *CYLD* in RCC and a higher survival rate in RCC patients with high *SMG7* expression, which may be due to the higher CYLD level promotes tumor cell death via apoptosis.

SMG7-targeted lncRNAs *Pvt1* and *Adapt33* protect TNFα-induced apoptosis

As shown in Figure 8-3, SMG7 affected not only NMD targets but also a cluster of lncRNAs. The CRISPRa screen experiment indicated that two lncRNAs *Pvt1* and *Adapt33* as well as one protein-coding gene *Tnfrsf11b*, a decoy TNF receptor, showed protection against TNFα-induced apoptosis. Given that TNF activation of NF-κB is still possible, it is unlikely that TNFRSF11B is acting as a decoy TNF receptor at the membrane; thus, I focused on the two lncRNAs. *Pvt1* and *Adapt33* were highly increased in *Smg7 -/-* cells. Surprisingly, cells overexpressing *Pvt1* and *Adapt33* by CRISPRa were adequate to prevent parental MF cells from TNFα-induced apoptosis (Figure 8-20A). Therefore, I speculated that apart from NMD, SMG7 regulates the expression of CYLD by targeting lncRNAs, thereby inducing survival signals. However, the interaction among SMG7, *Pvt1* and CYLD can be mechanistically complicated. *Pvt1* was firstly reported in 1984 in mice [107]. It lies in the region of the famous cancer-related chromosome 8q24.21, downstream of and regulating MYC [109], which in turn is the source of a large proportion of Burkitt's lymphomas. *SMG7* was found to be highly elevated in Burkitt's lymphoma cells [189]. In MYC-driven HCT116 colon cancer cells, *PVT1* depletion dramatically diminished its tumorigenic potency, as higher MYC expression level is consistently *PVT1*-dependent [109]. It is still unknown whether *PVT1* lncRNA directly regulates CYLD, but it is clear that, in human HCC tissues, CYLD expression is negatively correlated with MYC expression level via JNK mediated signaling [190], providing a hint to this relationship.

It is widely known that lncRNAs can modulate multiple pathways simultaneously. *Pvt1* serves as a sponge for many miRNAs [116-121], especially for the mir-200 family [108]. The human *PVT1* encodes a cluster of six microRNAs [127]. *PVT1,* as well as its derived microRNAs, has oncogenic capacities [191]. Additionally, pointing to miRNAs, two miRNA miR-362-5p and miR-19 can target *CYLD* [192, 193]. Therefore, I hypothesized that those upregulated lncRNAs in *Smg7 -/-* cells could also be processed into miRNAs, subsequently target *Cyld* mRNA and cause its degradation. Indeed, *CYLD* has been shown to be targeted by many miRNAs [194-196] and *PVT1* encodes several distinct miRNAs [191, 197], although whether *PVT1* encoded miRNAs target CYLD has not been explored. Recently, several large-scale genomic studies throw some light on the functions of such multi-factorial transcripts in relation to cancers [198].

Adapt33 is broadly involved in TNF signaling and apoptosis

LncRNA *Adapt33* was reported to be induced by hydrogen peroxide or staurosporine and involved in apoptosis [158]. Recently, Zhao et al. reported that *Adapt33* promoted the proliferation of mouse ES cells by activating *Mid1* expression [159]. However, its function has not yet been demonstrated. Here in my thesis, I showed *Adapt33* was co-precipitated with RNAs involved in TNF signaling and apoptosis pathways, therefore suggesting the direction by which *Adapt33* may carry out its function. Moreover, there are several miscellaneous RNAs (misc RNAs) located within *Adapt33* locus. These misc RNAs may have a potential role in gene regulation, such as gene switches, turning genes on and off, or silencing genes with the help of RNAi [199].

RNA-RNA interactions (RRIs) analysis is an emerging experimental technique to address the complexity of many fundamental cellular activities [200]. I used 5 biotin-labeled oligos against *Adapt33* RNA to pulldown *Adapt33*-interactive RNAs in the UV light or glutaraldehyde cross-linking conditions. The top 200 enriched RNAs were mapped to the associated pathways. Interestingly, TNF signaling and apoptosis pathways were found to be the highest involved pathways, providing a hint that *Adapt33* has the capacity to participate in death and survival regulation by targeting a cluster of genes. However, the roles of *Adapt33* in controlling these genes are still unknown. Given that lncRNA can bind to RNAs and degrade the corresponding transcripts into endogenous siRNAs [75, 76], I checked the genes involved in apoptosis and NF-κB pathways with a decreased expression levels in *Smg7 -/-* cells and found a well-known gene, *Nfkbia*, which can inhibit NF-κB production (Table 8-5). *Nfkbia* is also known as IκBα, which can form an IκBα/NF-κB complex and mask the nuclear localization signals (NLS) of NF-κB, keeping it inactive in the cytoplasm [201]. IKKs promote IκB phosphorylation and

degradation, then NF-κB is released to active its target genes [202]. *Smg7 -/-* cells showed a decreased IκBα mRNA level (Log2(FC) = -0.54, Table 8-5), which may be degraded by *Adapt33* and contribute the survival signals expression. Indeed, A20, an NF-κB inducible effector, was upregulated in *Smg7 -/-* cells upon TNFα treatment (Figure 8-10C). TNF Alpha Induced Protein 3 (A20 or *TNFαip3*), a feedback inhibitor of NF-κB [203], was also found to be decreased in resting *Smg7-/-* cells (Log2(FC) = -0.73, Table 8-5). The upregulated protein level of A20 in *Smg7 -/-* cells in response to TNFα is consistent with its role in inhibiting cytokine-induced apoptosis [204]. Furthermore, *Polr3d* is an RNA polymerase and is able to transcribe miRNA [161], snRNA, tRNA and rRNA [162]. I observed depression of the *Polr3d* mRNA in *Smg7 -/-* cells compared to MF parental cells (Log2(FC) = -0.08, Table 8-5), which matches the miRNA downregulation in the global differentially expressed biotypes analysis (Figure 8-3B).

Smg7 -/- protects 3D spheroids

Unlike classical monolayer-based models, which lack many characteristics of the complex in vivo situation, 3D spheroids culture is much more similar to the original tumor, including volume growth kinetics and cellular heterogeneity [205, 206]. Thus, 3D spheroids can better mimic in vivo tissue and cellular communication and are more appropriate for pharmaceutical high-throughput screening [156]. In the present study, I generated a 3D spheroid model using *Smg7 -/-* and parental MF cells and treated these spheroids with 20 ng/mL TNFα in the presence or absence of 10 µM SC-514 IKK inhibitor. *Smg7 -/-* spheroids still showed the resistance to TNFα-induced apoptosis, while with the combination of IKK inhibitor, *Smg7 -/-* spheroids were resensitized to TNFα (Figure 8-22A), suggesting the survival due to the lack of *Smg7* was also NF-κB-dependent. These data further imply that tumor cells with a low SMG7 expression at the early stage may not be eliminated via apoptosis and have a higher chance of developing into a mature tumor. Thus, SMG7 may serve as a potential biomarker for early-stage cancer diagnosis.

Mouse xenografts are widely powerful research tools in oncology. In my study, I confirmed that MF cells could grow in the Matrigel matrix and still showed a response to TNFα induced-apoptosis. The next step would be to inject MF cells into immunocompromised mice under Matrigel conditions or use other *SMG7*-deficient human tumor cells to generate mouse models.

Cellular origins influence TNF/SMG7 induced apoptosis

The sensitivities of distinct cell lines against TNF-induced apoptosis may differ considerably, but cells can be susceptible when combined with protein synthesis inhibitors [134]. TNFα

induced apoptosis in L929 cells with or without the presence of CHX (Figure 8-23A). However, when combined with CHX, TNFα only mildly induced apoptosis in L929 cells, probably due to the fact that CHX itself caused a significant amount of cell death in both TNFα-treated and untreated groups. HCT-116 cells were sensitive to TNFα, especially with the presence of CHX. However, Hela cells can be only sensitized by TNFα in the presence of CHX. hTNFα was able to induce apoptosis in MCF-7 and HCT-116 cells in a time-dependent manner (Figure 8-23B), thus I used these two cell lines in the following experiments. These data suggest TNFα-induced apoptosis is cell type-dependent, and most of the cases, CHX promotes apoptosis when combined with TNFα.

SMG7 influences human cancer cell growth

Smg7 -/- cells showed a lower growth rate compared to parental MF cells (Figure 8-22B). Similarly, continuous knockdown of *SMG7* by CRISPRi in HCT-116 and MCF-7 cells also showed growth defects (Figure 8-24). However, the loss of SMG7 in human cells showed differential phenotypes than in mouse cells. In HCT-116 cells, loss of SMG7 resulted in cell disruption and cell death (Figure 8-24). Furthermore, this SMG7-derived cell disruption and death showed a negative correlation to the expression level of SMG7, that is, the lower the SMG7 level, the more cell death (Figure 8-24A and B). In MCF-7 cells, temporary knockdown of SMG7 by siRNA was found to be resistant to TNFα-induced apoptosis, while continuous knockdown of SMG7 resulted in growth arrest. Human cells may not tolerate the loss of SMG7 ultimately, as I could not generate *SMG7 -/-* human cell lines. Compared with the protein-coding genes, lncRNAs are often less highly conserved between species and tend to exhibit a higher degree of tissue specificity [207]. Therefore, human *SMG7* may regulate another cluster of targets in human cells rather than mouse *Smg7*-targeted lncRNAs in mouse, which leads to the cell growth defect. *SMG7* KD Hela cells did not show prominent upregulation of lncRNAs or miRNAs in the pan-transcriptome level (biotype DESeq2 analysis, log2(FC) = 0.33, p(adj) = 0.09 and log(FC) = -0.04, p(adj) = 0.94, Table 13-6), while protein-coding genes and lncRNAs made up 62% and 23% of the top 100 upregulated genes (Table 13-7), suggesting that *SMG7* only targets a specific cluster of lncRNAs other than modulates all lncRNAs in human cells. However, these human *SMG7*-targeted lncRNAs may be different than in mouse cells, which resulted in different phenotypes. Indeed, the expression levels of the entire *PVT1* gene and distinct *PVT1* transcripts were not massively changed in *SMG7* KD Hela cells (Figure 13-2). These data suggest that different from mouse *Smg7*, human *SMG7* may dominate other subtype lncRNAs to maintain cell growth and integrity in these two human cancer lines. Furthermore, human *SMG7* may also target another cluster of protein-coding

genes. Some of these shortened proteins due to lack of SMG7 are toxic to cells and affect cell phenotypes, including cell viability and growth arrest [208-211].

SMG7 does not target classic NMD β-globin transcripts

Mutated *β-globin* with a PTC at site 39 is a widely used reporter transcript in NMD functional analysis [45, 212]. In this study, I also employed a bi-directional promoter-based vector, which can transcribe a wild-type *β-globin* transcript and a mutant *β-globin* at site 39 with a PTC simultaneously under the induction of doxycycline. Unexpectedly, I did not detect a highly increased mutant *β-globin* transcript in *Smg7 -/-* cells compared to parental cells (Figure 8-25A) though *β-globin* was shown predominantly to be degraded by SMG5/SMG7-dependent pathway [45]. *Upf1 -/-* cells also showed a decreased mutant *β-globin* expression compared to wild-type *β-globin* level. Similarly, *Upf1* knockdown cells by shRNA were also detected at a comparable mutant *β-globin* level to wild-type (Figure 8-25C). These data indicate that *Smg7* and *Upf1* KO or KD independently may not abolish NMD sufficiently, at least these cells can still degrade mutant *β-globin* transcripts, or these transcripts were cleaved by other NMD factors preferentially. Indeed, Ottens et al. showed that PTC-containing transcripts constitutively involve SMG6-dependent exonucleolytic decay [174]. In Figure 8-25A, *Smg7 -/-* and *Upf1 -/-* cells were found to have even less mutant β-globin expression levels compared to parental MF cells, indicating a robust compensation regulation mechanism in response to *Smg7* and *Upf1* depletion [170]. Though the mRNA levels of most NMD factors except for *Smg5* and *Upf3b* remained unchanged in *Smg7 -/-* cells, the protein levels and biochemical kinetics of the main NMD factors still need to be further investigated to confirm the compensation regulation function. Besides the regulation at the translational level, whether there are other post-translational modifications in addition to the phosphorylation of UPF1 also need to be examined in the future. It would be also interesting to check whether double knockout of NMD factors, such as double knockout of *Smg7* and *Smg6*, can abolish the degradation of mutated *β-globin*.

Modeling SMG7 effect on apoptosis

SMG7 is an essential NMD factor and also has redundant functions in regulating apoptosis. Parental MF cells were sensitive to TNFα-induced apoptosis mediated by caspases while *Smg7 -/-* MF cells and 3D spheroids were resistant to TNFα-induced apoptosis. Loss of SMG7 resulted in lncRNAs upregulation, including *Pvt1* and *Adapt33*. Overexpression of *Pvt1* and *Adapt33* increased resistance to TNFα-induced apoptosis in parental MF cells. Moreover, CYLD played an important role in apoptosis where overexpressing *Cyld* led to apoptosis, while knockdown of *Cyld* resulted in survival against TNFα. Interestingly, SMG7 dictated CYLD

levels, which is possibly regulated by lncRNAs, including *Pvt1* and *Adapt33*, -derived miRNAs, thereby switching apoptosis to NF-κB-dependent survival upon TNFα treatment. Furthermore, *Adapt33* was co-precipitated with a cluster of RNAs involved in TNF signaling and apoptosis pathways, providing a direction for *Adapt33* to participate in the death-survival regulation.
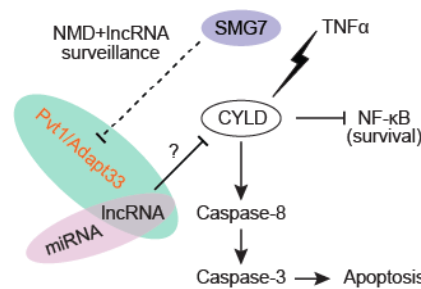
Figure 9-1. Modeling SMG7 effect on apoptosis.

Following TNFα treatment, loss of SMG7 surveillance of NMD and lncRNA targets leads to inhibition of CYLD by an uncharacterized mechanism and subsequent activation of the NF-κB survival pathway. By contrast, unmodified cells with normal SMG7/CYLD have reduced *Pvt1* and *Adapt33* levels and undergo apoptosis upon TNFα treatment. Data and figure legend were published in Molecular Oncology [136].

10. Conclusions

The extent to which long non-coding RNAs affect cell death pathways is a great unsolved question in oncology. In this study, I showed that losing the nonsense-mediated decay effector SMG7 uniquely prevented TNFα-induced apoptosis in several cell types. SMG7 degraded typical NMD targets and also showed the ability to target distinct lincRNAs. A pan-genomic mutagenesis TNFα screen indicated the insensitivity to the TNFα-induced apoptosis which is achieved by a dedicated SMG7 mechanism instead of by global destruction of NMD. A comparison of three RNA-seq data suggested *Smg7*, *Smg6* and *Upf1*-deficient mouse cells shared 6 lncRNAs out of 9 common genes in the top 1000 upregulated genes, and NMD factors could target specific alternatively spliced transcripts rather than the entire genes. NF-κB inhibitors re-sensitized *Smg7 -/-* cells and 3D spheroids to TNFα-sensitivity, indicating this resistance was NF-κB-dependent. Strikingly, this resistant effect to TNFα was coordinated through three distinct factors: CYLD, *Pvt1* and *Adapt33*. CYLD showed a positive correlation with SMG7, which was confirmed in SMG7-deficient cells and 1164 cancer cell lines from the CCLE database. CYLD overexpressing *Smg7 -/-* cells re-established TNFα-induced cell death while knockdown of *Cyld* by siRNA in parental MF cells showed partially increasing in cell viability, suggesting CYLD expression levels interferes with the cell viability. Moreover,

overexpression of *Pvt1* and *Adapt33* increased cell survival against TNFα treatment. The depressed expression level of CYLD is potentially mediated by miRNAs, including *Pvt1* derived miRNAs as *Pvt1* encodes 6 miRNAs and knockdown *Pvt1* in *Cyld* OE cells further decreased cell viability. RNA-RNA interactions analysis showed that lncRNA *Adapt33* is associated with TNF signaling pathway and apoptosis pathway. Furthermore, *Adpt33* negatively regulated two NF-κB inhibitors, *Nfkbia* and *TNFαip3*, by which they mediate NF-κB activation and generate survival signals. To summarize, these studies indicate a novel role of SMG7 in protecting TNFα-induced apoptosis through the regulation of the tumor suppressor CYLD and two lncRNA, *Pvt1* and *Adapt33*, and implicate a comprehensive role of NMD factor in the regulation of NF-κB.

11. Material and methods

11.1. Material

11.1.1. Instruments and equipment

Resource	Company
0.45 µm Millex Syringe Filter	Merck Millipore, Darmstadt, Germany
96-well plate for qPCR	Thomas Scientific, Swedesboro, NJ, USA
Bacterial culture flasks	BD, Heidelberg, Germany
Cell culture flasks	BD, Heidelberg, Germany
Cell culture plates	BD, Heidelberg, Germany
CO_2 incubator	Thermo Scientific, Waltham, MA, USA
Cooling cell culture centrifuge	Eppendorf, Hamburg, Germany
Corning 4515 plates	Corning, NY, USA
Incubator	Sartorius, Göttingen, Germany
Incubator Shaker I26	New Brunswick Scientific, Hamburg, Germany
LightCycler 480	Roche, Basel, Switzerland
Microcon centrifugal filters	Vivacon 500 30 kDa, Sartorius, Goettingen, Germany
Nanodrop 2000	Thermo Fisher Scientific, Waltham, USA
PerkinElmer Envision 2104	PerkinElmer, Waltham, MA, USA
PerkinElmer Operetta High Content Imaging System	PerkinElmer, Waltham, MA, USA

Pipettes	Eppendorf, Hamburg, Germany
Plastic filter tips TipOne (RNase free)	StarLab, Hamburg, Germany
Plastic pipettes	Greiner Bio-One, Frickenhausen, Germany
Plastic tips	Eppendorf, Hamburg, Germany
Precellys homogenizator	Bertin Technologies, Montigny‑le‑Bretonneux, France
PVDF membranes	Roth, Karlsruhe, Germany
SDS-PAGE chamber	Bio-Rad, München, Germany
semi‑dry western blot transfer system	Phase, Lübeck, Germany
Streptavidin Agarose Resin beeds	Thermo Scientific, Waltham, MA, USA
Tubes	Eppendorf, Hamburg, Germany
Ultimate 3000 nano‑RSLC	Thermo Scientific, Waltham, MA, USA
ViCell cell counter	Beckman Coulter, Brea, CA, USA

11.1.2. General chemicals

Resource	Company
4× Roti‑Load	Roth, Karlsruhe, Germany
Acrylamide/Bisacrylamide	Roth, Karlsruhe, Germany
Agar	Roth, Karlsruhe, Germany
Agarose	Biozym, Hessisch Oldendorf, Germany
Ammonium persulfate (APS)	Bio-Rad, München, Germany
Bovine serum albumin (BSA)	GE Healthcare, Freiburg, Germany
Dimethyl sulfoxide (DMSO)	Sigma-Aldrich, Taufkirchen, Germany
Dithiothreitol (DTT)	Sigma-Aldrich, Taufkirchen, Germany
DNA 1kb plus ladder	Invitrogen, Carlsbad, USA
dNTP-Mix	Thermo Fisher Scientific, Waltham, USA
Ethanol (p. a.)	Merck, Darmstadt, Germany
Ethidiumbromide	Roth, Freiburg, Germany
Ethylenediaminetetraacetic acid (EDTA)	Roth, Freiburg, Germany
formamide	Sigma-Aldrich, Taufkirchen, Germany
Glycerol	Roth, Freiburg, Germany
glycine	Sigma-Aldrich, Taufkirchen, Germany
HyperLadder 1kb, 200 Lanes	Thermo Fisher Scientific, Waltham, USA
Isopropyl alcohol (p.a.)	Merck, Darmstadt, Germany

LB	Roth, Freiburg, Germany
Lipofectamine RNAiMAX Transfection Reagent	Thermo Fisher Scientific, Waltham, USA
Lys−C	Wako Chemicals, Neuss, Germany
Methanol (p.a.)	Merck, Darmstadt, Germany
PageRuler Prestained Protein Ladder	Thermo Fisher Scientific, Waltham, USA
Paraformaldehyde (PFA)	Sigma-Aldrich, Taufkirchen, Germany
PMSF	Sigma-Aldrich, Taufkirchen,Germany
propidium iodide	Thermo Fisher Scientific, Waltham, USA
protease inhibitor cocktail	Sigma-Aldrich, Taufkirchen, Germany
SDS-PAGE buffer	Roth, Karlsruhe, Germany
skim milk	Sigma-Aldrich, Taufkirchen, Germany
Sodium chloride	Roth, Freiburg, Germany
Sodium dodecyl sulfate (SDS)	Roth, Freiburg, Germany
SSC buffer	Thermo Fisher Scientific, Waltham, USA
Tetramethylethylenediamine (TEMED)	Roth, Freiburg, Germany
Tris(hydroxymethyl)-aminomethan (Tris)	Roth, Freiburg, Germany
Trypsin	Promega, Madison, WI, USA
Tween 20	Roth, Freiburg, Germany
urea	Sigma-Aldrich, Taufkirchen, Germany
X-tremeGENE HP Transfection Reagent	Roche, Mannheim, Germany

11.1.3. Buffers and solutions

Solution	Information
Agar plates	LB (20 g/l), Agar (15 g/l)
APS-solution	APS (10 % (w/v))
Blocking buffer	BSA/milk in PBS-T (5 % (w/v))
Hybridization solution	NaCl (750 mM), SDS (1 %), Tris–HCl pH 7 (50 mM), EDTA (1 mM), formamide (15 %), PMSF (1x)
LB medium	LB (20 g/l)
Lysis buffer (MS)	Tris-HCl pH 8.5 (0.1 M), urea (8 M)
Lysis buffer (pulldown)	Tris-HCl pH 7 (50 mM), EDTA (10 mM), SDS (1 %), PMSF, protease inhibitor cocktail (1x)
Lysis buffer (WB)	Tris-HCl pH 6.8 (63 mM), glycerol (10 % (v/v)), SDS (2 % (w/v)), DTT (2.5 % (w/v)), 1x protease inhibitor cocktail
SDS-Blot-buffer	methanole (20 % (v/v)), SDS-PAGE buffer (1x)

Separation gel	Tris/HCl pH=8.8 (375 mM), Acrylamide/Bisacrylamide (6-18 %), SDS (0.1 %), APS (0.075 %), TEMED (0.05 %)
Stacking gel	Tris/HCl pH 6.8 (125 mM), Acrylamide/Bisacrylamide (5 %), SDS (0.1 %), APS (0.1 %), TEMED (0.1 %)
Stripping buffer	glycine (15 g/L), SDS (1 g/L), Tween-20 (1 % (v/v)) pH=2.2
TBS-T	Tris-HCl pH 7.5 (25mM), NaCl (150 mM), Tween-20 (0.1% (v/v))
TE (Tris EDTA) buffer	Tris/HCl pH 8.0 (10 mM), EDTA (1 mM)
Washing buffer	SSC buffer (2✗), SDS (0.5 %), PMSF (1x)

11.1.4. Cell lines

Name	Information
MCF-7	human breast adenocarcinoma cell line
NIH 3T3	mouse embryonic fibroblast cells
293T	human embryonic kidney cell line; transformed with SV40 large T antigen
L929	mouse fibroblast cell line
HT-22	mouse hippocampal neuronal cell line
Hela	human cervix cancer cell line
HCT-116	human colorectal carcinoma cell line
A549	adenocarcinomic human alveolar basal epithelial cells
MF cells	immortalized mouse fibroblasts

11.1.5. Cell culture

Resource	Company
Trypsin/EDTA	Life Technologies, Carlsbad, CA, USA
DMEM	Gibco, Grand Island, NY, USA
PBS	Thermo Fisher Scientific, Waltham, MA, USA
FBS superior	Biochrom, Berlin, Germany
Penicillin/streptomycin	Thermo Fisher Scientific, Waltham, MA, USA
L-Glutamine	Thermo Fisher Scientific, Waltham, MA, USA
F-12K	Thermo Fisher Scientific, Waltham, MA, USA
Zeocin	Life Technologies, Carlsbad, CA, USA
Puromycin	Sigma, St. Louis, MO, USA

| Blasticidine S hydrochloride | Sigma, St. Louis, MO, USA |
| Hygromycin B | Sigma, St. Louis, MO, USA |

11.1.6. Kits

Resource	Company
Caspase-Glo 3/7 Assay	Promega, Madison, WI, USA
Caspase-Glo 8 Assay	Promega, Madison, WI, USA
Wizard SV Gel and PCR Clean-Up System	Promega, Madison, WI, USA
Power SYBR Green PCR Master Mix	Thermo Fisher Scientific, Waltham, MA, USA
InviTrap Spin Cell RNA Mini Kit	Stratec, Birkenfeld, Germany
Gibson Assembly Master Mix	Ipswich, MA, USA
ECL prime western blotting detection reagent	GE Healthcare, Chicago, Illinois, USA
PureLink™ HiPure Plasmid Maxiprep Kit	Thermo Fisher Scientific, Waltham, MA, USA
Nucleospin Plasmid Mini kit for plasmid DNA purification	MACHEREY-NAGEL, Düren, Germany
KAPA HiFi plus dNTPs PCR Kit	Roche, Basel, Switzerland
RNeasy Mini Kit	Qiagen, Hilden, Germany

11.1.7. Cell viability assay

Resource	Company
hTNFα	Peprotech, Hamburg, Germany
mTNFα	Thermo Fisher Scientific, Waltham, MA, USA
Z-VAD-FMK	APExBIO Technology, Houston, TX, USA
Resazurin	Sigma, St. Louis, MO, USA
Cycloheximide	Merck, Darmstadt, Germany
TRAIL	Peprotech, Hamburg, Germany
TWEAK	Peprotech, Hamburg, Germany
LPS	Sigma, St. Louis, MO, USA
IFNγ	BioLegend, San Diego, CA, USA
SC-514	Sigma, St. Louis, MO, USA
MLN120B	Sigma, St. Louis, MO, USA

11.1.8. Enzymes

Enzyme	Company
BbsI	NEB, Ipswich, MA, USA
BsmBI	NEB, Ipswich, MA, USA
T4 ligase	NEB, Ipswich, MA, USA
AMV Reverse Transcriptase	NEB, Ipswich, MA, USA
PmeI	NEB, Ipswich, MA, USA
Proteinase K	NEB, Ipswich, MA, USA
Dnase I	Thermo Fisher Scientific, Waltham, MA, USA

11.1.9. Plasmids

Table 11-1. Plasmids used in this study.

Name (Addgene)	Identifier	RRID	Application
lenti sgRNA(MS2)_zeo backbone	61427	Addgene_61427	CRISPRa
dCAS-VP64_Blast	61425	Addgene_61425	CRISPRa
MS2-P65-HSF1_Hygro	61426	Addgene_61426	CRISPRa
pIRES Hyg3	Clontech		Cyld OE
pKLV-U6gRNA(BbsI)-Pgkpuro2ABFP	50946	Addgene_50946	UPF1 KO
pLV hU6-sgRNA hUbC-dCas9-KRAB-T2a-Puro	71236	Addgene_71236	CRISPRi
pHCMV-EcoEnv	15802	Addgene_15802	lentivirus
pRSV-Rev	12253	Addgene_12253	lentivirus
pMDLg/pRRE	12251	Addgene_12251	lentivirus
pSPAX2	12260	Addgene_12260	lentivirus
pMD2g	12259	Addgene_12259	lentivirus
pLVTHM empty Urquelle MV			shRNA
pTRE-Tight-BI-GI NORM-LacZA-TER-LacZB	86194	Addgene_86194	NMD
pLenti CMV rtTA3 Hygro	26730	Addgene_26730	NMD
CAGSlc7a1IRESPuro (mCAT1)			lentivirus

11.1.10. Antibodies

Table 11-2. Atibodies used in this study.

Name	Host	Clone	Source	Identifier	RRID
anti-A20/TNFAIP3	rabbit	D13H3	Cell Signaling	5630	AB_10698880
anti-cylindromatosis 1	mouse	E-10	Santa Cruz	sc-74435	AB_1122022
anti-Smg7	rabbit	polyclonal	Bethyl	A302-170A	AB_1659842
BID Antibody (FL-195)	rabbit	polyclonal	Santa Cruz	sc-11423	AB_2243383
Caspase-8	rabbit	D35G2	Cell Signaling	4790	AB_10545768
Cleaved Caspase-3 (Asp175)	rabbit	polyclonal	Cell Signaling	9661	AB_2341188
IκBα Mouse mAb (Amino-terminal Antigen)	mouse	L35A5	Cell Signaling	4814	AB_390781
p53	mouse	1C12	Cell Signaling	2524	AB_331743
Phospho-IκBα (Ser32/36)	mouse	5A5	Cell Signaling	9246	AB_2267145
Phospho-SAPK/JNK (Thr183/Tyr185)	rabbit	98F2	Cell Signaling	4671	AB_331338
RIP XP®	rabbit	D94C12	Cell Signaling	3493	AB_2305314
SAPK/JNK Antibody	rabbit	polyclonal	Cell Signaling	9252	AB_2250373
ß-Actin	mouse	8H10D10	Cell Signaling	3700	AB_2242334
ß-Actin	rabbit	13E5	Cell Signaling	4970	AB_2223172
TNF-R1 Antibody	mouse	H-5	Santa Cruz	sc-8436	AB_628377
TNF-R2 Antibody	rabbit	polyclonal	Cell Signaling	3727	AB_659912
TRAF2 Antibody	rabbit	polyclonal	Santa Cruz	sc-876	AB_632533
UPF1	rabbit	polyclonal	Elabscience	E-AB-13000	
anti-mouse	horse		Cell Signaling	7076	AB_330924
anti-rabbit	goat		Cell Signaling	7074	AB_2099233

11.1.11. siRNAs

Gene name	Organism	Catalogue	target sequence
SMG7	Human	EHU007301-20UG	GCAAAGAATCGAGCAAATCCGAATCGGAGTGAAG TTCAGGCAAACCTTTCTCTGTTCCTAGAGGCAGC TAGTGGCTTCTATACTCAGTTATTACAAGAACTGT GTACAGTATTTAATGTAGATTTACCATGCCGTGTG AAGTCTTCCCAATTGGGAATTATCAGCAATAAACA GACGCATACCAGCGCCATAGTGAAGCCACAGTCT AGCTCCTGTTCCTATATCTGCCAGCACTGCCTCG TCCACCTTGGAGACATTGCTCGATACAGAAACCA GACCAGCCAGGCAGAGTCCTACTATAGGCATGC AGCTCAGCTTGTCCCCTCCAATGGTCAGCCTTAT AATCAGTTGGCTATCTTAGCTTCTTCCAAAGGAGA CCATCTGACCACAATTTTCTACTACTGCAGAAGCA TTGCTGTGAAGTTCCCTTTCCCA
Smg7	Mouse	EMU150861-20UG	CCACAGAGACAGATGCACACTGTGCACAGAAGAA AACACAGCAGATGCCACTTTGGAGAGGGCAAGA GAAAGGAATAAACTCTATTTGATAATTTATATTAG GAGGAAAGAGGACTGAAGATGTTCTGTGTAGGAA CAGAAGAACGGACAGCATTTCTGTTAGTCATTTC CTGGAAAAGTAATATTTTAATGGGAAATTATGGAA ACAATCTAAATGTCCAATTGCTGTGCTAGGGTAG GGATTATTTTCTGGGAGGTGTGTGTGTGTGTGCG CGCGTGTGTGTCCCACACATGGCTTTCTACTCTC CCAGAGGGCAAGGGCTAAGTGTGGGAAATAGTG TGGAGCTTAGCTGAAGGACAGCTGTAGAGCAAA GCACATCCAGGAGCCCCAGGTGTCACTGGGGTC TGGGCAGCCCCGAAATGAGATGGGGTAAGGTAT TGCTCATTGCTCTTCAGAAAGAGTGCTTGAAGCC CCAGGCTTACTCTATTGCTCTTTTAGTTTGACATG G
EGFP		EHUEGFP-20UG	GTGAGCAAGGGCGAGGAGCTGTTCACCGGGGTG GTGCCCATCCTGGTCGAGCTGGACGGCGACGTA AACGGCCACAAGTTCAGCGTGTCCGGCGAGGGC GAGGGCGATGCCACCTACGGCAAGCTGACCCTG

			AAGTTCATCTGCACCACCGGCAAGCTGCCCGTG
			CCCTGGCCCACCCTCGTGACCACCCTGACCTAC
			GGCGTGCAGTGCTTCAGCCGCTACCCCGACCAC
			ATGAAGCAGCACGACTTCTTCAAGTCCGCCATGC
			CCGAAGGCTACGTCCAGGAGCGCACCATCTTCTT
			CAAGGACGACGGCAACTACAAGACCCGCGCCGA
			GGTGAAGTTCGAGGGCGACACCCTGGTGAACCG
			CATCGAGCTGAAGGGCATCGACTTCAAGGAGGA
			CGGCAACATCCTGGGGCACAAGCTGGAGTACAA
			CTACAACAGCCACAACGTCTATATCATGGCCGAC
			AAGCAGAAGAACGGCATCAAGGTGAACTTCAAGA
			TCCGCCACAACATCGAGGACGGCAGCGTGCAGC
			TCGCCGACCACTACCAGCAGAACACCCCCATCG
			GCGACGGCCCCGTGCTGCTGCCCGACAACCACT
			ACCTGAGCACCCAGTCCGCCCTGAGCAAAGACC
			CCAACGAGAAGCGCGATCACATGGTCCTGCTGG
			AGTTCGTGACCGCCGCCGGGATCACTCTCGGCA
			TGGACGAGCTGTA
			ATTGAGGTGGCCATTGAGAATTCAAGTGTACCTC
			TTGGTCCCTGATGCAGAAATGAAGTCCCCAGCAT
			GCTCAAGAAGAGCTTCCTTGGAGGATGAGAGGC
			ATGGGAATCTAAGTATACCCTTTAAGCGTTCCAG
			AAGGATTTTGAGATCCTTTCCTAAATCAAAGGTGG
			AATATTTGGGGATTTGGAAAATTGAGATGTGAAG
			CGTTGACTTAAGAGATGCCAAGTAACTCAGCAGA
Pvt1	Mouse	EMU19318	TGTCACACAGACGATAAATAGCAAAGATGGAAGT
		1-20UG	CTTCATGCCGGAGGCAATCCTATAAGACAGCTGA
			GTTCTGCAGAGCTGGTAGGAGACAGACTTGCTCA
			GGTGATAGATCCAGCCATGATACTGACCCTAAGA
			GAATGAGACGCTCTGCAGAAGACAGAAGATTCCT
			GAAACTGGGAAAGGTGCCTAGAAATCCTGATAAG
			AGTGAAGAAGGAGCTGGCAGAGCAGCCTTCCTC
			CGCACTATGAAAGACATCCAACAGAGAGCAAGTT
			CCC
CYLD	Mouse	EMU03111	TTTTGTTGGTGTGGACATGGATAACCCTATTGGC
		1-20UG	AACTGGGATGGAAGGTTTGATGGAGTACAGCTCT

84

GTAGTTTTGCAAGTGTTGAAAGTACAATTCTCCTG

CACATCAATGACATCATCCCAGATAGCGTGACAC

AGGAAAGGAGGCCTCCCAAACTTGCCTTTATGTC

AAGAGGTGTAGGTGACAAAGGTTCATCTAGTCAT

AATAAACCAAAGGTTACAGGATCTACCTCAGACC

CTGGAAGTAGAAACAGATCTGAATTATTTTATACC

TTAAATGGGTCATCTGTTGACTCACAACAATCCAA

GTCCAAAAATCCATGGTACATTGATGAAGTTGCA

GAAGACCCTGCAAAGTCACTTACAGAGATGTCTT

CGGACTTCGGACATTCATCTCCTCCACCGCAGCC

TCCTTCCATGAACTCCTTGTCTAGCGAGAACAGA

TTCCACTCCTTACCCTTCAGCCTGACA

11.1.12. PCR primers

Table 11-3. PCR primers used in this study.

Name	Sequence
Actin qPCR forward	CCTCTATGCCAACACAGTGC
Actin qPCR reverse	GTACTCCTGCTTGCTGATCC
Adapt33 qPCR forward	TCCTCATGAGAGAACGCTTTT
Adapt33 qPCR reverse	CATCACCGAGAACACAATTCC
Anril qPCR forward	AACCAAGAGCATGGTGTACTCA
Anril qPCR reverse	GAGGAGGTCGCTGTGTCAG
GAPD qPCR forward	GGGTTCCTATAAATACGGACTGC
GAPD qPCR reverse	CCATTTTGTCTACGGGACGA
Gas5 qPCR forward	GGCTCCTGTGACAAGTGGAC
Gas5 qPCR reverse	AATGGTAAAATTTTAACACAATATATCTGACAC
Hotair qPCR forward	GCCCCTTGAAACCCTCTT
Hotair qPCR reverse	GATGGGGATGATAAGGAGAGC
Malat1 qPCR forward	GACCCTTCACCCCTCACC
Malat1 qPCR reverse	AAGACGAATTGGGCATAACCT
Pvt1 qPCR forward	CGGAGGCAATCCTATAAGACA
Pvt1 qPCR reverse	GCTGGATCTATCACCTGAGCA
Smg1 qPCR forward	CTGTAAAGCAGCTGAAGGAGTTT
Smg1 qPCR reverse	TCATGAACAGCAGCCAAGAT

Smg5 qPCR forward	GCCTGTTACAGCCCAAAAGT
Smg5 qPCR reverse	GGTGAGGAGGGCAGGTAGA
Smg6 qPCR forward	TCTGAGCAGGAGAATGGTCTG
Smg6 qPCR reverse	TGGAGAAAACTGAGGATGAACC
Smg7 qPCR forward	TGCTGTGAAATTCCCTTTCC
Smg7 qPCR reverse	CTTCTCTCGAAGAGGGCTCA
Upf1 qPCR forward	AGATCACGGCACAGCAGAT
Upf1 qPCR reverse	CTCCAGAGTGGCTGAAGGAT
Upf2 qPCR forward	ACCTCCTAGCAGGGCTAGTTC
Upf2 qPCR reverse	GCACTACTGATACGCCTCTGG
Upf3b qPCR forward	TTTTGGAGAGTTATGCCACAGA
Upf3b qPCR reverse	AAGGGGCGTTGTCCTTTTAG
Cyld qPCR forward	CGGGGATTTTCTTTGGAGTAG
Cyld qPCR reverse	AAACACGCCACAGTCCTCAT
CYLD plasmid forward	GTACAGGCCTTAAGCCGGCGCGCTAGCGCCACCATGAGTTCAGGCCTGT
CYLD plasmid reverse	TTATCTATGTTAACGTACGATATCCTATTTGTACAGGCTCATGGTTGGA
OE library preparation forward	CCATCTCATCCCTGCGTGTCTCCGACTCAGCTAAGGTAACGGCTTTATATATCTTGTGGAAAGGACG
OE library preparation reverse	CCTCTCTATGGGCAGTCGGTGATCTGCAGACATGGGTGATCCTCAT
mUPF1 genotyping forward	GGTACTGTGCTCTGGGTTCT
mUPF1 genotyping reverse	GTAGAGGAGCACGGGATTCA

11.1.13. Guide sequences

Table 11-4. Guide sequences used in this study.

Name	Sequence
Mouse 2410004N09Rik CRISPRa guide 1	CGTTCGGCCGGTCCCTTTGT
Mouse 2410004N09Rik CRISPRa guide 2	GGCCGGAACGGACTGTACCA
Mouse 2410004N09Rik CRISPRa guide 3	AGGGAGAAGTGCATCGCGGG
Mouse 2410006H16Rik CRISPRa guide 1	GCGTGAGCGCCCTCCTCTTA
Mouse 2410006H16Rik CRISPRa guide 2	CCCCCGTTCTGTTGAGCGAG
Mouse 2410006H16Rik CRISPRa guide 3	TCGCTACCCAGAATCCCCCG

Mouse 2700099C18Rik CRISPRa guide 1	AGCGCGTTGAGCCGCCGATG
Mouse 2700099C18Rik CRISPRa guide 2	GTCGGTGTCGGCGACCTGAA
Mouse 2700099C18Rik CRISPRa guide 3	CGCCGACACCGACGATGACC
Mouse 5430416N02Rik CRISPRa guide 1	TACCGCGACTCGAGCTCTCG
Mouse 5430416N02Rik CRISPRa guide 2	TTGACCGGAAGGGCGGGCTT
Mouse 5430416N02Rik CRISPRa guide 3	AGGCGCCAGGCCTCTCCGAT
Mouse 6820431F20Rik CRISPRa guide 1	ATTGGGCGGAGCCTATGACC
Mouse 6820431F20Rik CRISPRa guide 2	TATGACCAGGCGCCCAGCTC
Mouse 6820431F20Rik CRISPRa guide 3	GTCATAGGCTCCGCCCAATG
Mouse Accsl CRISPRa guide 1	GCTTCAGCTGAAGTGTTCAC
Mouse Accsl CRISPRa guide 2	CCAAGGCCATCTAGATAATG
Mouse Accsl CRISPRa guide 3	TAGCCTCCTTCGAAGAGCAG
Mouse Agtpbp1 CRISPRa guide 1	GCGCAGCTTGTCTTCCCTCC
Mouse Agtpbp1 CRISPRa guide 2	GGGAAGGGCGCTTCCAGGGA
Mouse Agtpbp1 CRISPRa guide 3	AAGGTCGGGTGGGTACCAAG
Mouse AI662270 CRISPRa guide 1	CAAAATATAGGACCTCTGAT
Mouse AI662270 CRISPRa guide 2	GACCTTCTTTACTTGCTTAT
Mouse AI662270 CRISPRa guide 3	GCCACAGAAATAATACTAAG
Mouse Atp2b4 CRISPRa guide 1	GAAGCCCTGGGTAGGCCTGC
Mouse Atp2b4 CRISPRa guide 2	GAACAATTAGAACAGCCATG
Mouse Atp2b4 CRISPRa guide 3	CGAGAGTACCTTGCAGATCC
Mouse Car6 CRISPRa guide 1	AACAATTTACCAGGTCCAGC
Mouse Car6 CRISPRa guide 2	CTCAGTGGGCGCAGCAAGGG
Mouse Car6 CRISPRa guide 3	ATTGGCTATGGTAATGCCCT
Mouse Cngb1 CRISPRa guide 1	AGGACACTGCTGGACCCGTG
Mouse Cngb1 CRISPRa guide 2	GGATTAGCATGTGCAGAATC
Mouse Cngb1 CRISPRa guide 3	ACTAGATGGGCCGGGTGCAA
Mouse Cox7b2 CRISPRa guide 1	GACAGGTACTGGATTCGCCT
Mouse Cox7b2 CRISPRa guide 2	GGTAAATGAGGTCATTTGAT
Mouse Cox7b2 CRISPRa guide 3	GGTCAGATTGGAACATTGGA
Mouse Fam13b CRISPRa guide 1	GGGTGCGGAGGTCCTGTGCC
Mouse Fam13b CRISPRa guide 2	GGAGGATTCGGGAGGGATGA
Mouse Fam13b CRISPRa guide 3	CGCCGAATCCGGGTTGACCG
Mouse Gas5 CRISPRa guide 1	GGAGTTGCCGCGGGCACGAT
Mouse Gas5 CRISPRa guide 2	GCGGCTGAGTCGAGTATATA
Mouse Gas5 CRISPRa guide 3	AGGAGTCTGAGGGCGTGTGA

Mouse Gm20756 CRISPRa guide 1	CATGCTCCAGGCACGAACTC
Mouse Gm20756 CRISPRa guide 2	CATGAGTAGTCTAACTTGGC
Mouse Gm20756 CRISPRa guide 3	GCAGTTTTACTGCGCATGTT
Mouse Klf4 CRISPRa guide 1	AAGAAGCGCGCGGCGGCCGC
Mouse Klf4 CRISPRa guide 2	ACCATGGCAACGCGCAGTGG
Mouse Klf4 CRISPRa guide 3	ATAAACAAACTCCGCGCACG
Mouse Lars2 CRISPRa guide 1	GCCCTGGGCGAGCAGCTTGG
Mouse Lars2 CRISPRa guide 2	GCAGAATTTGTACCGATAGC
Mouse Lars2 CRISPRa guide 3	ATTGTAAGACCGGGACAATC
Mouse Nupr1 CRISPRa guide 1	AGAGGGCAGACATTCAGACA
Mouse Nupr1 CRISPRa guide 2	TATAAGTAGGGTGAGAAACT
Mouse Nupr1 CRISPRa guide 3	TGCTCAGGACTGCTGTCTAT
Mouse Parp6 CRISPRa guide 1	CGGAAGAGGACACCTGATCG
Mouse Parp6 CRISPRa guide 2	GCGCAGTGATCCAGAGTTGA
Mouse Parp6 CRISPRa guide 3	ACCGCGGTGCGTGCTGTACC
Mouse Poli CRISPRa guide 1	AGGCTAGGCCGTGGTTTCCT
Mouse Poli CRISPRa guide 2	AAACAGCCCGAGCGTGGCAG
Mouse Poli CRISPRa guide 3	GAATGAGAAAGATCTGGTTG
Mouse Pvt1 CRISPRa guide 1	GCGGCTCGCTCCCGGCCGCG
Mouse Pvt1 CRISPRa guide 2	GGGGGAGAAGCGCGCGCCAC
Mouse Pvt1 CRISPRa guide 3	CGCGTGTGTCCCCGATCTCC
Mouse Smg7 CRISPR guide	TACTCAGGTATACATGACCG
Mouse Smg7 CRISPRi guide	GCGGCGACCGCCAGCACCCG
Mouse Snhg1 CRISPRa guide 1	GGTAGAGGAATCCGCCCAAA
Mouse Snhg1 CRISPRa guide 2	AAAGAGGCGCAGGCGCTTTA
Mouse Snhg1 CRISPRa guide 3	TCGCAAAGGCCCACGGGATT
Mouse Snhg12 CRISPRa guide 1	CCTGATAGTGGTTTCGACCC
Mouse Snhg12 CRISPRa guide 2	ACCTGACGCACGGCGCCTCT
Mouse Snhg12 CRISPRa guide 3	GGCGCGAGAGTATATAATCC
Mouse Snhg15 CRISPRa guide 1	TAGTGGCGGTTGATCGAATG
Mouse Snhg15 CRISPRa guide 2	GTGGTGACGTTACGCGTGCG
Mouse Snhg15 CRISPRa guide 3	GCGGGTTAAACCCGCGCTCG
Mouse Snhg5 CRISPRa guide 1	AACGGAGATGCACGCGGCGG
Mouse Snhg5 CRISPRa guide 2	CTTTTCATGAAGCAACGCGT
Mouse Snhg5 CRISPRa guide 3	TCGCGTCCAATCAGTGACAG
Mouse Snhg6 CRISPRa guide 1	TGTGTTTCTAGTGGGGCGGA

Mouse Snhg6 CRISPRa guide 2	GCCTTAGGGTCGCGCACGCT
Mouse Snhg6 CRISPRa guide 3	CCGGAAGAGGCGGGGCCTAC
Mouse Snrnp48 CRISPRa guide 1	AAGGTGTTTCCACGCTCTTC
Mouse Snrnp48 CRISPRa guide 2	GCGGAATGATGCTCAAAGCT
Mouse Snrnp48 CRISPRa guide 3	CCGGGATGGCGCCAGCCTAT
Mouse Sulf1 CRISPRa guide 1	AATCTCAGGTTACTTGGCTG
Mouse Sulf1 CRISPRa guide 2	GTAGAGCGAATGAATTATTC
Mouse Sulf1 CRISPRa guide 3	CTCTTACGGATTGGAGGCGG
Mouse Sulf1 CRISPRa guide 4	AGCAGAGGCACAAGTTCCAC
Mouse Sulf1 CRISPRa guide 5	AAGATGCAGTTATATAAGCC
Mouse Sulf1 CRISPRa guide 6	TGTGATGATAATAATACGCC
Mouse Taf1d CRISPRa guide 1	AGGTGAGCGTCGATTTGTTG
Mouse Taf1d CRISPRa guide 2	TGAGTACACGTTGGTGGGCG
Mouse Taf1d CRISPRa guide 3	AAAGAAGGCCTTCCTGCAAG
Mouse Tnfrsf11b CRISPRa guide 1	CACCGCTGAGCTGAAGAACA
Mouse Tnfrsf11b CRISPRa guide 2	TTCTGCCAGCGGCTAGCCTC
Mouse Tnfrsf11b CRISPRa guide 3	CAGCTGTGACCTGTGGTGAG
Mouse Uggt2 CRISPRa guide 1	GTAGATTGGCATGGAAGGCT
Mouse Uggt2 CRISPRa guide 2	GCTGCAGTCCGTTAGTCCGC
Mouse Uggt2 CRISPRa guide 3	GGCGGCCCTGCGTAGGCAAG
Mouse Upf1shRNA_for	CGCGTCCCCGATGCAGTTCCGTTCC ATCTTCAAGAGAGATGGAACGGAACT GCATCTTTTTGGAAAT
Mouse Upf1shRNA_rev	CGATTTCCAAAAAGATGCAGTTCCGT TCCATCTCTCTTGAAGATGGAACGGA ACTGCATCGGGGA
Mouse mUpf1 CRISPR guide	GAGCCCTGCAGCATACCTGC
Human Smg7 CRISPRi guide 1	GCTCCTCCTCGCTCGGCAGG
Human Smg7 CRISPRi guide 2	GCGGCGGCCGCCAGCACCCG
Human Smg7 CRISPRi guide 3	CTCCTCCTCGCTCGGCAGGG
Human Smg7 CRISPRi guide 4	GGCGCAGGGACACTCCGACC
Human Smg7 CRISPRi guide 5	GGCTCCTCGGAGCGGCCCCG
Adapt33_pulldown_116	GTTTCCACCTCTCTACTCCC
Adapt33_pulldown_228	ACATCGAGAGCTCCTGTGCC
Adapt33_pulldown_377	CCAACGTCACGCATCTCTTC
Adapt33_pulldown_422	AACATCCTTTGATTTCATTC

11.2. Methods

The methods have been partially published in Molecular Oncology [136] as indicated in the citation.

11.2.1. Cell culture conditions

MCF-7, NIH 3T3, 293T, L929, HT-22, Hela, HCT-116 and A549 cells were acquired from American type culture collection (ATCC). MCF-7, immortalized mouse fibroblasts (MF) cells, NIH 3T3, 293T, L929, HT-22, Hela and HCT-116 were cultured in DMEM supplemented with 10% FBS Superior, 100 µg/mL streptomycin and 100 U/mL penicillin at 37°C in a humidified atmosphere incubator plus 5% CO_2. A549 cells were cultured in Ham's F-12K medium in the same condition. All cell lines were constantly checked for morphological compliance with ATCC specifications and mycoplasma were tested regularly. See the original publication in Molecular Oncology [136].

11.2.2. Cell viability assays

If not otherwise specified, cell viability assays were performed as follows. Cell viability assays were carried out on 96-well plates. $3x10^3$ cells were counted by a ViCell cell counter and seeded in each well treated with the respective compounds as indicated in the specific experiments. In the experiments, the respective compounds were first dissolved in 100 µL of medium as the initial concentration, followed by a series of dilutions by the 2-fold dilution method. Cells without drug treatment were used as a blank control. Cells were prepared in 100 µL of medium, 100 µL of medium containing respective compounds were added directly from above to a 96-well plate. 16 h later, resazurin was finally added to 200 µL of medium to reach a final concentration of 50 µM and incubated for 6 h. Fluorescence was measured using a PerkinElmer Envision 2104 Multilabel plate reader at 540 nm excitation / 590 nm emission. At least three technical repetitions of each condition were performed and the average was used to calculate the cell viability relative to respective control. The cell growth rate experiments were carried out in a 12-well plate. $3x10^4$ cells were seeded in each well and counted by a ViCell cell counter. See the original publication in Molecular Oncology [136].

11.2.3. Generation of cell lines

Knockout of *Smg7* by CRISPR Cas9 in MF was previously described [51]. Gene overexpression cell lines and gene knockdown cell lines were generated by the CRISPRa [154] and CRISPRi [137] techniques respectively. The gene transcriptional start sites were identified by FANTOM5 [213] and top guides within two hundred bp on either side of the gene transcription start sites were selected in the UCSC genome browser [214]. *Adapt33* or *Pvt1* overexpressing cell lines were generated using the CRISPRa technique and the same guides as used in the CRISPR activation screen experiment (Table 11-4). *Cyld* overexpression MF cell line was generated using the linearized pIREShyg3 vector containing *Cyld* cDNA. The full-length of murine *Cyld* ORF was amplified from the cDNA library of parental MF cell (Table 11-3). *Cyld* containing vector or empty control vector was transfected into MF *Smg7 -/-* cells with X-tremeGENE HP at a ratio of 1:3 (DNA:reagent). 48 h post transfection, cell pools were selected with 250 µg/mL Hygromycin B for one week. See the original publication in Molecular Oncology [136]. *Upf1* KO and KD were obtained by CRISPR and shRNA. The respective guides were cloned into pKLV-U6-gRNA(BbsI)-Pgkpuro2ABFP or pLVTHM empty Urquelle MV plasmid (Table 11-1). Then lentivirus was made to infect parental MF cells. KO or KD efficiency were confirmed by Western blot and qPCR.

11.2.4. CRISPR activation screen

In the CRISPR activation screen experiment, I chose the 31 upregulated genes from MF *Smg7 -/-* RNAseq data. Three guides were designed for each gene (six guides were designed for *Sulf* as *Sulf* has 2 TSSs, Table 11-4). In total, 96 guides were cloned into lenti sgRNA(MS2)_zeo backbone (gift from Feng Zhang, Addgene #61427) and 97 vectors (including one empty control) were used to make the mini lentiviral library. Next, lentiviral library was introduced to the MF-dCas9-MS2 screening cells as previously reported [154]. 48 h post infection, cells were treated with 200 µg/mL Zeocin for selection in a 10cm-dish for 5 days. After that, the surviving cells were transferred into a full six-well plate ($3x10^5$ cells per well) and challenged with 20 ng/mL TNFα. The total selection time was five days, and the fresh medium containing TNFα was changed every two days. After this step, genomic DNA was purified from TNFα-selected and untreated control pools and DNA fragments containing guide sequences was amplified with the specific primers as shown in Table 11-3. PCR products were sequenced on an Iontorrent platform and analyzed as described [51]. See the original publication in Molecular Oncology [136].

11.2.5.   siRNA knockdown

Mission esiRNAs of murine *Smg7* (EMU150861), murine *Cyld* (EMU031111), murine *Pvt1* (EMU193181), human *SMG7* (EHU007301) and *EGFP* (EHUEGFP) control were achieved from Sigma. The following is a brief description of the siRNA knockdown experiment. For mouse cells (MF and NIH 3T3) or human cancer cells (MCF-7), $5x10^4$ cells or $1x10^5$ cells in 500 µL medium were seeded in 24-well plates one day prior. The next day, 30 pmol siRNAs were added in 100 µL serum-free medium and mixed gently. Then 2 µL Lipofectamine RNAiMAX Transfection Reagent was added to the medium containing siRNA and incubated at room temperature for 10 min. Next, the siRNA solution was added directly onto the cells. Two days later, the cells were harvested and used in downstream experiments. See the original publication in Molecular Oncology [136].

11.2.6.   qPCR

Cells were collected and washed with PBS on ice and then frozen in liquid nitrogen. Total RNA was purified by InviTrap Spin Cell RNA Mini Kit according to the manufacturer's instructions. The concentration and quality were analyzed using Nanodrop. Then 500 ng RNA was mixed with random hexamer primer, dNTPs and AMV Reverse Transcriptase in a total volume of 10 µL for first-strand cDNA synthesis according to the manufacturer's instructions. The qPCR was conducted on a LightCycler 480 using the qPCR standard protocol. The qPCR program consists of 3 steps: an initial denaturation step of 95°C for 10 min; 40 cycles of denaturation at 95°C for 15 sec and annealing and extension at 60°C for 1 min; a melting curve analysis to demonstrate the uniqueness of the amplification product. Relative expression levels were calculated by the comparative $2^{-\Delta\Delta Cp}$ method by comparing to control conditions. *Gapdh* or *Actin* was employed as a reference gene. See the original publication in Molecular Oncology [136]. qPCR primers are listed in Table 11-3.

qPCR standard protocol

Component	Amount
cDNA (2.5 ng/µL)	4.9 µL
5' primer	0.05 µL
3' primer	0.05 µL
Power SYBR Green PCR Master Mix	5 µL
	In total10 µL

11.2.7. Western blotting

Cells were vortexed in lysis buffer evenly and lysed on ice for 30 min. Cell lysate was sonicated to break DNA and centrifuged for 20 min at max speed at 4°C. Then the clear supernatant was transferred to a new tube and mixed with respective volume of 4x Roti-Load buffer. Cell lysate as well as the proper marker were loaded on a 6-18% gradient SDS-PAGE gel. Next, the proteins were transferred onto methanol-activated PVDF membranes using electrophoretic semi-dry western blot transfer system. Membranes were blocked for 1 h in 5% skim milk TBS-T solution at room temperature then transferred into specific primary antibodies solutions (diluted 1:1000 in 2.5% BSA or 5% milk in TBS-T) overnight at 4°C. On the next morning, membranes were removed from primary antibodies and washed 3 times for 5 min in TBS-T. Then membranes were incubated in HRP-coupled secondary antibodies with the dilution of 1:2000 in 5% milk TBS-T for another 1 h at room temperature. Protein expression levels were detected by chemiluminescence using ECL prime Western blotting detection reagent following the manufacturer's instructions. The Western blotting results were confirmed at least twice independently. See the original publication in Molecular Oncology [136]. Antibodies used in this dissertation are listed in Table 11-2.

11.2.8. Lentiviral transduction

Lentivirus used in this dissertation were generated by the respective transfer vectors combined with vectors of pHCMV-EcoEnv (Addgene #15802), pMDLg/pRRE (Addgene #12251), pRSV-Rev (Addgene #12253) or pSPAX (Addgene #212260), pMD2g (Addgene #12259). Briefly, fresh 293T cells were seeded in a 10 cm dish one day prior to 70% confluency. Plasmids and X-tremeGENE HP were firstly diluted with 500 µL serum-free medium at a ratio of 1:3 (DNA:reagent) respectively. Then 500 µL of plasmids solution was mixed with 500 µL of X-tremeGENE HP solution and incubated at room temperature for 15 min, followed by the addition of 1 mL transfection complex onto 293T cells. 3 days later, the supernatant containing lentivirus was filtered through a 0.45 µM Millex Syringe Filter and introduced onto the respective cells. 2 days after infection, antibiotic drugs were used to select cells and generate pools. See the original publication in Molecular Oncology [136]. Human cell lines were transfected with mouse receptor for ecotropic virus (mCAT1, Table 11-1) one day before infection.

11.2.9. Luminescence assay

Caspase-8 and caspase-3/7 activities were measured by the Caspase-Glo 8 and 3/7 Assay Systems according to the manufacturer's operating manual. In short, in a 96-well plate,

1.5×10^4 *Smg7 -/-* or parental MF cells per well were seeded one day in advance. Cells were treated with 20 ng/mL TNFα for 8 h or left untouched on the second day. After removing the medium, the cells were washed twice with 100 µL PBS. 50 µL reagent and 50 µL PBS were mixed together in the 96-well plate and incubated at room temperature with constant shaking. The luminescence was measured after 20 min using an Envision 2104 Multilabel plate reader. All values were deducted from empty wells, which were used as blanks. See the original publication in Molecular Oncology [136].

11.2.10. 3D spheroid culture

To compensate for the different growth rates of the two cell lines, 1000 *Smg7 -/-* cells and 500 parental MF cells per well were seeded into Corning 4515 plates. 4 days later, cells were treated with 20 ng/mL TNFα in the presence of 10 µM SC-514 or not. On the second day, the medium was replaced by the fresh medium containing 20 ng/mL TNFα and 10 µM SC-514. On the third day, the medium was removed and the spheroids were stained with 1 µg/mL propidium iodide (PI) for 1 h. Then the spheroids were imaged under brightfield (BF) and 535/30 nm excitation and 595/70 nm emission channel by a PerkinElmer Operetta High Content Imaging System. See the original publication in Molecular Oncology [136].

11.2.11. Quantitative mass spectrometry

Triplicates of 1×10^7 *Smg7 -/-* and parental MF cells were lysed in lysis buffer using a Precellys homogenisator. Same amounts of protein were proteolyzed according a modified FASP method [215]. In short, proteins were reduced and alkylated using DTT and IAA, then centrifuged on Microcon centrifugal filters followed by 3 washes with lysis buffer and 2 washes with 50 mM ammonium bicarbonate. The proteins were digested by 0.5 µg Lys-C and 1 µg trypsin for 2 h at room temperature and 16 h at 37°C, respectively. Peptides were centrifuged at 14000 g for10 min to elute and acidified in 0.5% trifluoroacetic acid then stored at -20°C for the subsequent analysis. As mentioned before, approximately 0.5 µg of peptides for each sample were analyzed using a Q-Exactive HF mass spectrometer online coupled to an Ultimate 3000 nano-RSLC in data-independent acquisition (DIA) mode [216]. The raw data from mass spectrometer were analyzed by a series of software including the Spectronaut Pulsar software [217] (identification false discovery of peptide and protein < 1%), an in-house mouse spectral meta library (produced by Proteome Discoverer 2.1), the Byonic search engine (Protein Metrics) and the Swissprot Mouse database (release 2016_02). Quantification was conducted based on MS2 area levels of all unique peptides for each protein, meeting the percentile 0.3 setting. The relative fold-changes and *p*-values were calculated by the normalized protein quantifications. See the original publication in Molecular Oncology [136].

11.2.12. RNA sequencing and analysis

Triplicate samples were collected from *Smg7 -/-* and parental MF cells. Total RNA was isolated by a RNeasy Mini Kit and sent for RNAseq on an Illumina HiSeq 4000 platform. Ribosomal RNA (rRNA) was subtracted from total RNA and runs were performed as 150 bp paired-end. In this dissertation, RNAseq raw data were analyzed on Galaxy platform by alignment to mouse genome (mm10.gtf) using Salmon transcript quantification function [218]. Transcript-to-gene mapping was performed using gencode vM17 transcripts as a reference transcriptome and Broad IGV was used to visualize the transcripts data for *Smg7 -/-* and parental MF cells. Biotypes were annotated at Ensembl/gencode using the Biomart function. Transcript counts of less than one were not included in the study. DESeq2 was used to identify the significance of *Smg7 -/-* and parental cells for each biotype [219]. TopHat and Cufflinks were used to conduct differential gene expression analysis on rRNA-depleted samples [220] using the default program settings of Galaxy based on mouse genome (version mm10). The proportion of long non-coding RNA was calculated by TopHat alignment with the reference file gencode.vM12.lncRNA_transcripts.fa. The FPKM level of each gene was calculated by the default settings of the Cuffdiff program. See the original publication in Molecular Oncology [136]. *Smg6* and *Upf1* RNAseq data were downloaded from SRA (accession number: PRJNA215086 and PRJNA548061) and analyzed at Galaxy using Salmon transcript quantification function. Gencode vM25 transcripts with rRNA deletion were used as the reference transcriptome and differentially expressed genes (DEGs) analysis, as well as differentially expressed biotypes, was conducted by DESeq2. Biotypes were annotated at bioDBnet using db2db function (https://biodbnet-abcc.ncifcrf.gov/db/db2db.php#biodb). Human *SMG7* KD and corresponding control RNAseq data were downloaded from SRA with accession number PRJNA340370. DEGs analysis was performed at Galaxy using DESeq2 function. RNA-seq reads were mapped to gencode v34 transcripts using Salmon quant function. Differentially expressed biotype analysis was conducted using DESeq2 function with the replacement of "transcript ID to gene ID list" to "transcript ID to gene biotype list".

11.2.13. Gene set enrichment analysis

Gene set enrichment analysis (GSEA) in *Smg7 -/-* cells was performed using the top 100 up- and downregulated genes as described previously [221]. See the original publication in Molecular Oncology [136]. Gene set enrichment analysis of the top 200 upregulated genes in *Adapt33* RNA precipitation was performed by Metascape [160].

11.2.14. *SMG7* and *CYLD* correlation analysis

Cumulative CCLE [189] data of *SMG7* and *CYLD* RNA expression (Expression Public 19Q1) was acquired from the public database DepMap [150]. Then the data were imported into GraphPad Prism for linear regression and Pearson coefficient analysis. See the original publication in Molecular Oncology [136].

11.2.15. Association between *SMG7* and *CYLD* and patient survival

Transcriptome information of Kidney Renal Clear Cell Carcinoma (KIRC) and patient data were acquired from the The Cancer Genome Atlas [151] on 15th December 2019. The relevance of *SMG7* and *CYLD* RNA expression levels were presented by Pearson values using R (version 3.53). The correlation between SMG7 protein expression levels and patient survival rates were shown in a Kaplan-Meier plot. Significance analysis was established using Log-rank test and univariate Cox regression and the plot figures were generated using ggplot2 [222]. In short, 40 tumor samples were centered into nearest neighbor values based on the expression levels of *CYLD*. See the original publication in Molecular Oncology [136].

11.2.16. Global NMD examination in MF cells

β-globin expressing plasmid (pTRE-Tight-BI-Gl NORM-LacZA-TER-LacZB) and pLenti CMV rtTA3 Hygro were co-transfected into *Smg7* -/-, *Upf1* -/-, *Ufp1* KD and parental cells MF cells using X-tremeGENE HP Transfection Reagent. *β-globin* expression was induced by 1 μg/mL Doxi for 36 h. Cells were harvested and RNA was purified by InviTrap Spin Cell RNA Mini Kit. Plasmid DNA was removed by DNase I then *β-globin* relative expression levels were determined by qPCR.

11.2.17. *Adapt33* RNA cross-link precipitation

30 million *Smg 7-/-* cells were cross-linked on ice with 254 nm UV-C at 200 mJ/cm^2 or at room temperature with 1% glutaraldehyde in 20 mL of PBS for 10 min. Then 2 ml of 1.25 M glycine was added to quench glutaraldehyde for 5 min. Cross-linked *Smg 7-/-* cells were lysed in 2 ml lysis buffer and sonicated, following with the subsequential centrifugation at 14000 g 4°C for 20 min. Then 50 μL High Capacity Streptavidin Agarose Resin beads were washed 3 times in lysis buffer and added into the lysate mixed with 2 mL of Hybridization solution for pre-clearing for 30 min at 4°C. After removing the beads by centrifugation, 200 pmol probes were added into the UV and glutaraldehyde cross-linked samples and hybridized rotating at 37°C for 4 h. In parallel, 200 μL Streptavidin beads were blocked in hybridization solution for 30 min at 4°C. Afterwards, the blocked beads were added into the samples containing probes and rotated at

37°C for 30 min to harvest the RNAs. The beads were washed five times with 1 mL washing buffer for 5 min at 37°C then treated with Proteinase K at 50°C for 30 min on a thermostatic shaker. The RNA was extracted using InviTrap Spin Cell RNA Mini Kit and eluted in 50 µL H_2O for 15 min at 95°C shaking. The enrichment of *Adapt33* mRNA was checked by qPCR and then sent to RNAseq. Data analysis was performed using DEseq2 by comparing to *Smg7 -/-* cells.

11.2.18. 3D cell culture in Matrigel

Matrigel was thawed on ice. 100µL Matrigel was mixed with 100µL ice-cold medium containing 2×10^3 cells and TNFα at the final concentration of 20 ng/mL. Cell viabilities were measured 12, 48, and 96 h post-treatment by the addition of Resazurin to a final concentration of 50 µM.

11.2.19. Statistics / Data analysis

GraphPad Prism was used to conduct the general statistics and graphical analysis. If not specified otherwise, significance was calculated using Student's two-tailed, unpaired t-test versus corresponding control. See the original publication in Molecular Oncology [136].

12. Acknowledgments

For the last four years, I have had a lot of great moments and many memories here that I'll never forget. I enjoyed a lot in Munich and learned a lot through my project.

Firstly, I express my sincere gratitude to my supervisor Dr. Joel Schick for giving me this opportunity to join his lab and experiencing a great time in the past four years. His cheerful and optimistic personality, as well as rigorous attitudes for scientific research, inspired me to work harder and get promoted. Owning to the useful help and warm encouragement he offered, I had overcome lots of difficulties during my Ph.D. study. Furthermore, besides the study, he did help me a lot in my life in Munich. The technique and knowledge I learned in his lab will become an essential foundation for my further study in science.

My sincere thanks to Prof. Dr. Rainer Glaß, thank him for being an exemplary doctor father and in my Thesis Committee. His scientific advice and inspiring talk helped a lot to solve problems in my thesis.

I would like to say thanks to Prof. Dr. Thomas Floss for attending my Thesis Committee and giving me constructive suggestions. Thank Dr. Thomas Schwarzmayr and Susanne Pfeiffer for the RNAseq experiment; Juliane Merl-Pham and Stefanie M. Hauck for quantitative mass spectrometry experiment and analysis; Xuanwen Bao for human cancer date analysis; Susanne Pfeiffer and Vanessa Kraft for their helps with my experiments and figure optimization.

Special thanks to the Chinese scholarship council for financial support during my study in Germany.

I would like express my heartfelt thanks to my colleagues, Moritz Ludwig, Prof. Dr. Martin Göttlicher, Dr. Torben Gehring, Thomas Seeholzer, Hongli Yin, Shan Xin, Vera Kühne, Franz Kiefer, Dr. Kenji Schorpp, Thomas O´Neill, Dr. Sean Lin, Dr. Andreas Gewies, Stefanie Brandner, Johanna Kössl and Scarllet Dornauer for their scientific and non-scientific helps and their companionship. This will leave a great memory in my PhD study. Special thanks to Hongli Yin for proof reading my thesis and Susanne Pfeiffer for reviewing the Zusammenfassung.

Thank my friends Yuan Guo, Xiang Zhang, Xin Cao, Zhongmin Li, Xianming Wang, Jiangli Zhang, etc. We spent so many unforgettable moments together and I hope our friendship will last forever.

Finally, I would like to show my appreciation to my family. Their supports and encouragements reaffirmed my confidence and made my academic life more colorful. Whenever I meet difficulties, they will help me without any hesitation. I am indebted to my dear parents for the

love and care they gave me and my brother Lifu Yang for taking care of my parents when I study in Germany. Special thanks to dear Jing for six years of companionship and wish us to have a bright future.

13. Appendix

13.1. Supplemental tables

Table 13-1. DESeq2 analysis results in *Smg7-/-* cells.

In the DESeq2 analysis process, "transcript ID to gene ID list" was replaced by "transcript ID to gene biotype list". All the subtypes of pseudogenes, TR genes, and IG genes were merged into one category, respectively. NA, not available.

Biotypes	Base mean	log2(FC)	StdErr	Wald-Stats	P-value	P-adj
lincRNA	806129.96	1.15	0.03	43.49	0	0
antisense	199552.96	0.61	0.03	17.5	0	0
protein_coding	95938450.5	-0.39	0.03	-13.45	0	0
pseudogene	2041739.59	-0.33	0.03	-12.91	0	0
nonsense_mediated_decay	3233943.56	0.26	0.03	9.93	0	0
miRNA	2573.54	-0.62	0.06	-9.78	0	0
sense_intronic	22955.6	0.47	0.05	9.16	0	0
IG_gene	87.99	-2.48	0.27	-9.08	0	0
snoRNA	5076.17	-0.34	0.05	-7.5	0	0
snRNA	1988.59	0.49	0.08	6.52	0	0
TEC	223118.8	0.19	0.03	5.73	0	0
retained_intron	3483563.59	-0.14	0.03	-5.37	0	0
non_stop_decay	2301.04	0.33	0.07	4.89	0	0
bidirectional_promoter_lncRNA	22027.97	-0.13	0.03	-3.79	0	0
sense_overlapping	1296	-0.27	0.11	-2.48	0.01	0.02
ribozyme	60.64	-0.76	0.31	-2.45	0.01	0.02
macro_lncRNA	287.56	0.36	0.16	2.31	0.02	0.03
processed_transcript	2989534.78	-0.05	0.03	-1.65	0.1	0.14
TR_gene	41.14	0.53	0.36	1.48	0.14	0.18

scaRNA	187.17	0.25	0.19	1.32	0.19	0.23
rRNA	167.45	0.18	0.22	0.83	0.41	0.49
Mt_tRNA	6527.85	0.05	0.06	0.79	0.43	0.49
misc_RNA	1451.05	-0.05	0.08	-0.6	0.55	0.6
scRNA	0.87	0.1	0.21	0.5	0.62	0.64
3prime_overlapping_ncRNA	1	0.04	0.22	0.19	0.85	0.85
sRNA	0	NA	NA	NA	NA	NA

Table 13-2. DESeq2 analysis results in *Smg6* KO cells.

In the DESeq2 analysis process, "transcript ID to gene ID list" was replaced by "transcript ID to gene biotype list". All the subtypes of pseudogenes, TR genes, and IG genes were merged into one category, respectively.

Biotypes	Base mean	log2(FC)	StdErr	Wald-Stats	P-value	P-adj
lincRNA	1453723.02	0.32	0.08	3.89	0	0
sense_intronic	58641.12	-0.27	0.1	-2.7	0.01	0.06
TEC	1487606.69	0.18	0.07	2.71	0.01	0.06
bidirectional_promoter_lncRNA	32282.43	-0.29	0.13	-2.33	0.02	0.08
Mt_rRNA	158235.72	0.36	0.15	2.35	0.02	0.08
nonsense_mediated_decay	9281421.92	0.25	0.1	2.38	0.02	0.08
misc_RNA	46438.59	0.34	0.16	2.17	0.03	0.11
antisense	507107.69	-0.1	0.07	-1.42	0.16	0.48
pseudogene	9567822.37	-0.16	0.12	-1.38	0.17	0.48
sense_overlapping	4966	-0.19	0.17	-1.12	0.26	0.68
processed_transcript	9697995.13	0.11	0.11	1.02	0.31	0.73
retained_intron	11110225.53	0.09	0.11	0.82	0.41	0.89
3prime_overlapping_ncRNA	39.07	0.01	0.04	0.21	0.83	0.96
IG_gene	125.17	-0.01	0.08	-0.16	0.87	0.96

macro_lncRNA	164.31	0.04	0.09	0.4	0.69	0.96
miRNA	227655.14	0.04	0.14	0.28	0.78	0.96
Mt_tRNA	30407	-0.09	0.17	-0.56	0.57	0.96
non_stop_decay	8032.08	0.04	0.16	0.26	0.79	0.96
protein_coding	147206925.7	0.01	0.12	0.08	0.93	0.96
ribozyme	8299.84	0.09	0.14	0.66	0.51	0.96
scaRNA	886.1	0.01	0.14	0.05	0.96	0.96
scRNA	5.99	-0.01	0.03	-0.24	0.81	0.96
snoRNA	21086.34	0.03	0.13	0.2	0.84	0.96
snRNA	11623.96	0.1	0.16	0.6	0.55	0.96
sRNA	2.24	0	0.03	-0.05	0.96	0.96
TR_gene	250.02	-0.01	0.09	-0.14	0.89	0.96

Table 13-3. DESeq2 analysis results in *Upf1 KD* cells.

In the DESeq2 analysis process, "transcript ID to gene ID list" was replaced by "transcript ID to gene biotype list". All the subtypes of pseudogenes, TR genes, and IG genes were merged into one category, respectively.

Biotypes	Base mean	log2(FC)	StdErr	Wald-Stats	P-value	P-adj
miRNA	82801.47	3.87	0.08	51.51	0	0
retained_intron	780450.54	-0.12	0.02	-6.67	0	0
snRNA	852.89	0.48	0.08	6.3	0	0
lincRNA	250370.99	-0.14	0.03	-5.49	0	0
ribozyme	585.62	0.54	0.1	5.29	0	0
misc_RNA	13116.13	0.6	0.12	5.15	0	0
protein_coding	21103933.19	-0.18	0.04	-4.41	0	0
TEC	50298.33	0.23	0.05	4.35	0	0

	Base mean	log2(FC)	StdErr	Wald-Stats	P-value	P-adj
processed_transcript	571160.33	-0.15	0.04	-4.15	0	0
bidirectional_promoter_lncRNA	3457.93	-0.2	0.05	-4.02	0	0
non_stop_decay	1962.33	-0.23	0.06	-3.79	0	0
IG_gene	123.09	-1	0.28	-3.62	0	0
scRNA	2.58	2.07	0.71	2.92	0	0.01
snoRNA	444.07	0.19	0.08	2.35	0.02	0.04
pseudogene	567570.18	0.07	0.03	2.26	0.02	0.04
sense_intronic	3929.14	0.16	0.08	1.95	0.05	0.08
macro_lncRNA	4.85	0.9	0.55	1.63	0.1	0.16
Mt_rRNA	19591.43	0.07	0.06	1.29	0.2	0.28
sense_overlapping	328.86	-0.15	0.18	-0.83	0.41	0.56
scaRNA	56.71	0.11	0.16	0.72	0.47	0.62
antisense	29872.74	-0.01	0.02	-0.6	0.55	0.68
Mt_tRNA	648.97	0.05	0.13	0.42	0.68	0.8
nonsense_mediated_decay	635528.64	0.01	0.01	0.37	0.71	0.8
sRNA	0.08	0.16	1.04	0.15	0.88	0.95
3prime_overlapping_ncRNA	1	-0.02	0.86	-0.02	0.98	0.99
TR_gene	120.84	0	0.21	0.01	0.99	0.99

Table 13-4. DESeq2 results from 9 common genes under 3 conditions.

Gene ID	Condition	Base mean	log2(FC)	StdErr	Wald-Stats	P-value	P-adj
	Smg7	8776.36	3.18	0.04	75.99	0	0
Snhg12	Smg6	18577.5	2.2	0.17	13.35	0	0
	Upf1	259.5	0.48	0.07	6.69	0	0
	Smg7	9999.44	2.21	0.04	53.25	0	0
Ddit3	Smg6	2830	1.16	0.21	5.41	0	0

Gene	Condition	Base mean	log2(FC)	StdErr	Wald-Stats	P-value	P-adj
	Upf1	948.35	0.51	0.15	3.33	0	0.01
Zfas1	Smg7	26720.54	3.27	0.03	118.91	0	0
	Smg6	48936.36	2.97	0.15	19.72	0	0
	Upf1	927.43	0.51	0.06	8.85	0	0
Rasgrf2	Smg7	44.35	2.25	0.42	5.4	0	0
	Smg6	106.17	1.38	0.38	3.67	0	0
	Upf1	2.75	0.48	0.15	3.29	0	0.01
Pvt1	Smg7	25279.84	3.6	0.03	122.9	0	0
	Smg6	4609.28	1.24	0.17	7.12	0	0
	Upf1	143.71	0.6	0.1	6.02	0	0
Gm42546	Smg7	4862.67	1.54	0.04	37.16	0	0
	Smg6	3395.05	1.56	0.2	7.85	0	0
	Upf1	31.68	0.52	0.15	3.45	0	0
2410006H16Rik	Smg7	24421.58	2.68	0.03	85.06	0	0
	Smg6	50345.63	2.53	0.17	15.01	0	0
	Upf1	1098.56	0.52	0.05	9.58	0	0
Snhg6	Smg7	8067.23	2.28	0.04	62.89	0	0
	Smg6	31793.05	2.21	0.15	14.85	0	0
	Upf1	192.67	0.48	0.09	5.55	0	0
Snhg16	Smg7	4992	2.77	0.05	52.18	0	0
	Smg6	7463.06	1.24	0.19	6.66	0	0
	Upf1	149.19	0.58	0.12	4.96	0	0

Table 13-5. DESeq2 results on transcripts of 9 common genes under 3 conditions.

Condition	Transcript ID	Base mean	log2(FC)	StdErr	Wald-Stats	P-value	P-adj
Smg7	Snhg12-206	8678.23	3.43	0.05	68.3	0	0

	Snhg12-207	113.26	-0.65	0.24	-2.65	0.01	0.03
Smg6	Snhg12-206	11406.53	3.49	0.11	32.99	0	0
	Snhg12-202	1006.47	1.55	0.25	6.21	0	0
Upf1	Snhg12-206	183.89	0.47	0.08	6.06	0	0
	Snhg12-208	31.27	0.6	0.18	3.43	0	0.01
Smg7	Ddit3-201	9238.45	2.42	0.05	49.62	0	0
	Ddit3-203	627.71	1.09	0.16	6.64	0	0
Smg6	Ddit3-203	998.96	1.1	0.24	4.65	0	0
	Ddit3-201	1418.89	0.94	0.2	4.63	0	0
Upf1	Ddit3-201	777.71	0.26	0.06	4.66	0	0
Smg7	Zfas1-205	26510.4	3.71	0.03	112.61	0	0
	Zfas1-201	1049.74	0.58	0.1	5.94	0	0
Smg6	Zfas1-206	19799.13	3.54	0.11	33.66	0	0
	Zfas1-205	1412.35	3.11	0.25	12.23	0	0
	Zfas1-203	22703.72	3.19	0.12	26.79	0	0
	Zfas1-201	2657.69	0.89	0.13	6.82	0	0
Upf1	Zfas1-205	724.88	0.57	0.04	13.09	0	0
	Zfas1-204	25.34	0.68	0.18	3.69	0	0
	Zfas1-201	84.19	0.42	0.15	2.74	0.01	0.04
Smg7	Rasgrf2-205	20.27	2.24	0.53	4.22	0	0
Upf1	Rasgrf2-202	1.66	0.83	0.23	3.53	0	0
Smg7	Pvt1-201	7790.31	3.9	0.06	66.26	0	0
	Pvt1-204	1657.45	3.56	0.09	41.69	0	0
	Pvt1-207	4228.02	3.66	0.07	50.31	0	0
	Pvt1-208	6206.59	3.78	0.05	69.35	0	0

	Pvt1-210	1631.78	3.63	0.1	34.95	0	0
	Pvt1-203	2667.19	3.13	0.1	30.21	0	0
	Pvt1-205	428.44	3.2	0.17	18.41	0	0
	Pvt1-206	348.05	2.59	0.29	8.87	0	0
	Pvt1-202	187.49	0.49	0.19	2.59	0.01	0.03
Smg6	Pvt1-208	529.91	1.47	0.25	5.8	0	0
	Pvt1-210	865.6	1.38	0.25	5.5	0	0
	Pvt1-201	750.72	1.44	0.28	5.19	0	0
	Pvt1-206	683.32	1.08	0.3	3.62	0	0
	Pvt1-205	133.87	1.11	0.36	3.12	0	0.02
Upf1	Pvt1-201	34.45	0.71	0.23	3.14	0	0.01
	Pvt1-210	23.89	0.61	0.2	2.99	0	0.02
Smg7	Gm42546-201	4853.9	1.53	0.04	39.42	0	0
Smg6	Gm42546-201	3327.31	1.44	0.21	6.74	0	0
Upf1	Gm42546-201	31.65	0.58	0.16	3.59	0	0
Smg7	2410006H16Rik-201	24355.83	2.67	0.03	90.13	0	0
Smg6	2410006H16Rik-201	48928.25	2.43	0.16	15.65	0	0
Upf1	2410006H16Rik-201	1097.78	0.51	0.05	10.53	0	0
Smg7	Snhg6-203	6208.16	2.43	0.04	66.97	0	0
	Snhg6-204	1092.51	2.21	0.08	26.23	0	0
	Snhg6-205	401.77	-0.31	0.13	-2.39	0.02	0.05
Smg6	Snhg6-203	10527.17	2.38	0.1	23.51	0	0
	Snhg6-204	17973.34	2.12	0.12	18.11	0	0
Upf1	Snhg6-204	58.54	0.67	0.16	4.16	0	0
Smg7	Snhg16-204	3609	4.05	0.14	29.68	0	0

Smg6	Snhg16-205	716.67	1.26	0.2	6.33	0	0
	Snhg16-214	193.26	1.2	0.39	3.07	0	0.02
Upf1	Snhg16-207	11.29	0.99	0.24	4.09	0	0
	Snhg16-204	53.85	0.59	0.22	2.65	0.01	0.05

Table 13-6. DESeq2 analysis results in *SMG7* KD Hela cells.

Biotype	Base mean	log2(FC)	StdErr	Wald-Stats	P-value	P-adj
TEC	34168.73	0.48	0.09	5.15	0.00	0.00
snoRNA	3081.25	-0.62	0.13	-4.68	0.00	0.00
ribozyme	1185.11	-0.68	0.19	-3.63	0.00	0.00
scRNA	1492.28	-0.99	0.28	-3.54	0.00	0.00
rRNA	11919.05	0.61	0.19	3.22	0.00	0.01
lncRNA	1456128.77	0.33	0.16	2.13	0.03	0.09
Mt_tRNA	46752.39	0.3	0.14	2.22	0.03	0.09
snRNA	3084.80	-0.34	0.16	-2.16	0.03	0.09
Mt_rRNA	481747.79	0.29	0.16	1.84	0.07	0.15
misc_RNA	27515.12	0.32	0.18	1.73	0.08	0.17
vaultRNA	6.47	0.65	0.41	1.59	0.11	0.22
scaRNA	144.14	-0.4	0.27	-1.48	0.14	0.22
TR_gene	14.41	-0.53	0.36	-1.49	0.14	0.22
non_stop_decay	26251.74	-0.16	0.21	-0.74	0.46	0.69
processed_transcript	2930189.41	-0.05	0.08	-0.65	0.52	0.72
retained_intron	3603177.15	-0.06	0.11	-0.54	0.59	0.77
IG_gene	45.78	-0.06	0.38	-0.15	0.88	0.94
miRNA	1167.02	-0.04	0.17	-0.22	0.83	0.94
nonsense_mediated_decay	2513969.87	-0.02	0.10	-0.24	0.81	0.94
protein_coding	52788345.33	-0.01	0.09	-0.13	0.90	0.94
pseudogene	647962.03	0	0.12	0.02	0.99	0.99
sRNA	0	NA	NA	NA	NA	NA

Table 13-7. Biotypes of top 100 up and down genes in human *SMG7* KD Hela cells.

Biotype	up	Biotype	down
protein_coding	62	protein_coding	40
lncRNA	23	lncRNA	22
processed_transcript	6	processed_pseudogene	12
retained_intron	3	retained_intron	5
nonsense_mediated_decay	2	unprocessed_pseudogene	5
processed_pseudogene	2	nonsense_mediated_decay	4
TEC	1	processed_transcript	4
unprocessed_pseudogene	1	snoRNA	3
		transcribed_unprocessed_pseudogene	2
		transcribed_processed_pseudogene	1
		transcribed_unitary_pseudogene	1
		miRNA	1

13.2. Supplemental figures
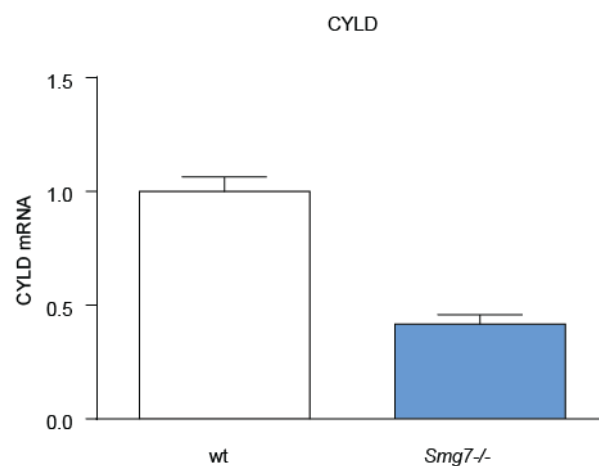
Figure 13-1. *Cyld* expression level in *Smg7 -/-* cells.

qPCR quantification of *Cyld* mRNA in *Smg7 -/-* and parental MF cells. Experiment was conducted by Susanne Pfeiffer and me.
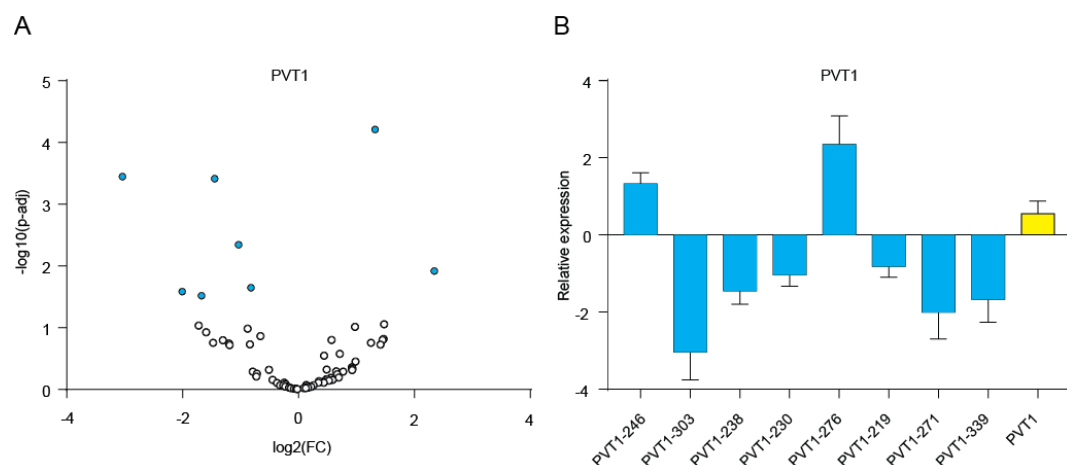
Figure 13-2. Expression levels of *PVT1* in human *SMG7* KD Hela cells.

(**A**) Volcano plot of all the *PVT1* transcripts in *SMG7* KD Hela cells compared to control cells. Blue dots indicate the expression levels with significant *p*-adj ≤ 0.05. (**B**) Bar chart of *PVT1* transcripts in *SMG7* KD Hela cells with significant *p*-adj ≤ 0.05. Yellow bar represents the expression level of the entire *PVT1* gene. Data are shown as log2(FC) ± SD. RNASeq data were downloaded from SRA with accession number PRJNA340370 and analyzed with DESeq2 at Galaxy platform.

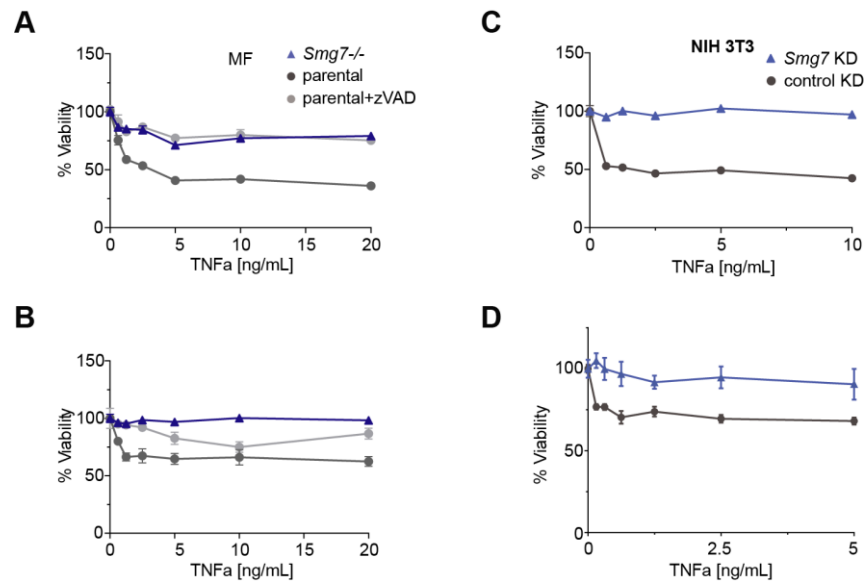**Figure 13-3. TNFα dose-response curves in *Smg7 -/-* MF cells and *Smg7* KD NIH 3T3 cells.**

(**A** and **B**) The other two replicate experiments of Figure 8-1A. (**C** and **D**) Two other representative experiments of Figure 8-1B. Viability is represented as mean ± SEM of n = 4 (**A**, **B** and **C**) or 3 (**D**) technical replicates.
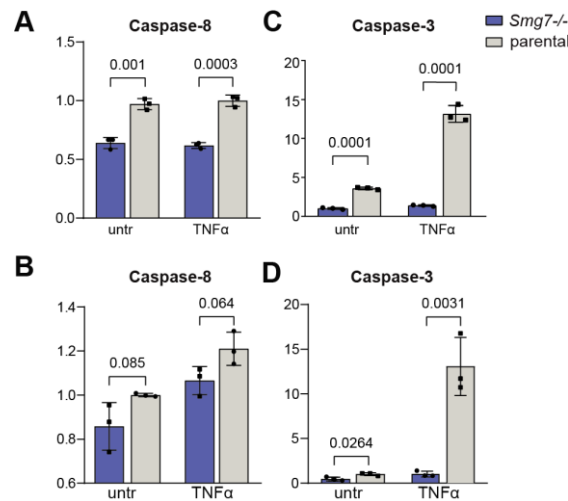

Figure 13-4. *Smg7 -/-* blocks caspases-8 and -3 activities.

The other two representative experiments of Figure 8-10A. Data were shown as mean ± SD of n = 3 technical replicates. untr, untreated.
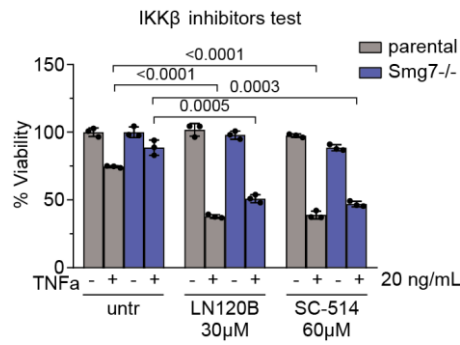
Figure 13-5. IKKβ inhibitors SC-514 and MLN120B sensitize cells to apoptosis.

A similar experiment corresponding to Figure 8-12A. Cells were pre-treated with IKK inhibitors (30 µM of MLN120B or 60 µM of SC-514) for 2 h followed by 20 ng/mL TNFα treatment. Viability is represented as mean ± SD of n = 3 technical replicates. untr, untreated.
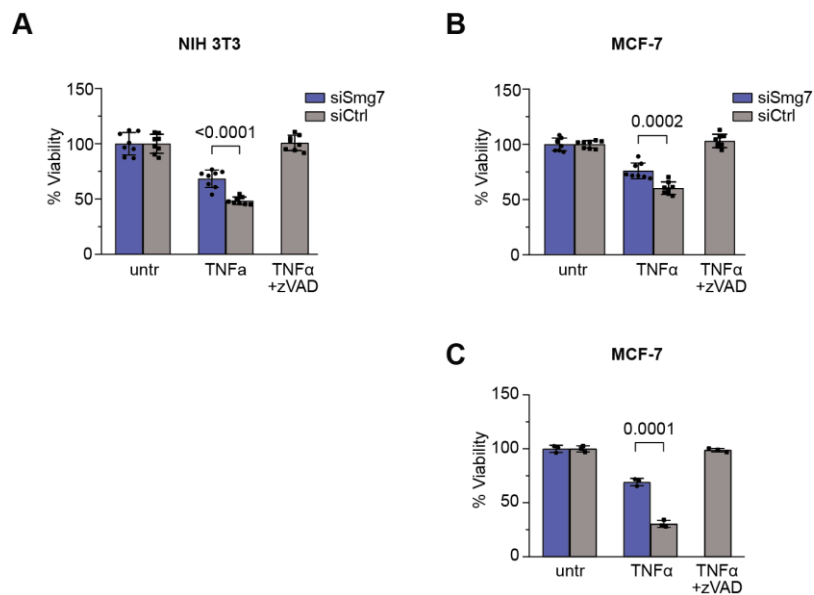

Figure 13-6. *SMG7* KD rescues cells from TNFα-induced apoptosis.

(**A**) An additional representative experiment of Figure 8-13A. (**B** and **C**) Two replicated experiments of Figure 8-13B. Viability data are represented as mean ± SD of n = 8 (**A** and **B**) or 3 (**C**) technical replicates. untr, untreated.
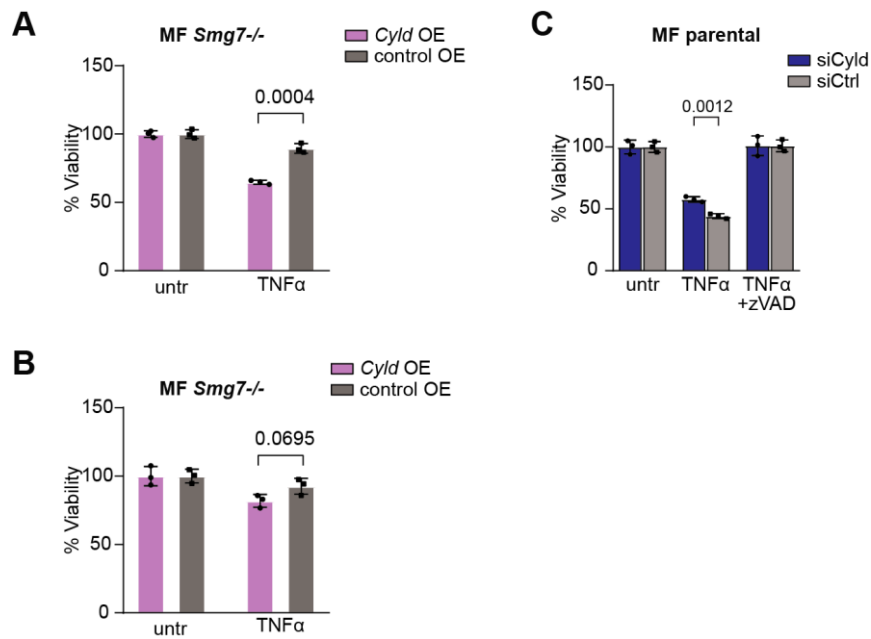
Figure 13-7. CYLD controls apoptosis in MF cells.

(**A** and **B**) Two similar repetitions of Figure 8-14A. (**C**) An alternative representative experiment of Figure 8-14B. Viability data are represented as mean ± SD of n = 3 technical replicates. untr, untreated.
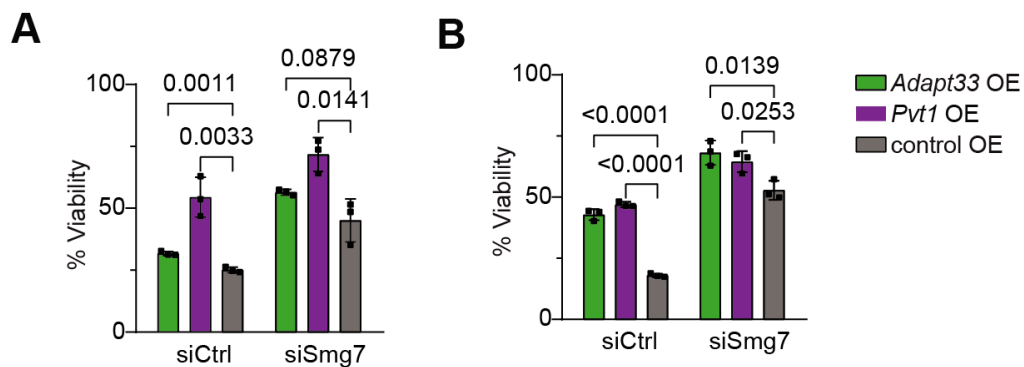

Figure 13-8. Overexpression of *Pvt1* and *Adapt33* decrease sensitivity to apoptosis.

Another two typical results of Figure 8-20A. Viability is shown as mean ± SD of n = 3 technical replicates.
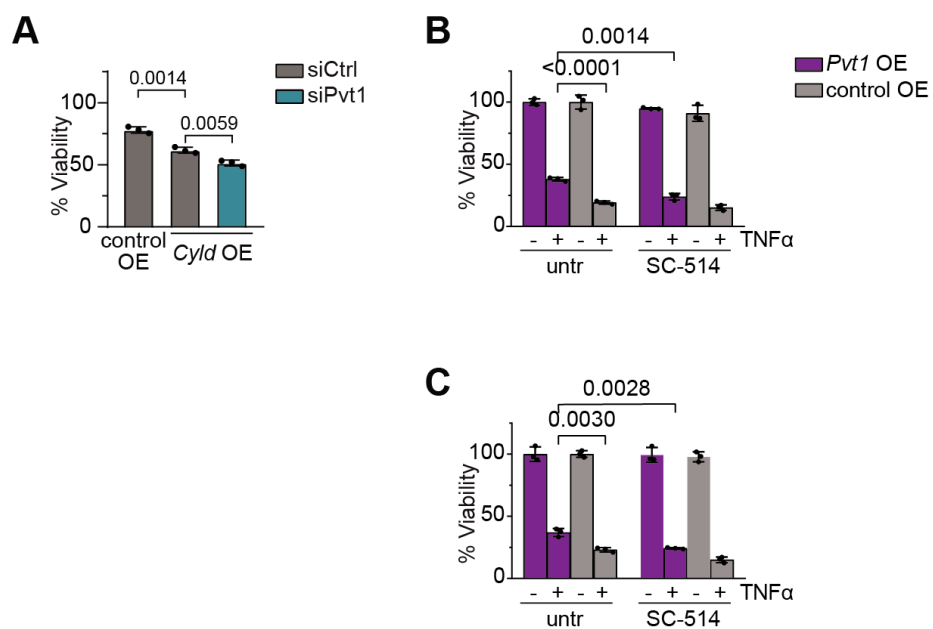
Figure 13-9. Overexpressing cells can be re-sensitized by *Pvt1* KD and SC-514.

The relevant unpublished data of Figure 8-21A (**A**) and Figure 8-21B (**B** and **C**). Viability is shown as mean ± SD of n = 3 technical replicates. untr, untreated.
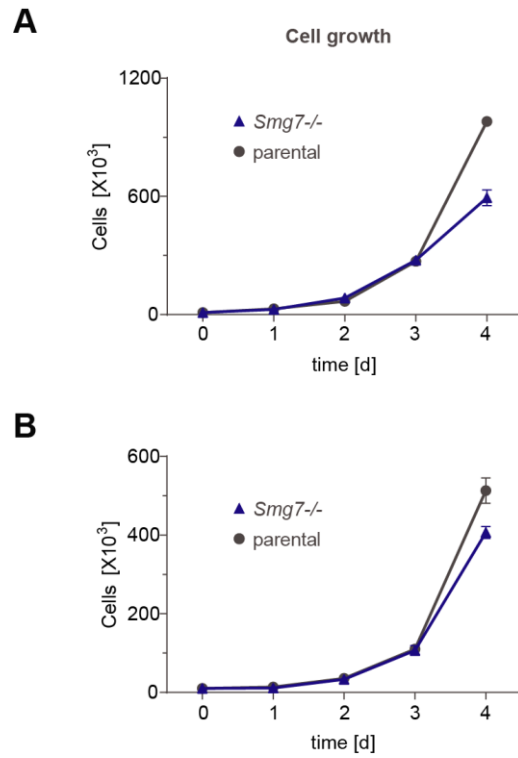
Figure 13-10. Growth characteristics of *Smg7 -/-* MF cells.

Similar experiments corresponding to Figure 8-22B. Cells were counted in n = 3 technical replicates. 1 or $2x10^4$ cells were seeded in (**A**) or (**B**).
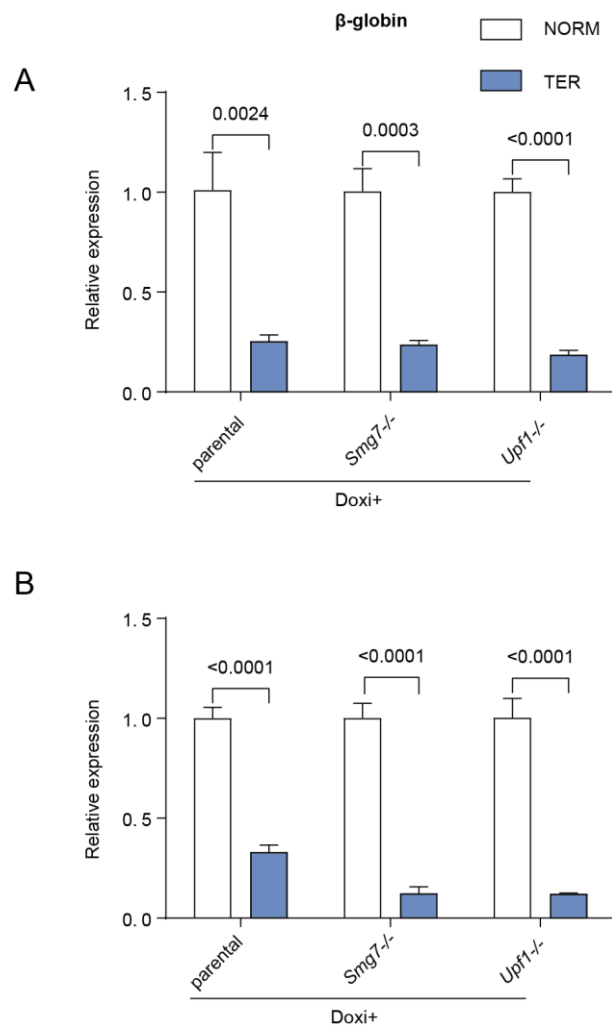
Figure 13-11. Global NMD examination in MF cells.

Two similar experiments of Figure 8-25A. Data are shown as mean ± SD of n = 3 technical replicates. NORM, wt β-globin. TER, mutated β-globin. Doxi, doxycycline.

13.3. Publication

Yang L, Kraft V A N, Pfeiffer S, et al. Nonsense‑mediated decay factor SMG7 sensitizes cells to TNFα‑induced apoptosis via CYLD tumor suppressor and the noncoding oncogene *Pvt1*[J]. Molecular Oncology, 2020.

* Part of the data in this dissertation has been published in Molecular Oncology [136] under a Creative Commons Attribution (CC BY) License.

13.4. Affidavit

Yang Limeng

_____

Surname, first name

_____

Street

_____

Zip code, town, country

I hereby declare, that the submitted thesis entitled:

Nonsense-mediated decay factor SMG7 sensitizes cells to TNFα-induced apoptosis via CYLD tumor suppressor and the noncoding oncogene *Pvt1* and lncRNA *Adapt33*

………

is my own work. I have only used the sources indicated and have not made unauthorized use of services of a third party. Where the work of others has been quoted or reproduced, the source is always given.

I further declare that the submitted thesis or parts thereof have not been presented as part of an examination degree to any other university.

Shanghai, 16052022   Limeng Yang

_____   _____

place, date   Signature doctoral candidate

13.5. Confirmation of congruency

Yang Limeng

_____

Surname, first name

_____

Street

_____

Zip code, town, country

I hereby declare, that the submitted thesis entitled:

Nonsense-mediated decay factor SMG7 sensitizes cells to TNFα-induced apoptosis via CYLD tumor suppressor and the noncoding oncogene *Pvt1* and lncRNA *Adapt33*

………………………………………………………………………………………………………

.

is congruent with the printed version both in content and format.

Shanghai, 16052022   Limeng Yang

_____   _____

place, date   Signature doctoral candidate

14. List of references

1.	Maquat LE, Kinniburgh AJ, Rachmilewitz EA, Ross J. Unstable β-globin mRNA in mRNA-deficient β0 thalassemia. Cell. 1981;27(3):543-53.
2.	Losson R, Lacroute F. Interference of nonsense mutations with eukaryotic messenger RNA stability. Proceedings of the National Academy of Sciences. 1979;76(10):5134-7.
3.	Peltz SW, Brown AH, Jacobson A. mRNA destabilization triggered by premature translational termination depends on at least three cis-acting sequence elements and one trans-acting factor. Genes & development. 1993;7(9):1737-54.
4.	Kurihara Y, Matsui A, Hanada K, Kawashima M, Ishida J, Morosawa T, Tanaka M, Kaminuma E, Mochizuki Y, Matsushima A. Genome-wide suppression of aberrant mRNA-like noncoding RNAs by NMD in Arabidopsis. Proceedings of the National Academy of Sciences. 2009;106(7):2453-8.
5.	Frischmeyer PA, Van Hoof A, O'Donnell K, Guerrerio AL, Parker R, Dietz HC. An mRNA surveillance mechanism that eliminates transcripts lacking termination codons. Science. 2002;295(5563):2258-61.
6.	Karousis ED, Nasif S, Muhlemann O. Nonsense-mediated mRNA decay: novel mechanistic insights and biological impact. Wiley Interdiscip Rev RNA. 2016;7(5):661-82.
7.	Kurosaki T, Maquat LE. Nonsense-mediated mRNA decay in humans at a glance. J Cell Sci. 2016;129(3):461-7.
8.	Karousis E, Mühlemann O. In vitro study of aberrant translation termination in the context of NMD-sensitive mRNAs. 2017.
9.	Brogna S, McLeod T, Petric M. The meaning of NMD: translate or perish. Trends in Genetics. 2016;32(7):395-407.
10.	He F, Jacobson A. Nonsense-Mediated mRNA Decay: Degradation of Defective Transcripts Is Only Part of the Story. Annu Rev Genet. 2015;49:339-66.
11.	Leeds P, Peltz S, Jacobson A, Culbertson M. The product of the yeast UPF1 gene is required for rapid turnover of mRNAs containing a premature translational termination codon. Genes & development. 1991;5(12a):2303-14.
12.	Maquat L. Nonsense-mediated mRNA decay: a comparative analysis of different species. Current Genomics. 2004;5(3):175-90.
13.	Ender C, Krek A, Friedlander MR, Beitzinger M, Weinmann L, Chen W, Pfeffer S, Rajewsky N, Meister G. A human snoRNA with microRNA-like functions. Molecular cell. 2008;32(4):519-28.
14.	Yamashita A, Izumi N, Kashima I, Ohnishi T, Saari B, Katsuhata Y, Muramatsu R, Morita T, Iwamatsu A, Hachiya T, Kurata R, Hirano H, Anderson P, Ohno S. SMG-8 and SMG-9, two novel subunits of the SMG-1 complex, regulate remodeling of the mRNA surveillance complex during nonsense-mediated mRNA decay. Genes Dev. 2009;23(9):1091-105.
15.	Kashima I, Yamashita A, Izumi N, Kataoka N, Morishita R, Hoshino S, Ohno M, Dreyfuss G, Ohno S. Binding of a novel SMG-1-Upf1-eRF1-eRF3 complex (SURF) to the exon junction complex triggers Upf1 phosphorylation and nonsense-mediated mRNA decay. Genes Dev. 2006;20(3):355-67.
16.	Le Hir H, Izaurralde E, Maquat LE, Moore MJ. The spliceosome deposits multiple proteins 20–24 nucleotides upstream of mRNA exon–exon junctions. The EMBO journal. 2000;19(24):6860-9.
17.	Le Hir H, Sauliere J, Wang Z. The exon junction complex as a node of post-transcriptional networks. Nat Rev Mol Cell Biol. 2016;17(1):41-54.
18.	Nagy E, Maquat LE. A rule for termination-codon position within intron-containing genes: when nonsense affects RNA abundance. Trends in biochemical sciences. 1998;23(6):198-9.
19.	Ware M, DeSilva D, Sinilnikova O, Stoppa-Lyonnet D, Tavtigian S, Mazoyer S. Does nonsense-mediated mRNA decay explain the ovarian cancer cluster region of the BRCA2 gene? Oncogene. 2006;25(2):323-8.

20.   Eberle AB, Stalder L, Mathys H, Orozco RZ, Muhlemann O. Posttranscriptional gene regulation by spatial rearrangement of the 3' untranslated region. PLoS Biol. 2008;6(4):e92.

21.   Barbosa C, Peixeiro I, Romão L. Gene expression regulation by upstream open reading frames and human disease. PLoS Genet. 2013;9(8).

22.   Ruiz-Echevarría MJ, Peltz SW. The RNA binding protein Pub1 modulates the stability of transcripts containing upstream open reading frames. Cell. 2000;101(7):741-51.

23.   Thermann R, Neu‐Yilik G, Deters A, Frede U, Wehr K, Hagemeier C, Hentze MW, Kulozik AE. Binary specification of nonsense codons by splicing and cytoplasmic translation. The EMBO journal. 1998;17(12):3484-94.

24.   Grosswendt S, Rajewsky N. Essentials of miRNA-dependent Control of mRNA Translation and decay, miRNA Targeting Principles, and Methods for Target Identification. Essentials of Noncoding RNA in Neuroscience2017. p. 19-38.

25.   Rao DD, Vorhies JS, Senzer N, Nemunaitis J. siRNA vs. shRNA: similarities and differences. Adv Drug Deliv Rev. 2009;61(9):746-59.

26.   Mack GS. MicroRNA gets down to business. Nature biotechnology. 2007;25(6):631-8.

27.   Holbrook JA, Neu-Yilik G, Hentze MW, Kulozik AE. Nonsense-mediated decay approaches the clinic. Nature genetics. 2004;36(8):801-8.

28.   Holbrook JA, Neu-Yilik G, Hentze MW, Kulozik AE. NMD and human disease. Madame Curie Bioscience Database [Internet]: Landes Bioscience; 2013.

29.   Pusch M. Myotonia caused by mutations in the muscle chloride channel gene CLCN1. Human mutation. 2002;19(4):423-34.

30.   Rivolta C, Berson EL, Dryja TP. Dominant Leber congenital amaurosis, cone‐rod degeneration, and retinitis pigmentosa caused by mutant versions of the transcription factor CRX. Human mutation. 2001;18(6):488-98.

31.   Rosenfeld PJ, Cowley GS, McGee TL, Sandberg MA, Berson EL, Dryja TP. A null mutation in the rhodopsin gene causes rod photoreceptor dysfunction and autosomal recessive retinitis pigmentosa. Nature genetics. 1992;1(3):209-13.

32.   Patton M, Afzal A. Robinow syndrome. Journal of medical genetics. 2002;39(5):305-10.

33.   Schwabe GC, Tinschert S, Buschow C, Meinecke P, Wolff G, Gillessen-Kaesbach G, Oldridge M, Wilkie AO, Kömec R, Mundlos S. Distinct mutations in the receptor tyrosine kinase gene ROR2 cause brachydactyly type B. The American Journal of Human Genetics. 2000;67(4):822-31.

34.   Wada M, Lokugamage KG, Nakagawa K, Narayanan K, Makino S. Interplay between coronavirus, a cytoplasmic RNA virus, and nonsense-mediated mRNA decay pathway. Proceedings of the National Academy of Sciences. 2018;115(43):E10157-E66.

35.   Popp MW, Maquat LE. Nonsense-mediated mRNA decay and cancer. Current opinion in genetics & development. 2018;48:44-50.

36.   Kalathiya U, Padariya M, Pawlicka K, Verma CS, Houston D, Hupp TR, Alfaro JA. Insights into the Effects of Cancer Associated Mutations at the UPF2 and ATP-Binding Sites of NMD Master Regulator: UPF1. International journal of molecular sciences. 2019;20(22):5644.

37.   Karam R, Carvalho J, Bruno I, Graziadio C, Senz J, Huntsman D, Carneiro F, Seruca R, Wilkinson M, Oliveira C. The NMD mRNA surveillance pathway downregulates aberrant E-cadherin transcripts in gastric cancer cells and in CDH1 mutation carriers. Oncogene. 2008;27(30):4255-60.

38.   Jonchere V, Lagrange A, Bertrand R, Svrcek M, Marisa L, Buhard O, Greene M, Demidova A, Jia J, Adriaenssens E. Targeting nonsense-mediated mRNA decay in colorectal cancers with microsatellite instability. Oncogenesis. 2018;7(9):1-9.

39.   Hu Z, Yau C, Ahmed AA. A pan-cancer genome-wide analysis reveals tumour dependencies by induction of nonsense-mediated decay. Nature communications. 2017;8:15943.

40.   Cali BM, Kuchma SL, Latham J, Anderson P. smg-7 is required for mRNA surveillance in Caenorhabditis elegans. Genetics. 1999;151(2):605-16.

41.   Fukuhara N, Ebert J, Unterholzner L, Lindner D, Izaurralde E, Conti E. SMG7 is a 14-3-3-like adaptor in the nonsense-mediated mRNA decay pathway. Molecular cell. 2005;17(4):537-47.

42.   D'Andrea LD, Regan L. TPR proteins: the versatile helix. Trends in biochemical sciences. 2003;28(12):655-62.

43.   Jonas S, Weichenrieder O, Izaurralde E. An unusual arrangement of two 14-3-3-like domains in the SMG5–SMG7 heterodimer is required for efficient nonsense-mediated mRNA decay. Genes & development. 2013;27(2):211-25.

44.   Unterholzner L, Izaurralde E. SMG7 acts as a molecular link between mRNA surveillance and mRNA decay. Molecular cell. 2004;16(4):587-96.

45.   Metze S, Herzog VA, Ruepp M-D, Mühlemann O. Comparison of EJC-enhanced and EJC-independent NMD in human cells reveals two partially redundant degradation pathways. Rna. 2013;19(10):1432-48.

46.   Loh B, Jonas S, Izaurralde E. The SMG5–SMG7 heterodimer directly recruits the CCR4–NOT deadenylase complex to mRNAs containing nonsense codons via interaction with POP2. Genes & development. 2013;27(19):2125-38.

47.   Park J, Seo J-W, Ahn N, Park S, Hwang J, Nam J-W. UPF1/SMG7-dependent microRNA-mediated gene regulation. Nature communications. 2019;10(1):1-15.

48.   Cowen LE, Tang Y. Identification of nonsense-mediated mRNA decay pathway as a critical regulator of p53 isoform beta. Sci Rep. 2017;7(1):17535.

49.   Luo H, Cowen L, Yu G, Jiang W, Tang Y. SMG7 is a critical regulator of p53 stability and function in DNA damage stress response. Cell discovery. 2016;2:15042.

50.   Li W, Middha M, Bicak M, Sjoberg DD, Vertosick E, Dahlin A, Haggstrom C, Hallmans G, Ronn AC, Stattin P, Melander O, Ulmert D, Lilja H, Klein RJ. Genome-wide Scan Identifies Role for AOX1 in Prostate Cancer Survival. European urology. 2018;74(6):710-9.

51.   Trumbach D, Pfeiffer S, Poppe M, Scherb H, Doll S, Wurst W, Schick JA. ENCoRE: an efficient software for CRISPR screens identifies new players in extrinsic apoptosis. BMC genomics. 2017;18(1):905.

52.   M Reichardt H, Luhder F. The ambivalent role of apoptosis in experimental autoimmune encephalomyelitis and multiple sclerosis. Current pharmaceutical design. 2012;18(29):4453-64.

53.   King KL, Cidlowski JA. Cell cycle and apoptosis: common pathways to life and death. Journal of cellular biochemistry. 1995;58(2):175-80.

54.   He B, Lu N, Zhou Z. Cellular and nuclear degradation during apoptosis. Current opinion in cell biology. 2009;21(6):900-12.

55.   Brown DA, Yang N, Ray SD. Apoptosis. In: Wexler P, editor. Encyclopedia of Toxicology (Third Edition). Oxford: Academic Press; 2014. p. 287-94.

56.   Kruidering M, Evan GI. Caspase‐8 in apoptosis: the beginning of "the end"? IUBMB life. 2000;50(2):85-90.

57.   Parrish AB, Freel CD, Kornbluth S. Cellular mechanisms controlling caspase activation and function. Cold Spring Harbor perspectives in biology. 2013;5(6):a008672.

58.   Urbanik T, Koehler BC, Wolpert L, Elßner C, Scherr A-L, Longerich T, Kautz N, Welte S, Hövelmeyer N, Jäger D. CYLD deletion triggers nuclear factor-κB-signaling and increases cell death resistance in murine hepatocytes. World Journal of Gastroenterology: WJG. 2014;20(45):17049.

59.   Kiraz Y, Adan A, Yandim MK, Baran Y. Major apoptotic mechanisms and genes involved in apoptosis. Tumor Biology. 2016;37(7):8471-86.

60.   Jia J, Furlan A, Gonzalez-Hilarion S, Leroy C, Gruenert D, Tulasne D, Lejeune F. Caspases shutdown nonsense-mediated mRNA decay during apoptosis. Cell Death & Differentiation. 2015;22(11):1754-63.

61.   Wang D, Wang Z, Li Y, Chen X, Sun GY. Nimodipine inhibits N-methyl-N-nitrosourea-induced retinalphotoreceptor apoptosis in vivo. Indian journal of pharmacology. 2013;45(2):149.

62.   Goetz AE, Wilkinson M. Stress and the nonsense-mediated RNA decay pathway. Cellular and Molecular Life Sciences. 2017;74(19):3509-31.

63.	Medghalchi SM, Frischmeyer PA, Mendell JT, Kelly AG, Lawler AM, Dietz HC. Rent1, a trans-effector of nonsense-mediated mRNA decay, is essential for mammalian embryonic viability. Human molecular genetics. 2001;10(2):99-105.

64.	Oliveira V, Romanow WJ, Geisen C, Otterness DM, Mercurio F, Wang HG, Dalton WS, Abraham RT. A protective role for the human SMG-1 kinase against tumor necrosis factor-α-induced apoptosis. Journal of Biological Chemistry. 2008;283(19):13174-84.

65.	Blythe AJ, Fox AH, Bond CS. The ins and outs of lncRNA structure: how, why and what comes next? Biochimica et Biophysica Acta (BBA)-Gene Regulatory Mechanisms. 2016;1859(1):46-58.

66.	Dunham I, Birney E, Lajoie BR, Sanyal A, Dong X, Greven M, Lin X, Wang J, Whitfield TW, Zhuang J. An integrated encyclopedia of DNA elements in the human genome. Nature. 2012;489(7414):57-74.

67.	Harrow J, Frankish A, Gonzalez JM, Tapanari E, Diekhans M, Kokocinski F, Aken BL, Barrell D, Zadissa A, Searle S. GENCODE: the reference human genome annotation for The ENCODE Project. Genome research. 2012;22(9):1760-74.

68.	Fernandes JC, Acuña SM, Aoki JI, Floeter-Winter LM, Muxel SM. Long non-coding RNAs in the regulation of gene expression: physiology and disease. Non-coding RNA. 2019;5(1):17.

69.	Kung JT, Colognori D, Lee JT. Long noncoding RNAs: past, present, and future. Genetics. 2013;193(3):651-69.

70.	Mercer TR, Mattick JS. Structure and function of long noncoding RNAs in epigenetic regulation. Nature structural & molecular biology. 2013;20(3):300.

71.	Zhang B, Arun G, Mao YS, Lazar Z, Hung G, Bhattacharjee G, Xiao X, Booth CJ, Wu J, Zhang C. The lncRNA Malat1 is dispensable for mouse development but its transcription plays a cis-regulatory role in the adult. Cell reports. 2012;2(1):111-23.

72.	Garding A, Bhattacharya N, Claus R, Ruppel M, Tschuch C, Filarsky K, Idler I, Zucknick M, Caudron-Herger M, Oakes C. Epigenetic upregulation of lncRNAs at 13q14. 3 in leukemia is linked to the In Cis downregulation of a gene cluster that targets NF-kB. PLoS genetics. 2013;9(4):e1003373.

73.	Peng B, Liu A, Yu X, Xu E, Dai J, Li M, Yang Q. Silencing of lncRNA AFAP1-AS1 suppressed lung cancer development by regulatory mechanism in cis and trans. Oncotarget. 2017;8(55):93608.

74.	Andersen RE, Hong SJ, Lim JJ, Cui M, Harpur BA, Hwang E, Delgado RN, Ramos AD, Liu SJ, Blencowe BJ. The long noncoding RNA Pnky is a trans-acting regulator of cortical development in vivo. Developmental cell. 2019;49(4):632-42. e7.

75.	Wilusz JE, Sunwoo H, Spector DL. Long noncoding RNAs: functional surprises from the RNA world. Genes & development. 2009;23(13):1494-504.

76.	Sana J, Faltejskova P, Svoboda M, Slaby O. Novel classes of non-coding RNAs and cancer. Journal of translational medicine. 2012;10(1):103.

77.	Xu F, Zhang J. Long non-coding RNA HOTAIR functions as miRNA sponge to promote the epithelial to mesenchymal transition in esophageal cancer. Biomedicine & Pharmacotherapy. 2017;90:888-96.

78.	Chen L, Yang W, Guo Y, Chen W, Zheng P, Zeng J, Tong W. Exosomal lncRNA GAS5 regulates the apoptosis of macrophages and vascular endothelial cells in atherosclerosis. PLoS One. 2017;12(9):e0185406.

79.	Li J, Zhang M, An G, Ma Q. LncRNA TUG1 acts as a tumor suppressor in human glioma by promoting cell apoptosis. Experimental Biology and Medicine. 2016;241(6):644-9.

80.	Wang J, Xu C, Wu H, Shen S. LncRNA SNHG12 promotes cell growth and inhibits cell apoptosis in colorectal cancer cells. Brazilian Journal of Medical and Biological Research. 2017;50(3).

81.	Yang Y, Chen D, Liu H, Yang K. Increased expression of lncRNA CASC9 promotes tumor progression by suppressing autophagy-mediated cell apoptosis via the AKT/mTOR pathway in oral squamous cell carcinoma. Cell Death & Disease. 2019;10(2).

82.	Zhang C, Wang P, Jiang P, Lv Y, Dong C, Dai X, Tan L, Wang Z. Upregulation of lncRNA HOTAIR contributes to IL-1β-induced MMP overexpression and chondrocytes apoptosis in temporomandibular joint osteoarthritis. Gene. 2016;586(2):248-53.

83.	Yu Y, Lv F, Liang D, Yang Q, Zhang B, Lin H, Wang X, Qian G, Xu J, You W. HOTAIR may regulate proliferation, apoptosis, migration and invasion of MCF-7 cells through regulating the P53/Akt/JNK signaling pathway. Biomedicine & Pharmacotherapy. 2017;90:555-61.

84.	Yang S-z, Xu F, Zhou T, Zhao X, McDonald JM, Chen Y. The long non-coding RNA HOTAIR enhances pancreatic cancer resistance to TNF-related apoptosis-inducing ligand. Journal of Biological Chemistry. 2017;292(25):10390-7.

85.	Yu Y, Zhang X, Li Z, Kong L, Huang Y. LncRNA HOTAIR suppresses TNF-α induced apoptosis of nucleus pulposus cells by regulating miR-34a/Bcl-2 axis. Biomedicine & Pharmacotherapy. 2018;107:729-37.

86.	Wapinski O, Chang HY. Long noncoding RNAs and human disease. Trends Cell Biol. 2011;21(6):354-61.

87.	Gibb EA, Brown CJ, Lam WL. The functional role of long non-coding RNA in human carcinomas. Molecular cancer. 2011;10:38.

88.	Chen G, Wang Z, Wang D, Qiu C, Liu M, Chen X, Zhang Q, Yan G, Cui Q. LncRNADisease: a database for long-non-coding RNA-associated diseases. Nucleic acids research. 2012;41(D1):D983-D6.

89.	Bao Z, Yang Z, Huang Z, Zhou Y, Cui Q, Dong D. LncRNADisease 2.0: an updated database of long non-coding RNA-associated diseases. Nucleic acids research. 2019;47(D1):D1034-D7.

90.	Li W, Zhai L, Wang H, Liu C, Zhang J, Chen W, Wei Q. Downregulation of LncRNA GAS5 causes trastuzumab resistance in breast cancer. Oncotarget. 2016;7(19):27778.

91.	Gu J, Wang Y, Wang X, Zhou D, Shao C, Zhou M, He Z. Downregulation of lncRNA GAS5 confers tamoxifen resistance by activating miR-222 in breast cancer. Cancer letters. 2018;434:1-10.

92.	Zhang X-F, Liu T, Li Y, Li S. Overexpression of long non-coding RNA CCAT1 is a novel biomarker of poor prognosis in patients with breast cancer. International journal of clinical and experimental pathology. 2015;8(8):9440.

93.	Yildirim E, Kirby JE, Brown DE, Mercier FE, Sadreyev RI, Scadden DT, Lee JT. Xist RNA is a potent suppressor of hematologic cancer in mice. Cell. 2013;152(4):727-42.

94.	Gao C, Zhang J, Wang Q, Ren C. Overexpression of lncRNA NEAT1 mitigates multidrug resistance by inhibiting ABCG2 in leukemia. Oncology letters. 2016;12(2):1051-7.

95.	Bian Z, Jin L, Zhang J, Yin Y, Quan C, Hu Y, Feng Y, Liu H, Fei B, Mao Y. LncRNA—UCA1 enhances cell proliferation and 5-fluorouracil resistance in colorectal cancer by inhibiting miR-204-5p. Scientific reports. 2016;6:23892.

96.	Iguchi T, Uchi R, Nambara S, Saito T, Komatsu H, Hirata H, Ueda M, Sakimura S, Takano Y, Kurashige J. A long noncoding RNA, lncRNA-ATB, is involved in the progression and prognosis of colorectal cancer. Anticancer research. 2015;35(3):1385-8.

97.	Li H, An J, Wu M, Zheng Q, Gui X, Li T, Pu H, Lu D. LncRNA HOTAIR promotes human liver cancer stem cell malignant growth through downregulation of SETD2. Oncotarget. 2015;6(29):27847.

98.	Yang H, Zhong Y, Xie H, Lai X, Xu M, Nie Y, Liu S, Wan Y-JY. Induction of the liver cancer-down-regulated long noncoding RNA uc002mbe. 2 mediates trichostatin-induced apoptosis of liver cancer cells. Biochemical pharmacology. 2013;85(12):1761-9.

99.	Wang X, Sun W, Shen W, Xia M, Chen C, Xiang D, Ning B, Cui X, Li H, Li X. Long non-coding RNA DILC regulates liver cancer stem cells via IL-6/STAT3 axis. Journal of hepatology. 2016;64(6):1283-94.

100.	Gutschner T, Hammerle M, Eissmann M, Hsu J, Kim Y, Hung G, Revenko A, Arun G, Stentrup M, Gross M, Zornig M, MacLeod AR, Spector DL, Diederichs S. The noncoding RNA MALAT1 is a critical regulator of the metastasis phenotype of lung cancer cells. Cancer research. 2013;73(3):1180-9.

101.   Li W, Xu H, Xiao T, Cong L, Love MI, Zhang F, Irizarry RA, Liu JS, Brown M, Liu XS. MAGeCK enables robust identification of essential genes from genome-scale CRISPR/Cas9 knockout screens. Genome biology. 2014;15(12):554.

102.   Gupta RA, Shah N, Wang KC, Kim J, Horlings HM, Wong DJ, Tsai MC, Hung T, Argani P, Rinn JL, Wang Y, Brzoska P, Kong B, Li R, West RB, van de Vijver MJ, Sukumar S, Chang HY. Long non-coding RNA HOTAIR reprograms chromatin state to promote cancer metastasis. Nature. 2010;464(7291):1071-6.

103.   Cabanski CR, White NM, Dang HX, Silva-Fisher JM, Rauck CE, Cicka D, Maher CA. Pan-cancer transcriptome analysis reveals long noncoding RNAs with conserved function. RNA biology. 2015;12(6):628-42.

104.   Zhang K, Luo Z, Zhang Y, Zhang L, Wu L, Liu L, Yang J, Song X, Liu J. Circulating lncRNA H19 in plasma as a novel biomarker for breast cancer. Cancer Biomarkers. 2016;17(2):187-94.

105.   Ma S, Deng X, Yang Y, Zhang Q, Zhou T, Liu Z. The lncRNA LINC00675 regulates cell proliferation, migration, and invasion by affecting Wnt/β-catenin signaling in cervical cancer. Biomedicine & Pharmacotherapy. 2018;108:1686-93.

106.   Sanjana NE, Shalem O, Zhang F. Improved vectors and genome-wide libraries for CRISPR screening. Nature methods. 2014;11(8):783-4.

107.   Webb E, Adams JM, Cory S. Variant (6; 15) translocation in a murine plasmacytoma occurs near an immunoglobulin κ gene but far from the myc oncogene. Nature. 1984;312(5996):777-9.

108.   Colombo T, Farina L, Macino G, Paci P. PVT1: a rising star among oncogenic long noncoding RNAs. BioMed research international. 2015;2015.

109.   Tseng Y-Y, Moriarity BS, Gong W, Akiyama R, Tiwari A, Kawakami H, Ronning P, Reuland B, Guenther K, Beadnell TC. PVT1 dependence in cancer with MYC copy-number increase. Nature. 2014;512(7512):82-6.

110.   Kong R, Zhang E-b, Yin D-d, You L-h, Xu T-p, Chen W-m, Xia R, Wan L, Sun M, Wang Z-x. Long noncoding RNA PVT1 indicates a poor prognosis of gastric cancer and promotes cell proliferation through epigenetically regulating p15 and p16. Molecular cancer. 2015;14(1):82.

111.   Yang Y-R, Zang S-Z, Zhong C-L, Li Y-X, Zhao S-S, Feng X-J. Increased expression of the lncRNA PVT1 promotes tumorigenesis in non-small cell lung cancer. International journal of clinical and experimental pathology. 2014;7(10):6929.

112.   Huang C, Yu W, Wang Q, Cui H, Wang Y, Zhang L, Han F, Huang T. Increased expression of the lncRNA PVT1 is associated with poor prognosis in pancreatic cancer patients. Minerva medica. 2015;106(3):143-9.

113.   Ding C, Yang Z, Lv Z, Du C, Xiao H, Peng C, Cheng S, Xie H, Zhou L, Wu J. Long non‐coding RNA PVT1 is associated with tumor progression and predicts recurrence in hepatocellular carcinoma patients. Oncology letters. 2015;9(2):955-63.

114.   Guan Y, Kuo W-L, Stilwell JL, Takano H, Lapuk AV, Fridlyand J, Mao J-H, Yu M, Miller MA, Santos JL. Amplification of PVT1 contributes to the pathophysiology of ovarian and breast cancer. Clinical cancer research. 2007;13(19):5745-55.

115.   Cui D, Yu C-H, Liu M, Xia Q-Q, Zhang Y-F, Jiang W-L. Long non-coding RNA PVT1 as a novel biomarker for diagnosis and prognosis of non-small cell lung cancer. Tumor Biology. 2016;37(3):4127-34.

116.   Zhou Q, Chen F, Zhao J, Li B, Liang Y, Pan W, Zhang S, Wang X, Zheng D. Long non-coding RNA PVT1 promotes osteosarcoma development by acting as a molecular sponge to regulate miR-195. Oncotarget. 2016;7(50):82620.

117.   Zhao L, Kong H, Sun H, Chen Z, Chen B, Zhou M. LncRNA‐PVT1 promotes pancreatic cancer cells proliferation and migration through acting as a molecular sponge to regulate miR‐448. Journal of cellular physiology. 2018;233(5):4044-55.

118.   Li T, Meng X-l, Yang W-q. Long noncoding RNA PVT1 acts as a "Sponge" to inhibit microRNA-152 in gastric cancer cells. Digestive Diseases and Sciences. 2017;62(11):3021-8.

119. Li Y, Li S, Luo Y, Liu Y, Yu N. LncRNA PVT1 regulates chondrocyte apoptosis in osteoarthritis by acting as a sponge for miR-488-3p. DNA and cell biology. 2017;36(7):571-80.
120. Li P-D, Hu J-L, Ma C, Ma H, Yao J, Chen L-L, Chen J, Cheng T-T, Yang K-Y, Wu G. Upregulation of the long non-coding RNA PVT1 promotes esophageal squamous cell carcinoma progression by acting as a molecular sponge of miR-203 and LASP1. Oncotarget. 2017;8(21):34164.
121. Zhao Y, Zhao J, Guo X, She J, Liu Y. Long non-coding RNA PVT1, a molecular sponge for miR-149, contributes aberrant metabolic dysfunction and inflammation in IL-1β-simulated osteoarthritic chondrocytes. Bioscience reports. 2018;38(5).
122. Su H, Lin Z, Peng W, Guan F, Zhu G, Mao B, Dai B, Huang H, Hu Z. MiR-448 downregulates CTTN to inhibit cell proliferation and promote apoptosis in glioma. Eur Rev Med Pharmacol Sci. 2018;22(12):3847-54.
123. Dang Y-W, Zeng J, He R-Q, Rong M-H, Luo D-Z, Chen G. Effects of miR-152 on cell growth inhibition, motility suppression and apoptosis induction in hepatocellular carcinoma cells. Asian Pac J Cancer Prev. 2014;15(12):4969-76.
124. Xue W, Chen J, Liu X, Gong W, Zheng J, Guo X, Liu Y, Liu L, Ma J, Wang P. PVT1 regulates the malignant behaviors of human glioma cells by targeting miR-190a-5p and miR-488-3p. Biochimica et Biophysica Acta (BBA)-Molecular Basis of Disease. 2018;1864(5):1783-94.
125. Zhang X, Zhang Y, Liu X, Fang A, Li P, Li Z, Liu T, Yang Y, Du L, Wang C. MicroRNA-203 is a prognostic indicator in bladder cancer and enhances chemosensitivity to cisplatin via apoptosis by targeting Bcl-w and survivin. PloS one. 2015;10(11).
126. Lin RJ, Lin YC, Yu AL. miR‐149* induces apoptosis by inhibiting Akt1 and E2F1 in human cancer cells. Molecular carcinogenesis. 2010;49(8):719-27.
127. Wang Y, Li X, Liu W, Li B, Chen D, Hu F, Wang L, Liu XM, Cui R, Liu R. MicroRNA-1205, encoded on chromosome 8q24, targets EGLN3 to induce cell growth and contributes to risk of castration-resistant prostate cancer. Oncogene. 2019;38(24):4820-34.
128. Oeckinghaus A, Ghosh S. The NF-κB family of transcription factors and its regulation. Cold Spring Harbor perspectives in biology. 2009;1(4):a000034.
129. Dolcet X, Llobet D, Pallares J, Matias-Guiu X. NF-kB in development and progression of human cancer. Virchows archiv. 2005;446(5):475-82.
130. Hayden MS, Ghosh S, editors. Regulation of NF-κB by TNF family cytokines. Seminars in immunology; 2014: Elsevier.
131. Hoesel B, Schmid JA. The complexity of NF-κB signaling in inflammation and cancer. Molecular cancer. 2013;12(1):86.
132. Savinova OV, Hoffmann A, Ghosh G. The Nfkb1 and Nfkb2 proteins p105 and p100 function as the core of high-molecular-weight heterogeneous complexes. Molecular cell. 2009;34(5):591-602.
133. Van Antwerp DJ, Martin SJ, Kafri T, Green DR, Verma IM. Suppression of TNF-α-induced apoptosis by NF-κB. Science. 1996;274(5288):787-9.
134. Van Antwerp DJ, Martin SJ, Verma IM, Green DR. Inhibition of TNF-induced apoptosis by NF-κB. Trends in cell biology. 1998;8(3):107-11.
135. Carswell EA, Old LJ, Kassel RL, Green S, Fiore N, Williamson B. An endotoxin-induced serum factor that causes necrosis of tumors. Proc Natl Acad Sci U S A. 1975;72(9):3666-70.
136. Yang L, Kraft VAN, Pfeiffer S, Merl-Pham J, Bao X, An Y, Hauck SM, Schick JA. Nonsense-mediated decay factor SMG7 sensitizes cells to TNFalpha-induced apoptosis via CYLD tumor suppressor and the noncoding oncogene Pvt1. Mol Oncol. 2020.
137. Thakore PI, D'ippolito AM, Song L, Safi A, Shivakumar NK, Kabadi AM, Reddy TE, Crawford GE, Gersbach CA. Highly specific epigenome editing by CRISPR-Cas9 repressors for silencing of distal regulatory elements. Nature methods. 2015;12(12):1143.
138. Mitrovich QM, Anderson P. mRNA surveillance of expressed pseudogenes in C. elegans. Current biology : CB. 2005;15(10):963-7.

139. Li T, Shi Y, Wang P, Guachalla LM, Sun B, Joerss T, Chen YS, Groth M, Krueger A, Platzer M. Smg6/Est1 licenses embryonic stem cell differentiation via nonsense‐mediated mRNA decay. The EMBO journal. 2015;34(12):1630-47.

140. Lan T, Ma W, Hong Z, Wu L, Chen X, Yuan Y. Long non-coding RNA small nucleolar RNA host gene 12 (SNHG12) promotes tumorigenesis and metastasis by targeting miR-199a/b-5p in hepatocellular carcinoma. Journal of experimental & clinical cancer research. 2017;36(1):11.

141. Birgani MT, Hajjari M, Shahrisa A, Khoshnevisan A, Shoja Z, Motahari P, Farhangi B. Long non-coding rna snhg6 as a potential biomarker for hepatocellular carcinoma. Pathology & Oncology Research. 2018;24(2):329-37.

142. Chang L, Yuan Y, Li C, Guo T, Qi H, Xiao Y, Dong X, Liu Z, Liu Q. Upregulation of SNHG6 regulates ZEB1 expression by competitively binding miR-101-3p and interacting with UPF1 in hepatocellular carcinoma. Cancer letters. 2016;383(2):183-94.

143. Lu Y-F, Cai X-L, Li Z-Z, Lv J, Xiang Y-a, Chen J-J, Chen W-J, Sun W-Y, Liu X-M, Chen J-B. LncRNA SNHG16 functions as an oncogene by sponging MiR-4518 and up-regulating PRMT5 expression in glioma. Cellular Physiology Biochemistry. 2018;45(5):1975-85.

144. He A, He S, Li X, Zhou L. ZFAS 1: A novel vital oncogenic lnc RNA in multiple human cancers. Cell proliferation. 2019;52(1):e12513.

145. Zeng N, Zhang Z, Jiang H, Li R, Chang C, Wang F, Xu D, Fan Q, Wang T, Xiao Y. LncRNA-241 inhibits 1, 2-Dichloroethane-induced hepatic apoptosis. Toxicology in Vitro. 2019;61:104650.

146. Li T, Su L, Lei Y, Liu X, Zhang Y, Liu X. DDIT3 and KAT2A proteins regulate TNFRSF10A and TNFRSF10B expression in endoplasmic reticulum stress-mediated apoptosis in human lung cancer cells. Journal of Biological Chemistry. 2015;290(17):11108-18.

147. Hansen KD, Lareau LF, Blanchette M, Green RE, Meng Q, Rehwinkel J, Gallusser FL, Izaurralde E, Rio DC, Dudoit S. Genome-wide identification of alternative splice forms down-regulated by nonsense-mediated mRNA decay in Drosophila. PLoS genetics. 2009;5(6).

148. Mak TW, Yeh W-C. Signaling for survival and apoptosis in the immune system. Arthritis Research & Therapy. 2002;4(3):S243.

149. Sun SC. CYLD: a tumor suppressor deubiquitinase regulating NF-kappaB activation and diverse biological processes. Cell death and differentiation. 2010;17(1):25-34.

150. Tsherniak A, Vazquez F, Montgomery PG, Weir BA, Kryukov G, Cowley GS, Gill S, Harrington WF, Pantel S, Krill-Burger JM, Meyers RM, Ali L, Goodale A, Lee Y, Jiang G, Hsiao J, Gerath WFJ, Howell S, Merkel E, Ghandi M, Garraway LA, Root DE, Golub TR, Boehm JS, Hahn WC. Defining a Cancer Dependency Map. Cell. 2017;170(3):564-76.e16.

151. TGCA. The results shown here are in whole or part based upon data generated by the TCGA Research Network: https://www.cancer.gov/tcga. Accessed 15 December 2019.

152. Al-Lamki RS, Sadler TJ, Wang J, Reid MJ, Warren AY, Movassagh M, Lu W, Mills IG, Neal DE, Burge J, Vandenebeele P, Pober JS, Bradley JR. Tumor Necrosis Factor Receptor Expression and Signaling in Renal Cell Carcinoma. The American Journal of Pathology. 2010;177(2):943-54.

153. Mikami S, Mizuno R, Kosaka T, Saya H, Oya M, Okada Y. Expression of TNF-alpha and CD44 is implicated in poor prognosis, cancer cell invasion, metastasis and resistance to the sunitinib treatment in clear cell renal cell carcinomas. International journal of cancer. 2015;136(7):1504-14.

154. Konermann S, Brigham MD, Trevino AE, Joung J, Abudayyeh OO, Barcena C, Hsu PD, Habib N, Gootenberg JS, Nishimasu H, Nureki O, Zhang F. Genome-scale transcriptional activation by an engineered CRISPR-Cas9 complex. Nature. 2014;517:583.

155. Wang Y, Davies KJ, Melendez JA, Crawford DR. Characterization of adapt33, a stress‐inducible riboregulator. Gene expression. 2003;11(2):85-94.

156. Chatzinikolaidou M. Cell spheroids: the new frontiers in in vitro models for cancer drug validation. Drug discovery today. 2016;21(9):1553-60.

157. Trcek T, Sato H, Singer RH, Maquat LE. Temporal and spatial characterization of nonsense-mediated mRNA decay. Genes development. 2013;27(5):541-51.

158.   Wang Y, Crawford DR, Davies KJ. adapt33, a novel oxidant-inducible RNA from hamster HA-1 cells. Archives of biochemistry and biophysics. 1996;332(2):255-60.

159.   Zhao T, Cai M, Liu M, Su G, An D, Moon B, Lyu G, Si Y, Chen L, Lu W. lncRNA 5430416N02Rik Promotes the Proliferation of Mouse Embryonic Stem Cells by Activating Mid1 Expression through 3D Chromatin Architecture. Stem cell reports. 2020;14(3):493-505.

160.   Zhou Y, Zhou B, Pache L, Chang M, Khodabakhshi AH, Tanaseichuk O, Benner C, Chanda SK. Metascape provides a biologist-oriented resource for the analysis of systems-level datasets. Nature communications. 2019;10(1):1-10.

161.   Borchert GM, Lanier W, Davidson BL. RNA polymerase III transcribes human microRNAs. Nature structural & molecular biology. 2006;13(12):1097-101.

162.   Dieci G, Fiorino G, Castelnuovo M, Teichmann M, Pagano A. The expanding RNA polymerase III transcriptome. TRENDS in Genetics. 2007;23(12):614-22.

163.   Lebrec H, Ponce R, Preston BD, Iles J, Born TL, Hooper M. Tumor necrosis factor, tumor necrosis factor inhibition, and cancer risk. Current Medical Research and Opinion. 2015;31(3):557-74.

164.   Baxevanis CN, Voutsas IF, Tsitsilonis OE, Tsiatas ML, Gritzapis AD, Papamichail M. Compromised anti-tumor responses in tumor necrosis factor-alpha knockout mice. Eur J Immunol. 2000;30(7):1957-66.

165.   Xu J, Chakrabarti AK, Tan JL, Ge L, Gambotto A, Vujanovic NL. Essential role of the TNF-TNFR2 cognate interaction in mouse dendritic cell-natural killer cell crosstalk. Blood. 2007;109(8):3333-41.

166.   Hofmanová J, Vaculová A, Hyzd'Alová M, Kozubík A. Response of normal and colon cancer epithelial cells to TNF-family apoptotic inducers. Oncology reports. 2008;19(2):567-73.

167.   Xu X, Fu X-Y, Plate J, Chong AS. IFN-γ induces cell growth inhibition by Fas-mediated apoptosis: requirement of STAT1 protein for up-regulation of Fas and FasL expression. Cancer research. 1998;58(13):2832-7.

168.   Spanaus KS, Schlapbach R, Fontana A. TNF‑α and IFN‑γ render microglia sensitive to Fas ligand‑induced apoptosis by induction of Fas expression and down‑regulation of Bcl‑2 and Bcl‑xL. European journal of immunology. 1998;28(12):4398-408.

169.   Iguchi M, Hiroi M, Kanegae H, Ohmori Y. Costimulation of murine osteoblasts with interferon-γ and tumor necrosis factor-α induces apoptosis through downregulation of Bcl-2 and release of cytochrome c from mitochondria. Mediators of inflammation. 2018;2018.

170.   Shao AL. The Role of UPF3B in Pluripotency and Differentiation: UC San Diego; 2015.

171.   Avery P, Vicente-Crespo M, Francis D, Nashchekina O, Alonso CR, Palacios IM. Drosophila Upf1 and Upf2 loss of function inhibits cell growth and causes animal death in a Upf3-independent manner. Rna. 2011;17(4):624-38.

172.   Weischenfeldt J, Damgaard I, Bryder D, Theilgaard-Mönch K, Thoren LA, Nielsen FC, Jacobsen SEW, Nerlov C, Porse BT. NMD is essential for hematopoietic stem and progenitor cells and for eliminating by-products of programmed DNA rearrangements. Genes & development. 2008;22(10):1381-96.

173.   Colombo M, Karousis ED, Bourquin J, Bruggmann R, Mühlemann O. Transcriptome-wide identification of NMD-targeted human mRNAs reveals extensive redundancy between SMG6-and SMG7-mediated degradation pathways. Rna. 2017;23(2):189-201.

174.   Ottens F, Boehm V, Sibley CR, Ule J, Gehring NH. Transcript-specific characteristics determine the contribution of endo-and exonucleolytic decay pathways during the degradation of nonsense-mediated decay substrates. RNA. 2017;23(8):1224-36.

175.   Cesana M, Cacchiarelli D, Legnini I, Santini T, Sthandier O, Chinappi M, Tramontano A, Bozzoni I. A long noncoding RNA controls muscle differentiation by functioning as a competing endogenous RNA. Cell. 2011;147(2):358-69.

176.   Mercer TR, Qureshi IA, Gokhan S, Dinger ME, Li G, Mattick JS, Mehler MF. Long noncoding RNAs in neuronal-glial fate specification and oligodendrocyte lineage maturation. BMC neuroscience. 2010;11(1):14.

177.   Cai X, Cullen BR. The imprinted H19 noncoding RNA is a primary microRNA precursor. Rna. 2007;13(3):313-6.

178. Calviello L, Mukherjee N, Wyler E, Zauber H, Hirsekorn A, Selbach M, Landthaler M, Obermayer B, Ohler U. Detecting actively translated open reading frames in ribosome profiling data. Nature methods. 2016;13(2):165-70.

179. Carlevaro-Fita J, Rahim A, Guigó R, Vardy LA, Johnson R. Cytoplasmic long noncoding RNAs are frequently bound to and degraded at ribosomes in human cells. Rna. 2016;22(6):867-82.

180. Ingolia NT, Lareau LF, Weissman JS. Ribosome profiling of mouse embryonic stem cells reveals the complexity and dynamics of mammalian proteomes. Cell. 2011;147(4):789-802.

181. Ruiz-Orera J, Messeguer X, Subirana JA, Alba MM. Long non-coding RNAs as a source of new peptides. elife. 2014;3:e03523.

182. Rion N, Rüegg MA. LncRNA-encoded peptides: more than translational noise? Cell research. 2017;27(5):604-5.

183. O'Donnell MA, Perez-Jimenez E, Oberst A, Ng A, Massoumi R, Xavier R, Green DR, Ting AT. Caspase 8 inhibits programmed necrosis by processing CYLD. Nature cell biology. 2011;13(12):1437-42.

184. Wu P, Shi K, An J, Ci Y, Li F, Hui K, Yang Y, Xu C. The LEF1/CYLD axis and cIAPs regulate RIP1 deubiquitination and trigger apoptosis in selenite-treated colorectal cancer cells. Cell death & disease. 2014;5(2):e1085-e.

185. Verzella D, Fischietti M, Capece D, Vecchiotti D, Del Vecchio F, Cicciarelli G, Mastroiaco V, Tessitore A, Alesse E, Zazzeroni F. Targeting the NF-kappaB pathway in prostate cancer: a promising therapeutic approach? Current drug targets. 2016;17(3):311-20.

186. Stolting MN, Ferrari S, Handschin C, Becskei A, Provenzano M, Sulser T, Eberli D. Myoblasts inhibit prostate cancer growth by paracrine secretion of tumor necrosis factor-alpha. J Urol. 2013;189(5):1952-9.

187. Wright A, Reiley WW, Chang M, Jin W, Lee AJ, Zhang M, Sun S-C. Regulation of early wave of germ cell apoptosis and spermatogenesis by deubiquitinating enzyme CYLD. Developmental cell. 2007;13(5):705-16.

188. Lork M, Verhelst K, Beyaert R. CYLD, A20 and OTULIN deubiquitinases in NF-κ B signaling and cell death: so similar, yet so different. Cell Death & Differentiation. 2017;24(7):1172-83.

189. Barretina J, Caponigro G, Stransky N, Venkatesan K, Margolin AA, Kim S, Wilson CJ, Lehár J, Kryukov GV, Sonkin D, Reddy A, Liu M, Murray L, Berger MF, Monahan JE, Morais P, Meltzer J, Korejwa A, Jané-Valbuena J, Mapa FA, Thibault J, Bric-Furlong E, Raman P, Shipway A, Engels IH, Cheng J, Yu GK, Yu J, Aspesi P, de Silva M, Jagtap K, Jones MD, Wang L, Hatton C, Palescandolo E, Gupta S, Mahan S, Sougnez C, Onofrio RC, Liefeld T, MacConaill L, Winckler W, Reich M, Li N, Mesirov JP, Gabriel SB, Getz G, Ardlie K, Chan V, Myer VE, Weber BL, Porter J, Warmuth M, Finan P, Harris JL, Meyerson M, Golub TR, Morrissey MP, Sellers WR, Schlegel R, Garraway LA. The Cancer Cell Line Encyclopedia enables predictive modelling of anticancer drug sensitivity. Nature. 2012;483(7391):603-7.

190. Pannem RR, Dorn C, Ahlqvist K, Bosserhoff AK, Hellerbrand C, Massoumi R. CYLD controls c-MYC expression through the JNK-dependent signaling pathway in hepatocellular carcinoma. Carcinogenesis. 2014;35(2):461-8.

191. Beck-Engeser GB, Lum AM, Huppi K, Caplen NJ, Wang BB, Wabl M. Pvt1-encoded microRNAs in oncogenesis. Retrovirology. 2008;5:4.

192. Ye H, Liu X, Lv M, Wu Y, Kuang S, Gong J, Yuan P, Zhong Z, Li Q, Jia H, Sun J, Chen Z, Guo AY. MicroRNA and transcription factor co-regulatory network analysis reveals miR-19 inhibits CYLD in T-cell acute lymphoblastic leukemia. Nucleic acids research. 2012;40(12):5201-14.

193. Ni F, Zhao H, Cui H, Wu Z, Chen L, Hu Z, Guo C, Liu Y, Chen Z, Wang X, Chen D, Wei H, Wang S. MicroRNA-362-5p promotes tumor growth and metastasis by targeting CYLD in hepatocellular carcinoma. Cancer letters. 2015;356(2 Pt B):809-18.

194. Zhu M, Zhou X, Du Y, Huang Z, Zhu J, Xu J, Cheng G, Shu Y, Liu P, Zhu W. miR-20a induces cisplatin resistance of a human gastric cancer cell line via targeting CYLD. Molecular medicine reports. 2016;14(2):1742-50.

195.   Li D, Jian W, Wei C, Song H, Gu Y, Luo Y, Fang L. Down-regulation of miR-181b promotes apoptosis by targeting CYLD in thyroid papillary cancer. International journal of clinical and experimental pathology. 2014;7(11):7672.

196.   Song H, Li D, Wu T, Xie D, Hua K, Hu J, Deng X, Ji C, Deng Y, Fang L. MicroRNA-301b promotes cell proliferation and apoptosis resistance in triple-negative breast cancer by targeting CYLD. BMB reports. 2018;51(11):602.

197.   Alvarez ML, Khosroheidari M, Eddy E, Kiefer J. Role of microRNA 1207-5P and its host gene, the long non-coding RNA Pvt1, as mediators of extracellular matrix accumulation in the kidney: implications for diabetic nephropathy. PloS one. 2013;8(10):e77468.

198.   Esposito R, Bosch N, Lanzós A, Polidori T, Pulido-Quetglas C, Johnson R. Hacking the Cancer Genome: Profiling Therapeutically Actionable Long Non-coding RNAs Using CRISPR-Cas9 Screening. Cancer Cell. 2019;35(4):545-57.

199.   Fan G, Li J. Regions identity between the genome of vertebrates and non-retroviral families of insect viruses. Virology journal. 2011;8(1):511.

200.   Gong J, Ju Y, Shao D, Zhang QC. Advances and challenges towards the study of RNA-RNA interactions in a transcriptome-wide scale. Quantitative Biology. 2018;6(3):239-52.

201.   Jacobs MD, Harrison SC. Structure of an IκBα/NF-κB complex. Cell. 1998;95(6):749-58.

202.   Zandi E, Rothwarf DM, Delhase M, Hayakawa M, Karin M. The IκB kinase complex (IKK) contains two kinase subunits, IKKα and IKKβ, necessary for IκB phosphorylation and NF-κB activation. Cell. 1997;91(2):243-52.

203.   Sakakibara S, Espigol-Frigole G, Gasperini P, Uldrick T, Yarchoan R, Tosato G. A20/TNFAIP3 inhibits NF-κB activation induced by the Kaposi's sarcoma-associated herpesvirus vFLIP oncoprotein. Oncogene. 2013;32(10):1223-32.

204.   Vereecke L, Beyaert R, van Loo G. The ubiquitin-editing enzyme A20 (TNFAIP3) is a central regulator of immunopathology. Trends in immunology. 2009;30(8):383-91.

205.   Hirschhaeuser F, Menne H, Dittfeld C, West J, Mueller-Klieser W, Kunz-Schughart LA. Multicellular tumor spheroids: an underestimated tool is catching up again. Journal of biotechnology. 2010;148(1):3-15.

206.   Mueller-Klieser W. Multicellular spheroids. Journal of cancer research and clinical oncology. 1987;113(2):101-22.

207.   Zhang H, Liang Y, Han S, Peng C, Li Y. Long noncoding RNA and protein interactions: from experimental results to computational models based on network methods. International journal of molecular sciences. 2019;20(6):1284.

208.   Yoshida H, Yoshizawa T, Shibasaki F, Kanazawa I. Chemical chaperones reduce aggregate formation and cell death caused by the truncated Machado–Joseph disease gene product with an expanded polyglutamine stretch. Neurobiology of disease. 2002;10(2):88-99.

209.   Algül H, Treiber M, Lesina M, Nakhai H, Saur D, Geisler F, Pfeifer A, Paxian S, Schmid RM. Pancreas-specific RelA/p65 truncation increases susceptibility of acini to inflammation-associated cell death following cerulein pancreatitis. The Journal of clinical investigation. 2007;117(6):1490-501.

210.   Chen G, Ward BM, Kwang HY, Chinchar VG, Robert J. Improved knockout methodology reveals that frog virus 3 mutants lacking either the 18K immediate-early gene or the truncated vIF-2α gene are defective for replication and growth in vivo. Journal of virology. 2011;85(21):11131-8.

211.   Xu H-J, Xu K, Zhou Y, Li J, Benedict WF, Hu S-X. Enhanced tumor cell growth suppression by an N-terminal truncated retinoblastoma protein. Proceedings of the National Academy of Sciences. 1994;91(21):9837-41.

212.   Neu-Yilik G, Amthor B, Gehring NH, Bahri S, Paidassi H, Hentze MW, Kulozik AE. Mechanism of escape from nonsense-mediated mRNA decay of human β-globin transcripts with nonsense mutations in the first exon. Rna. 2011;17(5):843-54.

213.   Hon C-C, Ramilowski JA, Harshbarger JH, 2017 #46}, Bertin N, Rackham OJL, Gough J, Denisenko E, Schmeier S, Poulsen TM, Severin J, Lizio M, Kawaji H, Kasukawa T, Itoh M, Burroughs AM, Noma S, Djebali S, Alam T, Medvedeva YA, Testa AC, Lipovich L, Yip C-W, Abugessaisa I, Mendez M, Hasegawa A, Tang D, Lassmann T, Heutink P, Babina M, Wells

CA, Kojima S, Nakamura Y, Suzuki H, Daub CO, de Hoon MJL, Arner E, Hayashizaki Y, Carninci P, Forrest ARR. An atlas of human long non-coding RNAs with accurate 5′ ends. Nature. 2017;543:199.

214. Kent WJ, Sugnet CW, Furey TS, Roskin KM, Pringle TH, Zahler AM, Haussler D. The human genome browser at UCSC. Genome research. 2002;12(6):996-1006.

215. Wiśniewski JR, Zougman A, Nagaraj N, Mann M. Universal sample preparation method for proteome analysis. Nature Methods. 2009;6(5):359-62.

216. Lepper MF, Ohmayer U, von Toerne C, Maison N, Ziegler AG, Hauck SM. Proteomic Landscape of Patient-Derived CD4+ T Cells in Recent-Onset Type 1 Diabetes. J Proteome Res. 2018;17(1):618-34.

217. Bruderer R, Bernhardt OM, Gandhi T, Miladinovic SM, Cheng LY, Messner S, Ehrenberger T, Zanotelli V, Butscheid Y, Escher C, Vitek O, Rinner O, Reiter L. Extending the limits of quantitative proteome profiling with data-independent acquisition and application to acetaminophen-treated three-dimensional liver microtissues. Mol Cell Proteomics. 2015;14(5):1400-10.

218. Patro R, Duggal G, Love MI, Irizarry RA, Kingsford C. Salmon provides fast and bias-aware quantification of transcript expression. Nature Methods. 2017;14:417.

219. Love MI, Huber W, Anders S. Moderated estimation of fold change and dispersion for RNA-seq data with DESeq2. Genome biology. 2014;15(12):550.

220. Trapnell C, Roberts A, Goff L, Pertea G, Kim D, Kelley DR, Pimentel H, Salzberg SL, Rinn JL, Pachter L. Differential gene and transcript expression analysis of RNA-seq experiments with TopHat and Cufflinks. Nature protocols. 2012;7(3):562-78.

221. Subramanian A, Tamayo P, Mootha VK, Mukherjee S, Ebert BL, Gillette MA, Paulovich A, Pomeroy SL, Golub TR, Lander ES, Mesirov JP. Gene set enrichment analysis: A knowledge-based approach for interpreting genome-wide expression profiles. Proceedings of the National Academy of Sciences. 2005;102(43):15545.

222. Wickham H. ggplot2: elegant graphics for data analysis: Springer; 2016.